Vibrational Sum Frequency Generation Studies of Biological and Atmospheric Relevant Interfaces: Lipids, Organosulfur Species and Interfacial Water Structure

DISSERTATION

Presented in Partial Fulfillment of the Requirements for the Degree Doctor of Philosophy in the Graduate School of The Ohio State University

By

Xiangke Chen

Graduate Program in Chemistry

The Ohio State University

2010

Dissertation Committee:

Heather C. Allen, Advisor

Dennis Bong

Sherwin J. Singer

James Waldman

Abstract

The challenges to reveal the molecular organization and interactions at the biological and atmospheric relevant interfaces were confronted in this dissertation by using vibrational sum frequency generation (VSFG) spectroscopy. In particular, the interfaces of biological membrane represented by model phospholipid monolayers, and the aqueous organosulfur species (dimethyl suloxide, DMSO and methanesulfonic acid, MSA) are studied.

A condensing effect is observed for the model phospholipid (dipalmitoylphosphatidylcholine, DPPC) monolayer on concentrated DMSO subphases. When the DMSO molecules interact with the phospholipid membranes, DMSO molecules squeeze aside the phospholipids, which cause them to form tightly packed domain structures as well as causing the membrane to expand. In addition, the miscibility of DMSO with water and its powerful solvation of many substances make the formed pores a transportation corridor across the membrane, which as a result accounts for the enhanced permeability of membranes upon exposure to DMSO. Similar effects were found through "in-situ" Brewster angle microscopy (BAM) on dipalmitoylphosphatidyl ethanolamine (DPPE), glycerol (DPPG), and serine (DPPS) phospholipids, indicating that the condensing effect is not dependant upon the phospholipid headgroup structure.

Novel structural features of water confined in phospholipid monolayers are revealed. At the air/D_2O/monolayer interface, the dangling OD stretching mode showed a marked frequency red-shift as well as spectral structure upon increasing the monolayer surface coverage. Furthermore, the dangling OD was found to exist even when a D_2O surface was fully covered by the lipid molecules. This phenomenon was observed in monolayers formed with DPPC and with palmitic acid. The frequency red-shift of the dangling OD is interpreted to be due to the perturbation imposed by the lipid hydrophobic tail groups.

In addition, phase sensitive vibrational sum frequency generation is employed to investigate the ordering of water at phospholipid/water interfaces. Interfacial water molecules are found to be oriented preferentially by the electrostatic potential imposed by the phospholipids and have, on average, their dipole pointing towards the phospholipid tails for all phospholipids studied. Zwitterionic DPPC and DPPE reveal weaker water orienting capability relative to net negative DPPA, DPPG, and DPPS. Binding of calcium cations to the lipid phosphate group reduces ordering of the water molecules.

Besides biological interfaces, a comprehensive investigation of the molecular organization at the aqueous DMSO/MSA surface has been made. Surface reorganization causes a decrease in the dangling OH fraction at the surface and further confirms the strong surface propensity of DMSO and MSA. Both DMSO molecules and MSA molecules are found to have their CH_3 groups pointing outwards into the air but are differ in their tilt angle.

For surface DMSO molecules, the S=O group at surface forms strong hydrogen bond with water, which results in reorientation of interfacial water molecules with their hydrogens pointing up towards the S=O group. MSA molecules completely dissociate into hydrated ions at low concentrations (< 0.1 *x*). The interfacial water structure is therefore found to be affected by both the methanesulfonate anions and the hydronium ions residing at the surface.

Dedication

This dissertation is dedicated to Yinglin and my parents.

Acknowledgments

With the closing of this section, my five years PhD life has come to an end. I am sincerely grateful to my advisor, Professor Heather C. Allen, for her continuous support and mentorship. Professor Allen has always been an inspiring, kind and helpful mentor for her great insights in science, optimism in life and courteous attitude to people. I would also thank Dr. Gang Ma for his great help in both science and life. Throughout my PhD period, I have also had nice working experiences with Dr. Man Xu, Dr. Nadia Casillas-ituarte, and Dr. Cheng Y. Tang which is unforgettable. In addition, I would also extend my thank and best wishes for Dr. Roxana Sierra-Hernandez, Aaron Jubb, Wei Hua and Zishuai Huang and all Allen group members. In the end, I would dedicate my PhD degree to my family, my wife Yinglin and my parents, for their warm support during the past years. I pray sincerely for them for a healthy and happy life everyday.

Vita

2002.....B.S. Chemistry, Nanjing University, China

2005.....M.Sc. Chemistry, Nanjing University, China

2005 to 2008 .....Graduate Teaching Associate, Department of Chemistry, The Ohio State University

2008 to present .....Graduate Researching Associate, Department of Chemistry, The Ohio State University

Publications

- X. Chen, W. Hua, Z. Huang, H. C. Allen; Interfacial Water Structure Associated with Phospholipid Membranes Studied by Phase-Sensitive Vibrational Sum Frequency Generation Spectroscopy, *J. Am. Chem. Soc.*, **2010**, in press
- N. N. Casillas-Ituarte, X. Chen, H. Castada, H. C. Allen; Na^+ and Ca^{2+} effect on the hydration andorientation of the phosphate group of DPPC at air−water and air−hydrated silica interfaces, *J. Phys. Chem B*, **2010**, in press

- X. Chen, H. Allen; Interactions of Dimethylsulfoxide with a Dipalmitoylphosphatidylcholine Monolayer Studied by Vibrational Sum Frequency Generation; *J. Phys. Chem A*, **2009**, 113, 12655-12662.
- H. C. Allen, N. N. Casillas-Ituarte, M. R. Sierra-Hernandez, X. Chen, C. Y. Tang; PCCP Perspective: Shedding Light on Water Structure at Air-Aqueous Interfaces: Ions, Lipids, and Hydration; *Phys. Chem. Chem. Phys.*, **2009**,11, 5521-5852.
- M. Xu, C. Y. Tang, A. M. Jubb, X. Chen, H. C. Allen; Nitrate Anions and Ion Pairing at the Air/Aqueous Interface; *J. Phys. Chem. C*, **2009,** 113, 2082-2087.
- G. Ma, X. Chen, H. C. Allen; Dangling OD Confined in a Langmuir Monolayer; *J. Am. Chem. Soc.*, **2007**, 129, 14053-14057.

Fields of Study

Major Field: Chemistry.

Table of Contents

List of Figures

List of Abbreviations

VSFG	vibrational sum frequency spectroscopy
PS-VSFG	phase-sensitive vibrational sum frequency spectroscopy
BAM	Brewster angle microscopy
G	gas phase
LE	liquid expanded phase
LC	liquid condensed phase
MMA	mean molecular area
PA	palmitic acid
DDAB	dimethyldioctadecylammonium bromide salt
DPPC	1,2-Dipalmitoyl-*sn*-glycero-3-phosphocholine
DPPE	1,2-Dipalmitoyl-*sn*-glycero-3-phosphoethanolamine
DPPA	1,2-Dipalmitoyl-*sn*-glycero-3-phosphate sodium salt
DPPG	1,2-Dipalmitoyl-*sn*-glycero-3-phosphoglycerol sodium salt
DPPS	1,2-Dipalmitoyl-*sn*-glycero-3-phospho-L-serine sodium salt
IR	infrared
vis	visible
SF	sum frequency
fs	femto second
ps	pico second
x	mole fraction

Chapter 1: Introduction

The world does not exist in one phase of matter, and interfaces are ubiquitous in nature. Chemical processes at molecular interfaces such as biological interfaces, environmental interfaces, and material interfaces are among the central topics of modern chemistry. This dissertation presents studies of biological and atmospheric relevant air/aqueous interfaces, which include the molecular organization of phospholipids at the air/water interface, phospholipids at the air/aqueous DMSO interface, organosulfur species, i.e. dimethyl sulfoxide (DMSO) and methanesulfonic acid (MSA) at the air/aqueous interfaces, and interfacial water structure at the above mentioned interfaces.

Biological membranes define the boundary and interface of living systems, which not only prevent undesirable agents from the outside environment, but also selectively allow certain necessary substances to exchange through. Therefore they are active structures rather than static barriers. From the identification of lipids as a major component, to the bilayer structure of lipids, to the fluid mosaic model of lipids and proteins, the current picture of biological membranes is the legacy of a century of study.[1] Few biological processes do not involve the function of membranes. Most processes such as cell fusion, differentiation, recognization and signaling rely on both the structure of lipids and

proteins of membranes and their interactions, which lead to the two major approaches in membrane biology: the biophyics of the structure of the lipids and proteins and the biochemistry of the specific chemical interactions between the biomolecules.[2]

To understand how biological membranes function, fundamental properties such as *fluidity*, *permeability*, and *electrostatic potential* need to be investigated. Although lipid molecules show considerable structural diversity, such as sterols, fatty acids, phospholipids and glycolipids, the most important to the bilayer structure backbone are the phospholipids.[3] The amphiphilic structure of phospholipids gives rise to their unique ability to form elegant bilayers with the long alkyl chain tailgroups congregated together as a hydrophobic center and the charged headgroups facing out to the hydrophilic environment. Phospholipid bilayers can be formed with single constituents, such as dipalmitoylphosphatidylcholine (DPPC), dipalmitoylphosphatidylethanolamine (DPPE), dipalmitoylphosphatidylglycerol (DPPG) and dipalmitoylphosphatidylserine (DPPS), or multiple components of them. Despite all of phospholipids contain negatively charged phosphate in the headgroup, properties of phospholipids vary significantly due to the other polar group attached to the phosphate. For example, the headgroups of DPPC and DPPE are zwitterionic while the headgroups of DPPG and DPPS are net negatively charged. This difference in phospholipids headgroup results in different intermolecular interactions, leading to different packing ability.[4, 5] Due to the complexity of membrane strcture, simpler models such as lipid vesicles, lipid bilayers and Langmuir monolayers are most often studied.[6] Among which Langmuir monolayers formed at the air/water

interface provides most controllability, such as continuously well defined molecular density, surface pressure and phase.[7, 8]

Chapters 4 and 5 present the work on the structural characterization and phase behavior of phospholipid monolayers on water by using vibrational sum frequency generation spectroscopy (VSFG), Langmuir trough, and Brewster angle microscopy (BAM). The influence of the addition of DMSO into water on the structure and phase behavior of phospholipids monolayer is also investigated because the interactions between DMSO molecules and a phospholipid monolayer will change the fluidity and permeability of the phospholipid monolayer.

Chapters 6 and 7 present the study of interfacial water structure associated with phospholipid monolayers. The structure of the top few layers of neat water is also studied for comparison. Because a water molecule can be considered as a small and sensitive polarizable dipole probe, the interfacial water structure reflects the electrostatic potential of the phospholipid monolayer.

Besides biological interfaces, atmospheric relevant interfaces are also important due to their role in tropospheric aerosol formation and growth. Chapter 8 presents the work on the molecular organization of DMSO and MSA at the air/aqueous DMSO and MSA interfaces.

Tropospheric sulfur containing aerosols play an important role in climate as well as in related heterogeneous atmospheric chemical processes.[9] A significant sulfur source in the marine boundary layer (MBL) is the biogenic dimethyl sulfide (DMS) produced by metabolic processes of algae.[10, 11] Because of its high volatility and reactivity, DMS is easily oxidized in the atmosphere and produces many stable intermediates such as DMSO and MSA.[12, 13] Oxidation of DMSO, MSA, and other intermediates can take place at the aerosol surface and in the bulk of the aerosol through reactions with OH radicals, which eventually leads to the formation of H_2SO_4.[14] The sulfur containing aerosols serve as cloud condensation nuclei, influencing the formation of clouds and thereby modifying the earth's albedo.[15-17]

In addition, for the air/aqueous DMSO and MSA interfaces, the interfacial water structure, the hydrogen bonding between water and DMSO and MSA molecules are also discussed in Chapter 9.

Chapter 2: Vibrational Sum Frequency Generation Theory

2.1 Vibrational Sum Frequency Generation (VSFG)

VSFG is a second-order nonlinear optical process that occurs in noncentrosymmetric environments such as interfaces under the electric-dipole approximation. Within this approximation, the effects of optical magnetic fields and of multipoles are neglected. Detailed theoretical descriptions of VSFG process are available in the literatures.[18-21] In this chapter, a brief introduction of VSFG technique is given.

To drive a VSFG process, two pulsed laser beams, one visible (ω_{vis}) together with an infrared (ω_{IR}) are spatially and temporally overlapped at a sample interface, which in result generates a sum frequency light with its frequency at $\omega_{SF} = \omega_{vis} + \omega_{IR}$. From the energy diagram of VSFG shown in Figure 2.1, the VSFG process can be viewed as an coherent anti-stokes Raman process over an IR excited surface. With the co-propagating visible and IR pulses both the reflected and transmitted sum frequency pulses are generated as shown in Figure 1, but in most experiments, only the reflected sum frequency signal is detected. The direction of reflected sum frequency light is given under momentum conservation along the interface:

$$\frac{\sin\theta_{SF}}{\lambda_{SF}} = \frac{\sin\theta_{vis}}{\lambda_{vis}} + \frac{\sin\theta_{IR}}{\lambda_{IR}} \tag{2-1}$$

θ_i is the angle of the indicated light to the surface normal and λ is the wavelength of each light.

The intensity of the reflected sum frequency signal, I_{SF}, is proportional to the absolute square of the effective second-order susceptibility, $\chi_{eff}^{(2)}$, and to the visible and IR pulse intensities:

$$I_{SF} = \frac{8\pi^3 \omega_{SF}^{\ 2} \sec^2\theta_{SF}}{c^3 n_1(\omega_{SF}) n_1(\omega_{vis}) n_1(\omega_{IR})} \left|\chi_{eff}^{\ (2)}\right|^2 I_{vis} I_{IR} \tag{2-2}$$

with

$$\chi_{eff}^{\ (2)} = \left[L(\omega_{SF})\cdot\hat{e}(\omega_{SF})\right]\cdot\chi^{(2)} : \left[L(\omega_{vis})\cdot\hat{e}(\omega_{vis})\right]\cdot\left[L(\omega_{IR})\cdot\hat{e}(\omega_{IR})\right] \tag{2-3}$$

ω_i is the frequency of visible, IR and sum frequency pulses, $n_1(\omega)$ is the refractive index of the medium 1 at frequency ω (for air the value is 1). The effective second-order susceptibility $\chi_{eff}^{(2)}$ is related to the macroscopic second-order susceptibility $\chi^{(2)}$ by the Fresnel factors $L(\omega)$ and the unit electric field vector $\hat{e}(\omega)$.

The macroscopic second-order susceptibility $\chi^{(2)}$ has a maximum of 27 components in laboratory coordinate system $\chi_{ijk}^{(2)}$, but the non-zero components maybe less due to symmetry constraints. In a centrosymmetric environment, i.e. bulk solution, the $\chi_{ijk}^{(2)}$ should be identical under inversion symmetry operation:

$$\chi_{ijk}^{(2)} = \chi_{-i-j-k}^{(2)} \tag{2-4}$$

However, as a third rand tensor, a change in the sign of the three subscripts is equivalent to the reversing of axis system, which therefore reverses the sign of $\chi_{ijk}^{(2)}$:

$$\chi_{-i-j-k}^{(2)} = (-1)^3 \chi_{ijk}^{(2)} = -\chi_{ijk}^{(2)} \tag{2-5}$$

To satisfy both equation (2-4) and (2-5), the $\chi_{ijk}^{(2)}$must be 0. This gives rise to the surface selectivity of VSFG because the centrosymmetry is naturally broken at the surface.

$\chi_{ijk}^{(2)}$ is the macroscopic orientational average of microscopic molecular hyperpolarizability $\beta_{lmn}^{(2)}$ of all the interfacial molecules:

$$\chi_{ijk}^{(2)} = N_s \sum_{lmn} < R(\theta)R(\phi)R(\psi) > \beta_{lmn}^{(2)} \tag{2-6}$$

N_s is the number density of the interfacial molecules, $< R(\theta)R(\phi)R(\psi) >$ represents the Euler transformation between the laboratory coordinate system (*i,j,k*) and the molecular coordinate system (*l,m,n*) as shown in Figure 2, where the laboratory coordinate axis and molecular coordinate axis are labeled as x-y-z and a-b-c. θ, $\phi$and ψ are the tilt angle, azimuth angle and twist angle of the molecules respectively.

Both $\chi^{(2)}$ and $\beta^{(2)}$ are comprised of a nonresonant term and a sum of resonant terms:

$$\begin{aligned} \chi^{(2)} &= \chi_{NR}^{(2)} + \sum_{\nu} \frac{A_\nu}{\omega_{IR} - \omega_\nu - i\Gamma_\nu} \\ \beta^{(2)} &= \beta_{NR}^{(2)} + \sum_{\nu} \frac{\beta_\nu}{\omega_{IR} - \omega_\nu - i\Gamma_\nu} \end{aligned} \tag{2-7}$$

in which A_ν (β_ν), ω_ν and Γ_ν are the VSFG transition moment amplitude, transition frequency and line width of vibrational mode ν respectively. For dielectric substrates

such as water, $\chi_{NR}^{(2)}$ is usually very small.[20] Therefore the VSFG signal is mainly attributed to the resonant terms when the incident IR matches the vibrational transition frequencies of molecules.

2.2 Fresnel Factors

VSFG experiments can be conducted with a variety of polarization combinations of incident visible and IR pulses such as ssp, sps, pss and ppp, where the three polarizations refer to the polarization of sum frequency light, visible light and IR light in order. For instance, ssp means s-polarized output sum frequency signal with s-polarized incident visible and p-polarized incident IR pulses. The s-polarized light has its electric field vector perpendicular to the plane of incidence, while the p-polarized light has its electric field vector parallel to the plane of incidence. The Fresnel factors serve as the local-field correction factors of each electric field at the interface. For reflection VSFG geometry, Fresnel factors are functions of the refractive indices of the beam in different media, the incident (reflection) angle and the refractive angle:

$$
\begin{aligned}
L_{xx}(\omega_i) &= \frac{2n_1(\omega_i)\cos\gamma_i}{n_1(\omega_i)\cos\gamma_i + n_2(\omega_i)\cos\theta_i} \\
L_{yy}(\omega_i) &= \frac{2n_1(\omega_i)\cos\theta_i}{n_1(\omega_i)\cos\theta_i + n_2(\omega_i)\cos\omega_i} \\
L_{zz}(\omega_i) &= \frac{2n_2(\omega_i)\cos\theta_i}{n_1(\omega_i)\cos\gamma_i + n_2(\omega_i)\cos\theta_i}\left(\frac{n_1(\omega_i)}{n'(\omega_i)}\right)^2
\end{aligned}
\qquad (2\text{-}8)
$$

in which $n_m(\omega_i)$ is the refractive index of medium m (m = 1, 2, ') at frequency ω_i (i = SF, vis, IR), θ_i is the incident (reflection for SF) angle to the surface normal in medium 1 and γ_i is the refractive angle into medium 2 defined by Snell's $n_1(\omega_i)\sin\theta_i = n_2(\omega_i)\sin\gamma_i$. In

Fresnel factors, all variables are known values except for the refractive index of the interface $n'(\omega_i)$. The value of $n'(\omega_i)$ can be estimated from an empirical model with $n_1(\omega_i) = 1$:[19]

$$\left(\frac{1}{n'(\omega_i)}\right)^2 = \frac{4n_2^2(\omega_i)+2}{n_2^2(\omega_i)(n_2^2(\omega_i)+5)} \tag{2-9}$$

With equation (2-8), equation (2-3) can be rewritten for an isotropic interface in different polarization combinations:

$$\begin{aligned}
\chi^{(2)}_{eff,ssp} &= L_{yy}(\omega_{SF})L_{yy}(\omega_{vis})L_{zz}(\omega_{IR})\sin\theta_{IR}\chi_{yyz} \\
\chi^{(2)}_{eff,sps} &= L_{yy}(\omega_{SF})L_{zz}(\omega_{vis})L_{yy}(\omega_{IR})\sin\theta_{vis}\chi_{yzy} \\
\chi^{(2)}_{eff,pss} &= L_{zz}(\omega_{SF})L_{yy}(\omega_{vis})L_{yy}(\omega_{IR})\sin\theta_{SF}\chi_{zyy} \\
\chi^{(2)}_{eff,ppp} &= -L_{xx}(\omega_{SF})L_{xx}(\omega_{vis})L_{zz}(\omega_{IR})\cos\theta_{SF}\cos\theta_{vis}\sin\theta_{IR}\chi_{xxz} \\
&- L_{xx}(\omega_{SF})L_{zz}(\omega_{vis})L_{xx}(\omega_{IR})\cos\theta_{SF}\sin\theta_{vis}\cos\theta_{IR}\chi_{xzx} \\
&+ L_{zz}(\omega_{SF})L_{xx}(\omega_{vis})L_{xx}(\omega_{IR})\sin\theta_{SF}\cos\theta_{vis}\cos\theta_{IR}\chi_{zxx} \\
&+ L_{zz}(\omega_{SF})L_{zz}(\omega_{vis})L_{zz}(\omega_{IR})\sin\theta_{SF}\sin\theta_{vis}\sin\theta_{IR}\chi_{zzz}
\end{aligned} \tag{2-10}$$

Therefore the Fresnel factors have impact on VSFG intensity and should be considered in spectral normalization. However, for the simplicity of data process, the VSFG spectra presented in this dissertation are only normalized to the visible and IR intensities.

2.3 Molecular Orientational Analysis

The capability of quantitative determination of molecular orientation is a significant advantage of VSFG technique compared to other spectroscopic methods. It is shown in equation (2-6) that the macroscopic second-order susceptibility $\chi^{(2)}$ is related to the microscopic molecular hyperpolarizability $\beta^{(2)}$ through average molecular orientation. For

a certain vibrational mode, the nonvanishing components of $\beta^{(2)}$ are determined by the symmetry of the molecular group.

In this dissertation molecular groups with C_{3v} symmetry such as CH_3 and SO_3^- groups are investigated. For the symmetric stretch (SS) of C_{3v} groups, the nonvanishing $\beta^{(2)}$are $\beta_{aac} = \beta_{bbc}$ and β_{ccc}. Therefore equation (2-6) can be further derived for C_{3v} symmetric stretch as following:[18]

$$\begin{aligned}
\chi_{xxz}^{SS} &= \chi_{yyz}^{SS} = \frac{1}{2} N_s \beta_{ccc} [< \cos\theta > (1+R) - < \cos^3\theta > (1-R)] \\
\chi_{xzx}^{SS} &= \chi_{zxx}^{SS} = \chi_{yzy}^{SS} = \chi_{zyy}^{SS} = \frac{1}{2} N_s \beta_{ccc} (< \cos\theta > - < \cos^3\theta >)(1-R) \\
\chi_{zzz}^{SS} &= N_s \beta_{ccc} [< \cos\theta > R + < \cos^3\theta > (1-R)]
\end{aligned} \tag{2-11}$$

where θ is the tilt angle of the C_{3v} groups to the surface normal and $R = \beta_{aac}/\beta_{ccc}$ is the hyperpolarizability ratio which can be determined experimentally from polarized Raman spectra (see section 2.4).

2.4 Hyperpolarizability Ratio (R)

The hyperpolarizability ratio R used for orientational analysis can be obtained from Raman depolarization ratio (ρ). Because the VSFG process can be viewed as an antistokes Raman scattering on an IR excited surface, the hyperpolarizability ratio R can be expressed in terms of molecular polarizability and dipole moment derivatives:

$$R = \frac{\beta_{aac}}{\beta_{ccc}} = \frac{\alpha_{aa} \cdot \mu_c}{\alpha_{cc} \cdot \mu_c} = \frac{\alpha_{aa}}{\alpha_{cc}} \tag{2-12}$$

The Raman depolarization ratio ρ is given by:

$$\rho = \frac{I_{\perp}}{I_{\parallel}} = \frac{3\gamma^2}{45\alpha^2 + 4\gamma^2} \tag{2-13}$$

$I_{\perp}$ and $I_{//}$ are the measured intensities of scattered light with polarization perpendicular and parallel to the incident light, respectively. α is the mean polarizability derivative and γ is the anisotropy:

$$\alpha = \frac{1}{3}(\alpha_{aa} + \alpha_{bb} + \alpha_{cc})$$
$$\gamma^2 = \frac{1}{2}[(\alpha_{aa} - \alpha_{bb})^2 + (\alpha_{aa} - \alpha_{cc})^2 + (\alpha_{bb} - \alpha_{cc})^2] \tag{2-14}$$

For C_{3v} symmetry, $\alpha_{aa} = \alpha_{bb}$ so that equation (2-13) can be rewritten as:

$$\rho = \frac{3}{4 + 5\left(\frac{2R+1}{R-1}\right)^2} \tag{2-15}$$

Therefore the value of R can be retrieved:

$$R = \frac{Q-1}{Q+2} \quad \text{or} \quad R = \frac{Q+1}{Q-2} \tag{2-16}$$

with $Q = \sqrt{\frac{3}{5}\left(\frac{1}{\rho} - \frac{4}{3}\right)}$.

Only one of the retrieved R from solving the quadratic equation is physically correct, which can be validated from polarized VSFG experiment. For molecular groups with C_{3v} symmetry, the value of $R > 1$ is a simple check from the bond additive model.[19, 21]

The polarized Raman spectra of the CH_3 and SO_3^- groups of methanesulfonic acid (MSA) are shown in Figure 3. The Raman depolarization ratio ρ measured for the CH_3 symmetric stretch (at 2945 cm^{-1}) and SO_3^- symmetric stretch (at 1050 cm^{-1}) are 0.009 ± 0.001 and 0.039 ± 0.001, which yield the hyperpolarizability ratio R value of 1.49 ± 0.03 and 2.65 ± 0.05, respectively.

Combining equation (2-10) and (2-11) could allow to retrieve the orientation angle of C_{3v} groups from the VSFG intensity ratio of different polarization combinations, i.e. ssp and ppp. The retrieved orientational parameter D, defined as $\langle\cos\theta\rangle/\langle\cos^3\theta\rangle$, is based on the known value of Fresnel factors, the experiment geometry, and the hyperpolarizability ratio R.

For present analysis the value of the refractive index of the interface $n'(\omega_i)$ is chosen to be 1.18 for substances at the air/water interface according to Shen et al. In addition a δ-distribution of the orientation angle is assumed so that $\langle\cos\theta\rangle = \cos\theta$. Changing the distribution function of θ will result in change of the retrieved average orientation accordingly. Especially, as shown in a previous SHG study, the retrieved orientation angle and the distribution width are subjected to a very large uncertainty if the value of the orientational parameter D is close to 1.66. In that case, the apparent orientation angle retrieved is ~ 39°, which is the so-called "magic angle".[22]

2.5 Polarization Null Angle Method

As mentioned in section 2.3 the average molecular orientation can be retrieved from the measured ratio of VSFG intensities in different polarization combinations. However, sometimes the VSFG intensity of a specific polarization combination could be very low (For example, the ppp spectrum of DMSO CH_3 is more than 10 folds lower than ssp spectrum.), which as a result leads to large experimental errors in orientation analysis from a quantitative aspect.

Polarization null angle method, as shown in literatures,[21, 23] can improve the accuracy of the measured ratio of macroscopic second-order susceptibilities $\chi^{(2)}$. In VSFG experiment the polarization of the output sum frequency beam is determined by the polarization of incident visible and IR beams and the macroscopic second-order susceptibilities $\chi^{(2)}$ as shown in equation (2-2), (2-3) and (2-10). If we incorporate the polarization angle of each beam, equation (2-10) can be rewritten as:

$$\chi^{(2)}_{eff,total} = \chi^{(2)}_{eff,ssp} + \chi^{(2)}_{eff,sps} + \chi^{(2)}_{eff,pss} + \chi^{(2)}_{eff,ppp}$$

$$\begin{aligned}
\chi^{(2)}_{eff,total} &= \sin\Omega_{SF}\sin\Omega_{vis}\cos\Omega_{IR}L_{yy}(\omega_{SF})L_{yy}(\omega_{vis})L_{zz}(\omega_{IR})\sin\theta_{IR}\chi_{yyz} \\
&+ \sin\Omega_{SF}\cos\Omega_{vis}\sin\Omega_{IR}L_{yy}(\omega_{SF})L_{zz}(\omega_{vis})L_{yy}(\omega_{IR})\sin\theta_{vis}\chi_{yzy} \\
&+ \cos\Omega_{SF}\sin\Omega_{vis}\sin\Omega_{IR}L_{zz}(\omega_{SF})L_{yy}(\omega_{vis})L_{yy}(\omega_{IR})\sin\theta_{SF}\chi_{zyy} \\
&- \cos\Omega_{SF}\cos\Omega_{vis}\cos\Omega_{IR}L_{xx}(\omega_{SF})L_{xx}(\omega_{vis})L_{zz}(\omega_{IR})\cos\theta_{SF}\cos\theta_{vis}\sin\theta_{IR}\chi_{xxz} \\
&- \cos\Omega_{SF}\cos\Omega_{vis}\cos\Omega_{IR}L_{xx}(\omega_{SF})L_{zz}(\omega_{vis})L_{xx}(\omega_{IR})\cos\theta_{SF}\sin\theta_{vis}\cos\theta_{IR}\chi_{xzx} \\
&+ \cos\Omega_{SF}\cos\Omega_{vis}\cos\Omega_{IR}L_{zz}(\omega_{SF})L_{xx}(\omega_{vis})L_{xx}(\omega_{IR})\sin\theta_{SF}\cos\theta_{vis}\cos\theta_{IR}\chi_{zxx} \\
&+ \cos\Omega_{SF}\cos\Omega_{vis}\cos\Omega_{IR}L_{zz}(\omega_{SF})L_{zz}(\omega_{vis})L_{zz}(\omega_{IR})\sin\theta_{SF}\sin\theta_{vis}\sin\theta_{IR}\chi_{zzz}
\end{aligned} \tag{2-17}$$

where Ω_{SF}, Ω_{vis} and Ω_{IR} are the detection polarization angle of sum frequency beam, the incident polarization angle of visible beam and the incident polarization angle of IR beam, respectively. Here $\Omega = 0°$ for p-polarization and $\Omega = 90°$ for s-polarization. If the incident visible is s-polarized and IR is p-polarized then the effective susceptibility $\chi_{eff,total}^{(2)}$ is reduced to $\chi_{eff,ssp}^{(2)}$.

Typically, a p-polarized (0°) IR pulse and a -45° linear polarized (half s and half p polarized) visible pulse are used for in polarization null angle method. In this case, equation (2-17) is reduced as:

$$\chi_{eff,total}^{(2)} = \frac{\sqrt{2}}{2}(\chi_{eff,ppp}^{(2)} \cos\Omega_{SF} - \chi_{eff,ssp}^{(2)} \sin\Omega_{SF}) \tag{2-18}$$

Therefore a null angle in detection polarization is inferred from equation (2-18) at which the VSFG intensity will be vanished, with:

$$\begin{aligned} &\chi_{eff,total}^{(2)} = 0 \\ &\tan\Omega_{null,SF} = \chi_{eff,ppp}^{(2)} / \chi_{eff,ssp}^{(2)} \end{aligned} \tag{2-19}$$

Because the VSFG intensity is proportional to the absolute square of $\chi_{eff,total}^{(2)}$, the null angle can be retrieved through fitting of the measured VSFG intensity at a range of detection polarization angles as shown in equation (2-20):

$$I_{SF} = \left|\chi_{eff,total}^{(2)}\right|^2 = A\left|\sin(\Omega_{SF} - \Omega_{null,SF})\right|^2 \tag{2-20}$$

The macroscopic second-order susceptibility ratio obtained from the polarization null angle method is similar to the VSFG intensity ratio of different polarization, which can then be used for orientation analysis.

2.6 Phase-Sensitive Vibrational Sum Frequency Generation (PS-VSFG)

PS-VSFG, namely can provide phase information of the vibrational modes as compared to conventional VSFG discussed above. In this dissertation, the term VSFG refers to conventional VSFG in contrast with PS-VSFG.

As shown from equation (2-2) and (2-7), VSFG intensity is proportional to the absolute square of the macroscopic second-order susceptibility ($|\chi^{(2)}|^2$), which is the sum of all resonant terms and the nonresonant term. For the air/water interface studied in this dissertation, the nonresonant term is small as compared to the resonant enhanced terms. However, the interference from overlapping resonant modes generally makes the spectra appear more complex as fitting parameters obtained from VSFG spectra are not unique if the phase information of each mode is unknown.[24] Figure 4 shows the simulated VSFG spectra of two overlapping peaks in the same phase and opposite phase according to equation (2-7). The simulated $|\chi^{(2)}|^2$ spectra are hardly distinguishable although the actual phase of each peak and subsequently the physical implication are completely different. Unlike the VSFG $|\chi^{(2)}|^2$ spectra, the imaginary part of $\chi^{(2)}$ reveals unambiguously the phase information as shown in equation (2-21):

$$\mathrm{Im}\,\chi^{(2)} = \sum_{\nu} \frac{A_\nu \Gamma_\nu}{(\omega_{IR} - \omega_\nu)^2 + \Gamma_\nu^{\,2}} \tag{2-21}$$

The strength of each mode, A_ν, is nonvanishing only if the assembly of contributing molecules has a net polar orientation. For the isotropic (C_∞ symmetry) air/water interface the net polar orientation is either up or down, which determines the relative sign of A_ν.

To obtain the imaginary part of $\chi^{(2)}$ (Im $\chi^{(2)}$ spectra), heterodyne detection based on the interference of sample VSFG signal with another local oscillator of the same frequency is often employed. This was pioneered by Shen and coworkers who reported the first Im $\chi^{(2)}$ spectra of quartz/water (2005) and air/water interfaces (2008) by using pico-second scanning laser system.[24, 25] Heterodyne detected VSFG based on femto-second broadband laser system has also been reported recently by Stiopkin et al[26] and Nihonyanagi et al.[27] Similar Im $\chi^{(2)}$ spectrum of air/water interface is reported as obtained by Shen and coworkers on scanning system.

Our experimental setup of PS-VSFG system is similar as reported by Nihonyanagi et al. Briefly, the sample sum frequency signal is interfered with a local oscillator delayed by a time ΔT (~ 2.5 ps), so that the total sum frequency electric field can be expressed as follows:[28]

$$E_{total}(t) = E_{sample}(t - \Delta T) + E_{LO}(t) \tag{2-22}$$

Equation (2-22) is Fourier transformed into the frequency domain to give:

$$E_{total}(\omega) = \int_{-\infty}^{+\infty} dt E_{total}(t) \exp(i\omega t) = E_{sample}(\omega) \exp(i\omega\Delta T) + E_{LO}(\omega) \tag{2-23}$$

The raw VSFG spectra of the total signal can therefore be expressed as follows:

$$I_{SF} \propto \left|E_{total}\right|^2 = \left|E_{sample}\right|^2 + \left|E_{LO}\right|^2 + E_{sample} E_{LO}{}^{*} \exp(i\omega\Delta T) + E_{sample}{}^{*} E_{LO} \exp(-i\omega\Delta T) \tag{2-24}$$

from which a fringe pattern in the detected VSFG intensity is seen in the cross terms.

The data process of the raw VSFG spectra (interferograms) to obtain the PS-VSFG spectra is shown in Figure 5. The raw interferograms were inverse Fourier transformed to the time domain using OriginPro software (version 7.5). The $|E_{sample}|^2$ and $|E_{LO}|^2$ signals at $t = 0$ in time domain were filtered out and only the cross terms were kept and followed by Fourier transform back to the frequency domain. The resulted frequency spectra contain phase information (φ) of the complex $E_{sample}E_{LO}^{*}exp(i\omega\Delta T)$. Because quartz does not have any resonance in this infrared region, the phase of *z*-cut quartz can be used as a reference. Therefore, the real and imaginary $\chi^{(2)}$ spectra can be obtained by dividing the sample interferogram by the quartz reference, through which the contribution from E_{LO} is completely removed. Moreover, the final spectra need to be normalized to the different reflectivities of the incident visible and IR beams on quartz and samples. The expression of Im $\chi^{(2)}$ spectrum is as follows:

$$\mathrm{Im}\,\chi^{(2)} \propto \frac{r_{vis,quartz}r_{IR,quartz}\left|E_{sample}E_{LO}\right|}{r_{vis,sample}r_{IR,sample}\left|E_{quartz}E_{LO}\right|}\sin(\varphi_{sample}-\varphi_{quartz}) \tag{2-25}$$

r is the reflectivity of incident visible or IR beams on quartz or samples. Phase of quartz and samples (φ) is obtained directly from software after Fourier transformation.

For water OH symmetric stretch with C_{2v} symmetry, similar to the C_{3v} symmetry as shown in equation (2-11), the macroscopic second-order susceptibility $\chi^{(2)}$ can be expressed as follows:[27]

$$\chi_{yyz}^{OH,SS} = \frac{1}{2} N_s \{(<\cos^2\psi> \beta_{aac} + <\sin^2\psi> \beta_{bbc} + \beta_{ccc}) <\cos\theta> + <\sin^2\psi> \beta_{aac} + <\cos^2\psi> \beta_{bbc} - \beta_{ccc}) <\cos^3\theta>\} \quad (2\text{-}26)$$

where θ is the tilt angle between water dipole (along C_{2v} axis from oxygen to hydrogen) and the outwards surface normal, ψ is twist angle.

By plug into the relative $\beta^{(2)}$ values (assuming $\beta_{ccc} = 1$) for the water OH symmetric stretch, $\beta_{aac} = 1.296$, $\beta_{bbc} = 0.557$ and $\beta_{ccc} = 1$,[29] equation (2-26) is:

$$\chi_{yyz}^{OH,SS} = \frac{1}{2} N_s \beta_{ccc} \{(1.296 + 0.557 \frac{<\cos^3\theta>}{<\cos\theta>}) <\cos^2\psi> + (0.557 + 1.296 \frac{<\cos^3\theta>}{<\cos\theta>}) <\sin^2\psi> + (1 - \frac{<\cos^3\theta>}{<\cos\theta>})\} <\cos\theta> \quad (2\text{-}27)$$

From equation (2-27) it can be concluded that when $\cos\theta > 0$, $0° < \theta < 90°$, $\chi_{yyz}^{OH,SS}$ is also positive. This suggests that a positive OH stretch band observed in Im $\chi^{(2)}$ spectrum corresponds to water molecules have a net orientation with hydrogens pointing up.

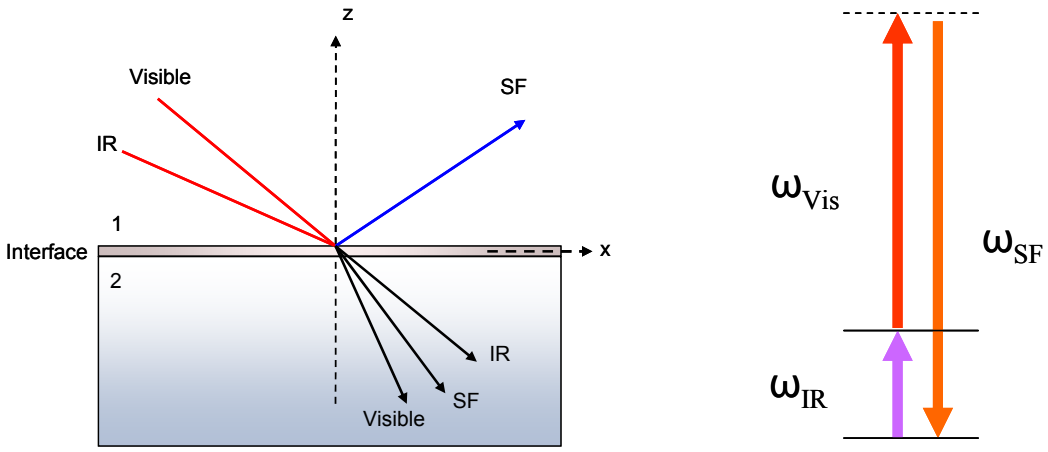

Figure 2.1. Co-propagating VSFG setup and the energy diagram.

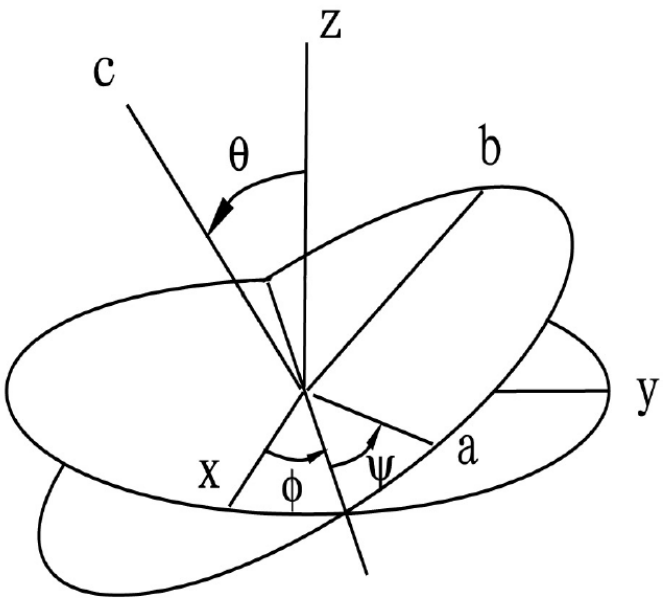

Figure 2.2. The Euler transformation between laboratory coordinates and molecular coordinates.

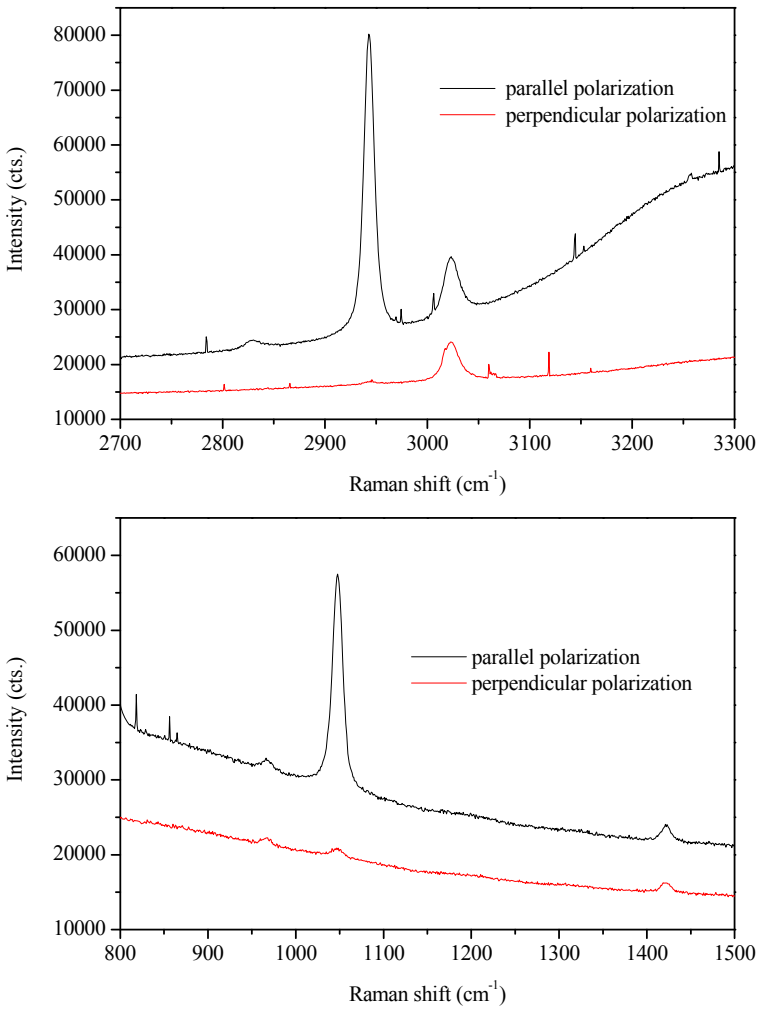

Figure 2.3. Polarized Raman spectra of the CH_3 and SO_3^- groups of methanesulfonic acid (MSA).

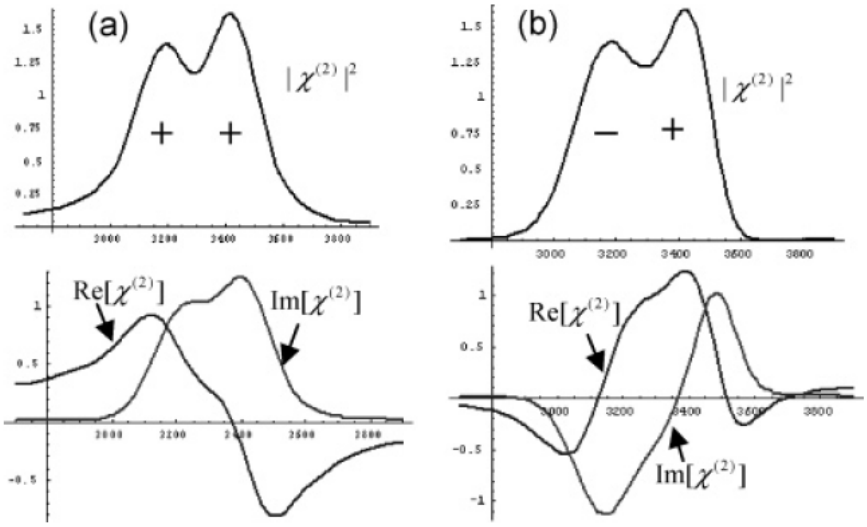

Figure 2.4. The simulated VSFG spectra of two overlapping peaks in the same phase and opposite phase. (from Ref. 24)

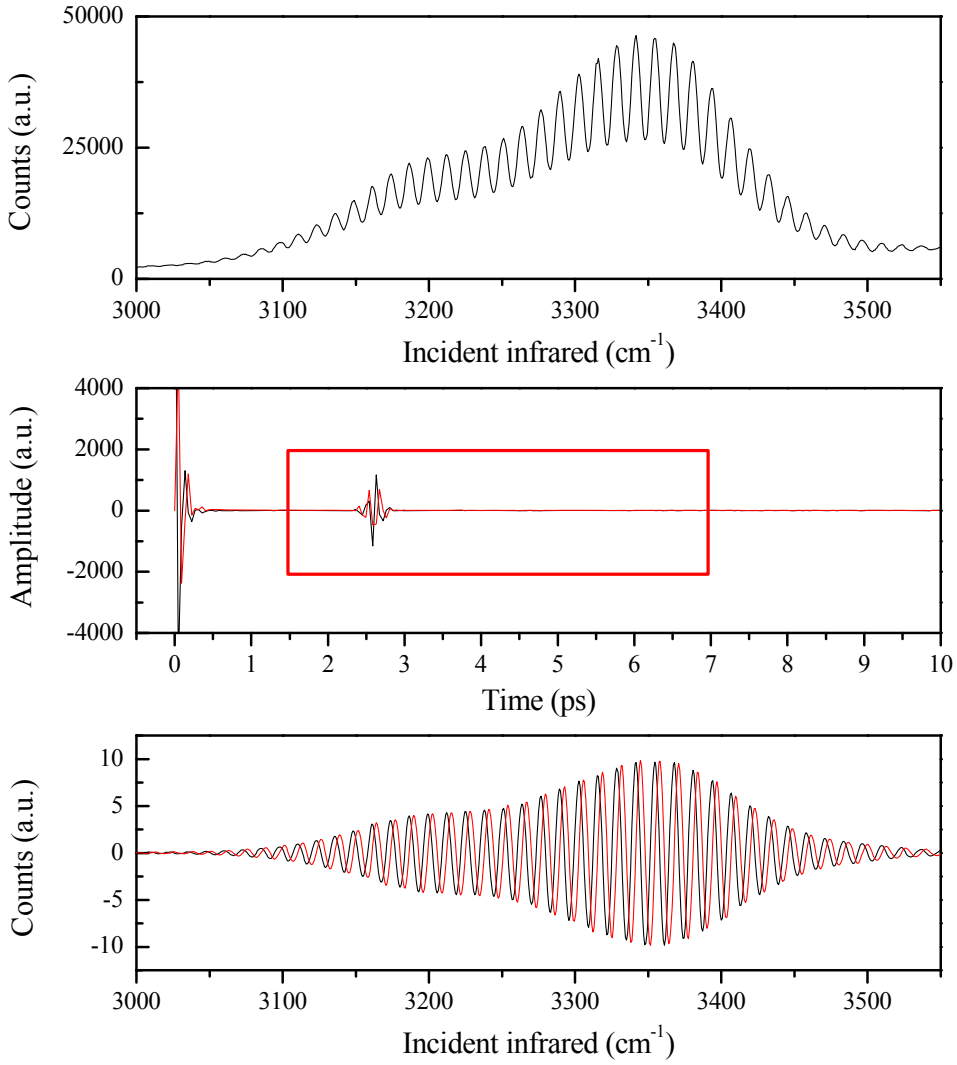

Figure 2.5. Upper panel: Raw interferogram of z-cut quartz with GaAs. Middle panel: Time domain Real (black) and Imaginary (red) signals. The cross term at ~ 2.5 ps is extracted to yield heterodyne frequency spectra. Lower panel: Real (black) and Imaginary (red) parts of heterodyne frequency spectra of z-cut quartz with GaAs. Phase information (φ) is therefore obtained.

Chapter 3: Instrumentation

3.1 Materials.

DMSO and MSA (> 99% purity) was purchased from Fisher. 1,2-Dipalmitoyl-*sn*-glycero-3-phosphocholine (DPPC), 1,2-Dipalmitoyl-*sn*-glycero-3-phosphoethanolamine (DPPE), 1,2-Dipalmitoyl-*sn*-glycero-3-phosphate sodium salt (DPPA), 1,2-Dipalmitoyl-*sn*-glycero-3-phosphoglycerol sodium salt (DPPG)， 1,2-Dipalmitoyl-*sn*-glycero-3-phospho-L-serine sodium salt (DPPS), Dimethyldioctadecylammonium bromide salt (DDAB), and palmitic acid (PA) were purchased from Avanti Polar Lipids (Alabaster, AL). Chain fully deuterated 1,2-dipalmitoyl-*sn*-glycero-3-phosphocholine (DPPC-*d62*) and 1,2-dipalmitoyl-*sn*-glycero-3-phosphate sodium salt (DPPA-*d62*) were also purchased from Avanti Polar Lipids. Molecular structures of lipids are shown in Figure 3.1. Spectrophotometric-grade chloroform was purchased from Sigma-Aldrich. Deionized water (not purged of CO_2) with a resistivity of 18.2 MΩ•cm and a measured pH of 5.5 was from a Barnstead Nanopure system.

3.2 VSFG instrumentation

The broad bandwidth VSFG system consists of two 1-kHz repetition rate regenerative amplifiers (Spectra-Physics Spitfire, femtosecond and picosecond versions), both of

which are seeded by sub-50 fs 792 nm pulses (the wavelength is tuned for system optimization) from a Ti:sapphire oscillator (Spectra-Physics, Tsunami) and pumped by a 527 nm beam from an all solid-state Nd:YLF laser (Spectra-Physics, Evolution 30). The two regenerative amplifiers provide 85 fs pulses and 2 ps pulses at 792 nm. The spectrally broad femtosecond pulses are used to drive the infrared generation in an OPA (optical parametric amplifier; TOPAS, Quantronix) and then produce broad bandwidth infrared pulses (~200 cm^{-1} FWHM). Stable infrared pulses are tunable in various wavelength regions ranging from 1000 cm^{-1} to 3800 cm^{-1}. The output energy of each 792 nm picosecond pulse was set to 300 μJ, and the IR energies were ~ 9μJ in the C-H stretching region, and ~ 3μJ in the PO_2^- symmetric stretching region at the sample stage.

The VSFG spectrum is polarization dependent. In this study, spectra with the polarization combination of *ssp* (*s*-SFG; *s*-visible; *p*-infrared) are shown. The *ppp* polarization combination (data not shown) was used to verify assignments and orientation. Spectral resolution was 8 cm^{-1}. The VSFG spectra were normalized against a nonresonant VSFG spectrum from a GaAs crystal (Lambda Precision Optics, Inc) to remove the spectral distortion caused by the energy profile of the infrared pulse. To calibrate the VSFG peak positions, a nonresonant VSFG spectrum from the GaAs crystal surface was obtained with a polystyrene film covering the OPA infrared output port. The resulting VSFG spectrum containing polystyrene infrared absorption bands was used for the calibration.

The broad bandwidth of IR energy in the OH stretch region can be achieved with pumping a fs pulse of over 1 W. The typical total energy of signal + idler in this region is over 220 μJ.

To get a broad IR profile for a one shot measurement for water spectra, it is critical to find a good overlap position on the difference frequency generation (DFG) crystal. The current DFG is based on a non-collinear design. However, if the angle separation of signal and idler is large, then the 3000 cm^{-1} and 3700 cm^{-1} edges of IR will not be easily focused at the same time on the sample surface. In addition, the compressor length in the Spitfire fs amplifier should be fine tuned because the IR energy at the spectral center and edges cannot be simultaneously maximized. Therefore it is important to sacrifice some SFG peak intensity from the spectral center wavelength (wavenumber) while increasing the SFG intensity arising from the IR profile edges by the fine tuning of the fs compressor length.

3.3 PS-VSFG instrumentation

Our PS-VSFG system is similar to the design reported by Nihonyanagi et al,[27] which is based on heterodyne detection of broad bandwidth signals and Fourier transform analysis. Our broad bandwidth VSFG system[30-32] was redesigned for this application as shown in Figure 3.2. A titanium:sapphire oscillator (Spectra-Physics, Tsunami) with an optimal center wavelength at 792 nm and a sub-50 fs pulse width seeds two 1 kHz regenerative amplifiers (Spectra-Physics, Spitfire, femtosecond and picosecond versions) that are

pumped by a solid state Nd:YLF laser (Spectra-Physics, Evolution 30) at 527 nm. The resulting laser beams from the two respective regenerative amplifiers are ~ 85 fs pulses at 792 nm (22 nm bandwidth, > 1 W) and 2 ps pulses at 792 nm (17 cm^{-1} bandwidth, > 500 mW, used as the visible beam). For the tunable broadband infrared generation in an optical parametric amplifier (Light Conversion, TOPAS), the broadband femtosecond laser pulses (~ 85 fs, > 1 W) are used to generate amplified parametric waves (signal and idler) via a BBO (beta barium borate) crystal using three general steps: superfluorescence generation, preamplification, and power amplification of the signal beam. The amplified signal and idler beams are then used to create an infrared beam via an $AgGaS_2$ crystal in a nonlinear difference-frequency generation system (Light Conversion, NDFG connected to the TOPAS). A 300 μJ visible beam (s-polarized, 792 nm) and a 10 μJ infrared beam (p-polarized, OH stretch region) were spatially and temporally overlapped at incident angles of 50˚ and 60˚ on sample stage 1 (for samples and z-cut quartz), respectively. The visible, infrared, and generated sum frequency (s-polarized) beams reflected from sample stage 1 were refocused by a gold concave mirror (f = 100 mm) onto a GaAs (Lambda Precision Optics) surface on sample stage 2 to generate another sum frequency beam (local oscillator, LO). The sum frequency beam from sample stage 1 was delayed ~ 2.5 ps by passing through an ~ 1 mm thick silica plate positioned before the gold concave mirror. The time difference between the sum frequency beams from two sample stages introduced an interference fringe in the frequency domain. This interferogram was stretched in a monochromator (Acton Research, SpectraPro SP-500 monochromator with a 1200 g/mm grating blazed at 750 nm) and then detected by a liquid-nitrogen cooled

charge-coupled device (CCD) (Roper Scientific, 1340 × 400 pixel array, LN400EB back illuminated CCD). The height of the sample surface which is critical for accurate phase determination is also checked by the image on the CCD. Spectra are averaged over two consecutive runs of 5 min integration times. Final spectra are processed from the raw interferograms through Fourier transformation.

3.4 Langmuir Trough

The surface pressure-area isotherm was obtained with a KSV minitrough (KSV, Finland). The rectangular trough (176.5 mm × 85 mm) is made of Teflon and two barriers are employed to provide symmetric film compression. The barriers, which are made of Delrin, prevent leakage of the monolayer. The surface pressure and mean molecular area were continuously monitored during film compression by the Wilhelmy plate method. The trough was filled with Nanopure water as the subphase. The surface pressure-area isotherm was always measured on a fresh water or 0.1 *x* (mole fractio) DMSO subphases. The compression rate of the barrier to obtain the isotherms was 5 mm/min. Before recording an isotherm, the surface pressure was zeroed for each subphase. The sample temperature was maintained at 22 ± 1°C.

3.5 Brewster Angle Microscopy (BAM)

The BAM experiments were carried out on a self-assembled symmetric goniometer system. The laser light source is from Research Electro-Optics, Inc and emits 17 W at 633 nm, which is incident at the Brewster angle of the subphase, i.e. 53.1° for water. The

incident beam is attenuated by a neutral density filter and passes through a half wave plate before reaching the liquid surface. An infinity corrected 20X Nikon lens together with a tube lens are used to form the image. The BAM image is collected on an Andor charge coupled device (CCD; Andor DV412) of 512 × 512 pixels. The scale of BAM image is 350 μm ×350 μm.

3.6 Polarized Raman Spectroscopy

Polarized Raman spectra were obtained by passing a ~ 200 mW 785 nm light source (Raman System Inc) from a continuous wave laser onto the sample and then detecting in a 90 degree direction. Two polarization sheets, one was placed before the sample and another was placed in front of the monochromator were used to achieve the parallel and perpendicular polarization combination. The incident 785 nm light was focused by a 7.5 mm Raman probe (InPhotonics) and the scattered light was focused onto the entrance slit of a 500 mm monochromator (Acton Research, SpectroPro SP-500), dispersed by a 1200 groove/mm grating blazed at 1 micron and then collected on a liquid nitrogen cooled CCD camera (Roper Scientific, LN400EB).

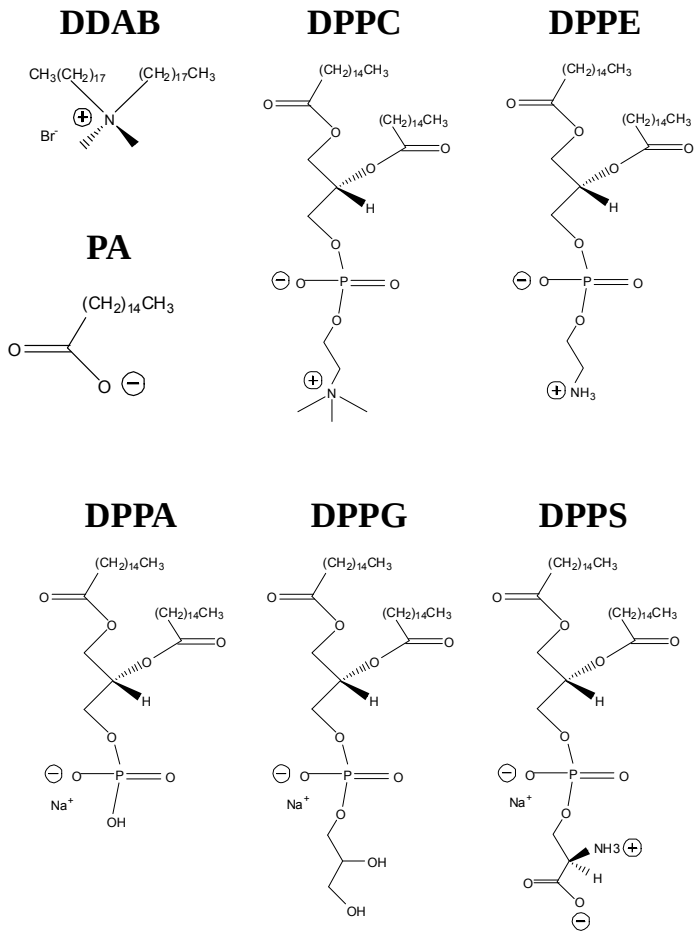

Figure 3.1. Molecular structures of the studied fatty acid, surfactant, and phospholipids.

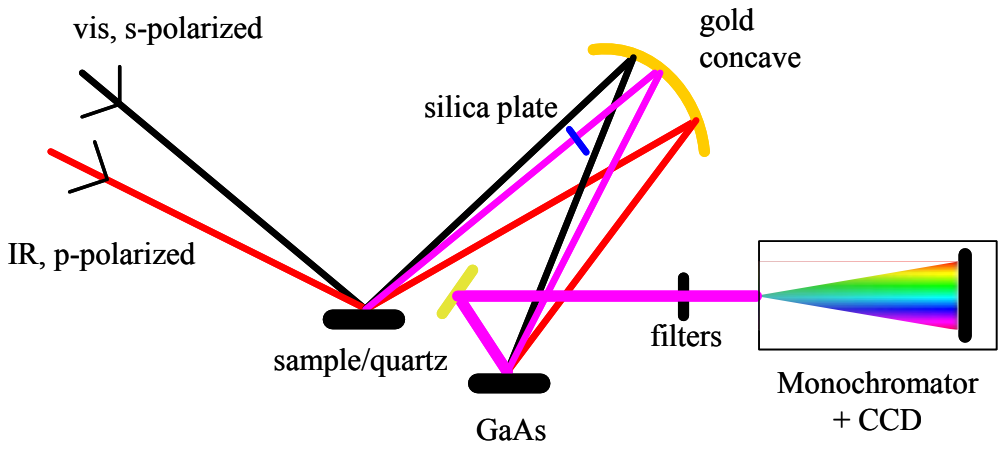

Figure 3.2. Schematic drawing of the PS-VSFG experiment configuration.

Chapter 4: Interactions of Dimethylsulfoxide (DMSO) with a Dipalmitoylphosphatidylcholine (DPPC) monolayer studied by Vibrational Sum Frequency Generation (VSFG)

Dimethylsulfoxide (DMSO) is considered a universal solvent and has found wide applications in pharmaceutical and biological sciences. The DMSO molecule consists of a polar S=O moiety and two non-polar CH_3 groups. Such small amphiphilic structure makes it feasible for DMSO molecules to incorporate into the lipid-water interface and therefore to penetrate into the cell membrane. As the most common cryoprotectant, DMSO is used for preservation of biological tissues at low temperature.[33-35] DMSO can penetrate into the cell interior and is therefore perceived to protect the cell by preventing ice formation in extracellular and intracellular spaces. DMSO has been used to improve drug delivery in diverse types of membranes[36-38] and has been shown to be effective in promoting penetration of both hydrophilic and lipophilic substances.[39] Moreover, DMSO is known as an agent that induces cell fusion[40] and promotes cell differentiation.[41] Given the importance of DMSO in various practical applications, the molecular level mechanisms responsible for these effects have been of great interest.[42]

It is generally thought that DMSO influences the structure and properties of membranes. The interaction of DMSO with model membranes has been studied previously by various experimental and theoretical approaches, i.e. differential scanning calorimetry (DSC),[43-45] X-ray diffraction (XRD),[43, 44, 46, 47] small-angle neutron diffraction,[48, 49] nuclear magnetic resonance (NMR),[50] infrared spectroscopy (IR),[45] and molecular dynamics (MD) simulations.[51-56] As one of the most common phospholipid, dipalmitoylphosphatidylcholine (DPPC) is often used in model biological membrane systems in research. The influence of DMSO on DPPC model membranes was shown to be concentration dependent, and significant structural changes to the membranes were observed in aqueous solutions of DMSO less than 30 mol%.[46, 57] The temperature of the main phase transition of DPPC vesicles in water/DMSO mixed solvent increases with DMSO concentration, revealing a stabilization effect by DMSO on the vesicle gel phase.[37] X-ray and neutron diffraction studies revealed that the repeat distance between the bilayers in multi-lamellar DPPC vesicles decreased with DMSO concentration. This decrease in intermembrane distance inside the vesicles was mainly attributed to the decrease of the intermembrane solvent layer thickness, namely, the removal of free water molecules in the intermembrane spaces.[46, 48, 49]

In addition to experimental efforts, MD simulations provide more insight. Sum *et al.* showed that DMSO penetrates readily into the polar headgroup region of a DPPC bilayer but only a few DMSO molecules actually cross the bilayer.[54] Most recently, Anwar and coworkers reported water pore formation within a DPPC bilayer induced by DMSO using

MD simulation.[55, 56] This finding presented an interesting explanation of the enhanced transdermal permeability by DMSO which cast light on the molecular interaction between DPPC and DMSO molecules.

Although many efforts have been made, probing the intermolecular interactions between DMSO and lipid model membranes directly in the interfacial region has not been reported; a molecular-specific technique is required to meet this need. Vibrational sum frequency generation (VSFG) is a powerful surface-selective and molecular-specific technique that has been successfully applied in many phospholipid studies.[31, 58-60] As a second-order optical spectroscopy, VSFG intensity arises from lack of inversion symmetry. Unlike in bulk solution, inversion symmetry is broken at a surface. This gives rise to the surface selectivity of VSFG. A perfect lipid bilayer is centrosymmetric and thus VSFG inactive;[61-63] therefore, lipid monolayers instead of bilayers are often used as model systems in VSFG studies.

Previous studies of DMSO-membrane interactions mainly focused on the gel phase of bilayers. The gel phase and fluid phase of a bilayer are analogous to the liquid condensed phase and liquid expanded phase of a monolayer, respectively. The use of the Langmuir trough allows investigating the monolayer in the liquid condensed phase and in the liquid expanded phase. In this chapter, we study the interaction between DMSO and DPPC molecules in monolayers by VSFG spectroscopy coupled with a Langmuir trough. A series of water/DMSO subphases were used to examine the concentration dependent

effect of DMSO on phospholipid monolayer structure. Both the head and tail groups of the DPPC molecules, as well as DMSO molecules, were probed to elucidate the interactions between the DMSO and the DPPC molecules.

4.1 Results and Discussion

Compression Isotherms

The interactions between DMSO and DPPC molecules influence the phase behavior of DPPC Langmuir monolayers. The phase behavior can be characterized by surface pressure-area isotherm measurements. The surface pressure-area isotherms of DPPC monolayers on subphases containing different DMSO concentrations are shown in Figure 4.1. The isotherm of a DPPC monolayer on a pure water subphase (black trace) shows several distinct phases, which are generally assigned to the gas (G, > 120 $Å^2$/molecule, not shown in Figure 4.1) phase, the gas-liquid expanded coexistence (G-LE) region, the liquid expanded (LE) phase, the liquid expanded-liquid condensed coexistence (LE-LC) region, the liquid condensed (LC) phase, and the collapse phase. As the DPPC monolayer is compressed, the surface pressure (difference between the surface tension of the subphase and the monolayer covered surface) rises when entering the LE phase. The first order LE-LC phase transition occurs at ~6 mN/m at the experiment temperature of 22 °C, and collapse occurs at ~72 mN/m.

Isotherms of DPPC monolayers on 3 mol%, 10 mol% and 20 mol% DMSO/water mixed subphases are shown in red, green and blue in Figure 4.1, respectively. With the addition

of 3 mol% DMSO in the subphase, the surface pressure of the LE to LC phase transition plateau (LE-LC region) decreases. This decrease is more pronounced as the phase transition surface pressure to the LC phase decreases to zero on the 10 mol% and the 20 mol% DMSO subphases. As a result, the LE phase is bypassed on these DMSO subphases and the DPPC monolayers undergo a phase transition from the G phase to the LC phase directly. Mohwald et al. reported similar observations and attributed this effect to the condensing effect of DMSO on DPPC monolayers.[47] The decreased LE to LC phase transition surface pressure is also in agreement with observations[37, 43] of an increased main phase transition temperature of the DPPC bilayer, which suggests that DMSO has a stabilization effect on the DPPC condensed phase. Additionally, a similar condensing effect on DPPC films induced by surfactants was previously observed.[64, 65]

Although the isotherm of the DPPC monolayer at large mean molecular area (MMA) is greatly changed by DMSO, the liquid condensed phase is only slightly influenced upon addition of DMSO. This result suggests that DMSO molecules are squeezed out from the condensed monolayer region. Similar conclusions were also drawn in a previous study on the influence of DMSO on a DPPC bilayer using nuclear magnetic resonance (NMR).[50]

The collapse pressure for each isotherm is also interesting. For a pure water subphase, the DPPC monolayer collapses at about 72 mN/m, which reveals that the DPPC monolayer can reach a near zero surface tension. This high collapse surface pressure (low surface tension) is consistent with previous isotherm measurements.[66, 67] The collapse pressures

of the DPPC monolayers on 3 mol%, 10 mol%, and 20 mol% DMSO subphases are 68, 62, and 56 mN/m respectively, which are about the same as the surface tensions of each DMSO subphase.[68] This result indicates that near zero surface tension can also be reached for DPPC monolayers on different DMSO subphases. When the DMSO concentration in a subphase is 40 mol%, the DPPC footprint area in the LC phase shifts much lower (< 30 $Å^2$/molecule, data not shown in Figure 4.1), indicating a loss of DPPC molecules to the subphase. The bulk solvation of a fraction of the DPPC monolayer in a concentrated 40 mol% DMSO/water subphase is supported by previous simulation.[56]

VSFG Spectroscopy of DPPC Headgroup

To gain further molecular level insight on the interactions between DPPC and DMSO molecules, VSFG was employed to investigate the phospholipid/aqueous DMSO interface. The headgroup of the DPPC molecule is zwitterionic, consisting of a negatively charged phosphate group and a positively charged choline group. VSFG spectra (*ssp* polarization) of the DPPC phosphate group at different MMAs are shown in Figure 4.2.

For a pure water subphase, there is no detectable VSFG intensity at low surface coverage (100 $Å^2$/molecule) as shown in Figure 4.2. Since VSFG intensity is largely dependent on the orientation and ordering of the molecules, the lack of notable intensity at low surface coverage could be due to a large orientation distribution of the DPPC headgroup in the G-LE region. One peak and a lower energy shoulder are observed when the MMA is compressed to 82 $Å^2$/molecule (LE phase). The main peak centered at 1094 cm^{-1} is

assigned to the headgroup PO_2^- symmetric stretch (SS).[69] The shoulder observed at ~1070 cm^{-1} is not as easy to assign since several possible vibrational modes fall within this frequency region. Since there is no VSFG peak observed for palmitic acid (PA, the chain portion of DPPC; data not shown) in this region, the shoulder is tentatively assigned to a DPPC headgroup C-O stretch. The VSFG spectra are nearly unchanged from the LE to the LE-LC region. Upon further compression to the LC phase (45 $Å^2$/molecule), the PO_2^- SS peak intensity increases. At the same time, the PO_2^- SS peak shifts from 1094 cm^{-1} to 1099 cm^{-1}.

The spectra of the DPPC monolayer on 3 mol% DMSO are similar to the spectra obtained on the water subphase as shown in Figure 4.2, indicating no significant influence on the DPPC headgroup by low concentrations of DMSO. However, on 10 mol% and 20 mol% DMSO subphases, the PO_2^- SS peak is observed at 1099 cm^{-1} at all DPPC surface coverages . This blue shift of the vibrational frequency of the phosphate group on concentrated DMSO subphases is direct evidence of a DMSO-induced dehydration of the DPPC headgroup.[55, 56]

Water molecules around the DPPC headgroup can be roughly divided into two different categories, bound and free.[70] Bound water molecules participate in the solvation of the headgroup and form the hydration shells around the hydrophilic moieties (such as $-PO_2^-$, $-N(CH_3)_3^+$ and –C=O) on the headgroup. Free water molecules do not interact in headgroup solvation although they are still hydrogen bonded to each other. The average

number of bound and free water molecules around a single DPPC headgroup in a gel phase bilayer was reported to be 10.8 and 4, respectively.[70] The average number of free water molecules for each headgroup was reported to decrease to1.1 at 14 mol% DMSO concentration, resulting in a decrease in the intermembrane solvent layer thickness.[46] Additionally, DSC measurements suggested that DMSO molecules do not penetrate into the bound water region when the concentration is below 30 mol%.[71] This result is consistent with our observation in the LC phase (45 and 48 $Å^2$/molecule) on all subphases in which the PO_2^- SS is observed at 1099 cm^{-1}.

As the MMA increases, the number of water molecules in the solvation shell increases, causing the red shift of the PO_2^- SS frequency to 1094 cm^{-1} due to an increase in hydrogen bonding of water molecules to the phosphate group.[31, 72, 73] Addition of DMSO to the subphase results in the replacement of water molecules by DMSO molecules at the interface, which leads to the dehydration of the DPPC headgroup at large MMA (82 and 100 $Å^2$/molecule) for the 10 and 20 mol% DMSO subphases. This is evidenced by the higher frequency of the PO_2^- SS (1099 cm^{-1}). Clearly, DMSO molecules cannot provide the same solvation effect as water molecules to the hydrophilic DPPC headgroup as DMSO does not favor interaction with DPPC headgroups since it is a hydrogen bond acceptor instead of a hydrogen bond donor.

On the 20 mol% DMSO subphase, it is very interesting that the VSFG intensity is notable at large MMA (100 $Å^2$/molecule), while no detectable intensity is observed for water, 3

mol%, and 10 mol% DMSO subphases as shown in Figure 4.2. This suggests that high concentration of DMSO (> 20 mol%) facilitates the aggregation of DPPC molecules and the formation of DPPC domains at the interface since DPPC ordering is observed. Recall that VSFG intensity is sensitive to the order and orientation of the molecules probed. Compared with the 3 mol% and the 10 mol% DMSO subphases, the surface tension of the 20 mol% DMSO subphase without lipid coverage is lower (56 mN/m), corresponding to a surface pressure of 16 mN/m relative to pure water. However, the LE to LC phase transition surface pressure for the DPPC monolayer on a water subphase is ~6 mN/m, which is well below the actual surface pressure of the 20 mol% DMSO subphase itself. Therefore, it is reasonable to consider that DMSO molecules act to corral the headgroups into domains at the interface. Hence the "pressure" from the DMSO molecules causes the aggregation of DPPC molecules, giving rise to a detectable VSFG intensity.

VSFG Spectroscopy of DPPC Tail Alkyl Chains

VSFG spectra (*ssp* polarization) of DPPC monolayers in the C-H stretching region on different subphases are shown in Figure 4.3. The structural change of the DPPC monolayer is monitored from the expanded region to the condensed region. For non-deuterated DPPC, both the tail acyl chains and the phosphocholine headgroup contribute to the VSFG spectra. However, due to conformation and orientation issues, VSFG intensity from the headgroup is relatively small compared to the tail groups in spectra with the *ssp* polarization combination. In the spectrum of the condensed DPPC monolayer (45 $Å^2$/molecule) on a pure water subphase, the small shoulder at 2840 cm^{-1} is

assigned to the CH_2 SS of the acyl chains. The peak at 2872 cm^{-1} is assigned to the CH_3 SS of the acyl chains. The small shoulder at ~2905 cm^{-1} is assigned to the CH_2 Fermi resonance (FR) of the acyl chains with a contribution from the CH_2 SS of the phosphocholine headgroup. The peak at ~2942 cm^{-1} is assigned to the CH_3 FR of the acyl chains, and the shoulder at ~2956 cm^{-1} has contribution from the CH_3 asymmetric stretch (AS) of the acyl chains and the CH_2 AS of the headgroup.[74]

Similar to the PO_2^- region, no VSFG intensity is detectable with an MMA of 100 $Å^2$/molecule on a pure water subphase. When the DPPC monolayer is compressed to 98 $Å^2$/molecule, surface pressure rises slightly to ~0.5 mN/m and the VSFG intensity is clearly detected with the CH_2 SS peak at 2844 cm^{-1} and the CH_3 SS peak at 2872 cm^{-1}. The peak intensities of the CH_2 SS and the CH_3 SS in the VSFG spectra contain information about the conformation and orientation of the acyl chains. The information extracted from the VSFG spectra can be understood based on symmetry of the vibrational modes, which is related to the nature of VSFG theory. When the CH_2 groups on the acyl chains are disordered and in gauche conformations, they are VSFG active. When the chain changes from a gauche conformation to an all *trans* conformation, local centers of inversion symmetry appear on the acyl chains, making the CH_2 modes VSFG inactive. For the tail-end CH_3 group, the VSFG intensity depends largely on the orientation angle and its distribution.

The ratio of the intensities of CH_3 SS to CH_2 SS can be used as an indication of monolayer ordering.[60, 75-78] As seen in the VSFG spectrum in Figure 4.3 of a DPPC monolayer at 98 $Å^2$/molecule on water, the intensity of the CH_2 SS peak is larger compared to the CH_3 SS peak, indicating that the acyl chains have many gauche conformations. Upon compression of the DPPC monolayer to the LE-LC region, the CH_3 SS peak intensity gradually increases while the CH_2 SS peak intensity is nearly unchanged. A sharp increase of the CH_3 SS peak intensity and a decrease of the CH_2 peak intensity is observed when the DPPC monolayer is compressed to the LC phase (45 $Å^2$/molecule). The observations above reveal a disordered DPPC monolayer in the LE phase and an ordered DPPC monolayer in the LC phase on a water subphase.

On a 3 mol% DMSO subphase at low surface coverage (100 $Å^2$/molecule), only the CH_3 SS peak from DMSO at 2914 cm^{-1} is observed. Additionally, the 2914 cm^{-1} peak intensity increases with increasing DMSO surface concentration. However, the observed increase is not as large as was shown in previous VSFG studies of aqueous DMSO[79] without the presence of lipids. Interestingly, when the surface pressure rises to 94 $Å^2$/molecule, the CH_2 SS and the CH_3 SS peaks from DPPC appear but the CH_3 SS of DMSO disappears. The vanishing of the DMSO CH_3 SS intensity is also seen on 10 mol% and 20 mol% DMSO subphases when DPPC monolayers are compressed from the G to the LC phase. DPPC CH_3 SS peak intensity only appears on the 20 mol% DMSO subphase at 100 $Å^2$/molecule (in accordance with the observation in the PO_2^- region).

Condensing Effect by DMSO

To the limit of our detection, VSFG intensity from DPPC monolayers is discernable at a very low surface number density (120 $Å^2$/molecule) in both the PO_2^- and the CH regions as shown Figure 4.4. It is noteworthy to point out that in the CH region spectrum (Figure 4.4b), the DPPC CH_3 SS (2872 cm^{-1}) coexists with the DMSO CH_3 SS (2910 cm^{-1}). Yet, the DPPC CH_2 SS peak is not detectable.

Given the above discussion about the ratio of the peak intensities of the DPPC CH_3 SS and the CH_2 SS, a notable CH_3 SS peak intensity together with lack of a CH_2 SS peak indicates that the DPPC monolayer on a 20 mol% DMSO subphase is well ordered even at a very large MMA. The surface covered by DPPC is incomplete at this MMA (120 $Å^2$/molecule); therefore, we conclude that the DPPC molecules form aggregates and coexist with the DMSO molecules at the interface. Consequently, the occupied molecular area at low surface coverage by each DPPC molecule decreases by adopting ordered chain conformations (fewer gauche defects) on the 20 mol% DMSO subphase. Figure 4.5 illustrates disordered DPPC chain conformations on a pure water subphase and ordered DPPC chain conformations on the 20 mol% DMSO subphase.

Chain Orientation of DPPC in the Liquid Condensed Phase

The chain orientation of DPPC in the liquid condensed phase on different aqueous DMSO subphases was also investigated. Previous studies suggested that the inclination angle of the acyl chains may change by DMSO perturbation.[49] Polarized VSFG

spectroscopy is used here to determine the average DPPC chain tilt angle in the ordered monolayers. For a DPPC monolayer with acyl chains in an all *trans* configuration, the angular relationship between the chain axis and the terminal CH_3 orientation is known to be about 41.5 degrees.[59, 80] Therefore, to calculate the DPPC chain tilt angle in the monolayer, the orientation angle of the CH_3 group is needed. This can be obtained by VSFG measurement using the ratio of the CH_3 SS to the CH_3 AS peak intensity in *ssp* polarization spectra.[81]

To avoid the spectral interferences between the terminal CH_3 vibrational modes and other CH moieties of the DPPC molecule, chain deuterated DPPC (DPPC-*d62*) was used here to determine the terminal methyl group orientation. VSFG spectra (*ssp* polarization) of condensed DPPC-*d62* monolayers on different subphases are shown in Figure 4.6. The CD_3 SS and CD_3 AS are observed at 2071 cm^{-1} and 2218 cm^{-1} respectively. The peak at 2121 cm^{-1} is assigned to the CD_3 FR.[31] For a water subphase, the average angle of the CD_3 group calculated from the intensity ratio of the CD_3 SS and the CD_3 AS is 16.5 degrees, so the average chain tilt angle of DPPC-*d62* is about 25 degrees.[31] This result agrees well with the results obtained by previous X-ray scattering experiments which gave a value of ~27 degrees.[82]

The VSFG spectra of the condensed DPPC-*d62* on DMSO subphases are almost identical to the spectrum obtained on a pure water subphase, indicating an insignificant tilt angle change of the acyl chains upon addition of DMSO. It should be noted that the VSFG

average orientation angle calculation includes the assumption of the angular relationship between the chain and the methyl group, which is different from an X-ray scattering experiment. Our previous VSFG results suggested that the chain orientation of a DPPC monolayer on a water subphase remains nearly unchanged from the LE to the LC phase;[31] but an X-ray scattering study showed an angle decrease from 37 degrees to 29 degrees.[47] With VSFG, the existence of gauche defects in the LE phase complicates the DPPC orientation determination in the LE phase, explaining the discrepancy between the two methods.[31] However, in the work presented here, the orientation determination is of well packed DPPC molecules in the LC phase where the acyl chains are in an all *trans* configuration.

DMSO Orientation at the DPPC/Water Interface

The vanishing of the DMSO CH_3 SS peak upon a surface pressure rise (Figure 4.3) is an interesting phenomenon related to the interaction between the DPPC monolayer and the DMSO molecules. As discussed above, there are arguments about whether the DMSO molecules penetrate into the polar headgroup region or just occupy positions beneath the lipid headgroup. We observe that DMSO molecules exist in the interfacial region. The observed DMSO CH_3 SS peak at low DPPC surface coverage indicates that the DMSO molecules are not completely disordered.

To elucidate the impact of phospholipids on the DMSO molecules, a DPPA-*d62* monolayer on a 10 mol% DMSO subphase was studied and compared to a DPPC-*d62*

monolayer as shown in Figure 4.7. Since the acyl chains of the lipids are deuterated and the DMSO CH_3 SS peak is absent, only CH modes from the lipid headgroup (CH_2 modes: ~2905 cm^{-1} and ~2956 cm^{-1}) are observed for the DPPC-*d62* covered interface. However, intensity from the DMSO CH_3 SS peak remains in the VSFG spectrum of the DPPA-*d62* monolayer. The biggest difference between these two phospholipids is the headgroup charge: DPPC is zwitterionic and DPPA is negatively charged. When the phospholipid monolayer is well packed, the interfacial region is polarized by the electric field induced by the headgroup charge. Previous MD simulation showed that the DPPC molecules adopt an L-shape conformation in the LC phase, that is, on average a near-flat headgroup orientation with intermolecular charge pairing between the phosphate from one DPPC to the choline of an adjacent DPPC molecule.[83, 84] The electric field induced by the DPPC headgroup is therefore nearly parallel to the surface. The DPPA headgroup is negatively charged, and thus, the double layer (sodium counter cation) creates an electric field along the surface normal of the interface as illustrated in Figure 4.8. Therefore DMSO CH_3 SS peak intensity indicates that the polar S=O bond of the DMSO molecules at the monolayer interface is well aligned in the electric field direction. Since the rotation of CH_3 groups about the –S=O bond is allowed, assuming free rotation, the net orientation vector of the CH_3 groups of DMSO is along the –S=O bond axis. Consequently, the DMSO CH_3 orientation vector is nearly parallel and perpendicular to the surface for DPPC and DPPA monolayers, respectively. DMSO orientation in the DPPC system explains the vanishing of the DMSO peak (for C_{3v} symmetry, VSFG intensity vanishes at an orientation parallel to the surface in *ssp* and *ppp* polarization).[21] VSFG spectra with

ppp polarization also reveal lack DMSO peak intensity (data not shown). The disappearance of DMSO VSFG intensity could also be possible when interfacial DMSO molecules become disordered although this scenario is unlikely due to the presence of the headgroup-induced electric field.

It should be pointed out that the disappearance of the DMSO peak intensity occurs only after the rise of surface pressure above ~0.5 mN/m. This suggests that a relatively strong electric field is needed to significantly perturb the orientation of the DMSO molecules. Figure 4.9 reveals the disappearance of the DMSO CH_3 SS peak at 2910 cm^{-1}on the 20 mol% DMSO subphase as a function of time. This result indicates that the surface electric field is established within a few minutes during monolayer compression.

Biological Implications

DMSO interactions play an important role for enhancement of membrane permeability. Recently, MD simulations of the interaction of DMSO with a model membrane revealed that DMSO molecules induce water pore formation within the lipid bilayer.[55, 56] The water pores formed at high DMSO concentration (> 10 mol%) were transient and dynamic. From a macroscopic point of view, existence of the water pores results in an increased area per lipid, and a "floppier bilayer". In the present study, the decrease in the area occupied by each DPPC molecule on concentrated DMSO-containing subphases (condensing effect) is observed, which at first appears to be different from the MD simulation results. The pressure that is exerted by DMSO on the DPPC monolayer causes

the observed condensing behavior. However, this pressure is also the cause of the pore formation as observed by MD simulations. DMSO action on the DPPC headgroups is more likely as compared to action on the DPPC acyl chains since very few DMSO molecules reside in the hydrophobic chain region of lipids.[54] It is then plausible that DMSO acts on the DPPC headgroups to corral the lipids into surface domains. This results in an increase of the average area per lipid in an unconfined system. In a confined system such as a Langmuir trough with rigid barriers, DMSO induces condensing of the lipids. From this argument, our experimental evidence provides support for the pore formation mechanism induced by DMSO and is therefore consistent with the MD simulations. Moreover, previous permeability studies showed that the permeability enhancement induced by DMSO is concentration dependent and occurs at high concentrations (usually ~60 wt%, or 26 mol%),[39] which is also in accordance with our findings.

4.2 Conclusion

A comprehensive picture of the interactions between DMSO molecules and a DPPC monolayer is presented. The impact of DMSO on DPPC monolayers is found to be concentration dependent. When the DMSO concentration is above 10 mol%, DMSO-induced dehydration of the DPPC phosphate group is observed. The high surface pressure of a concentrated DMSO subphase (> 20 mol%) induces a condensing effect on the DPPC monolayer, which causes DPPC molecules to adopt a well ordered conformation at very large mean molecular areas. When DPPC is in the liquid condensed phase, DMSO

has an insignificant effect on the monolayer structure, suggesting that DMSO molecules are expelled from the monolayer region. Study of the interaction between DMSO and DPPC and DPPA indicates that the interfacial DMSO molecules are also perturbed by the headgroup-induced electric field and reorient. In summary, our results provide a molecular basis that accounts for the DMSO-induced enhancement of biological membrane permeability.

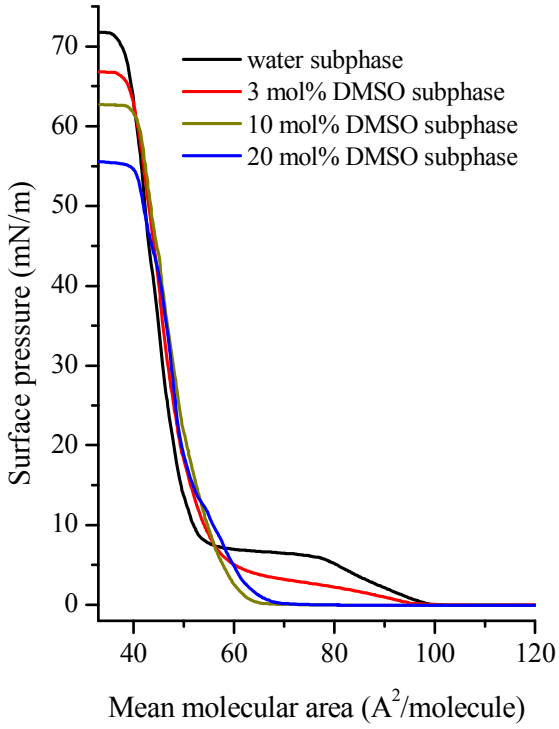

Figure 4.1. Isotherms of DPPC monolayers on different DMSO/water subphases.

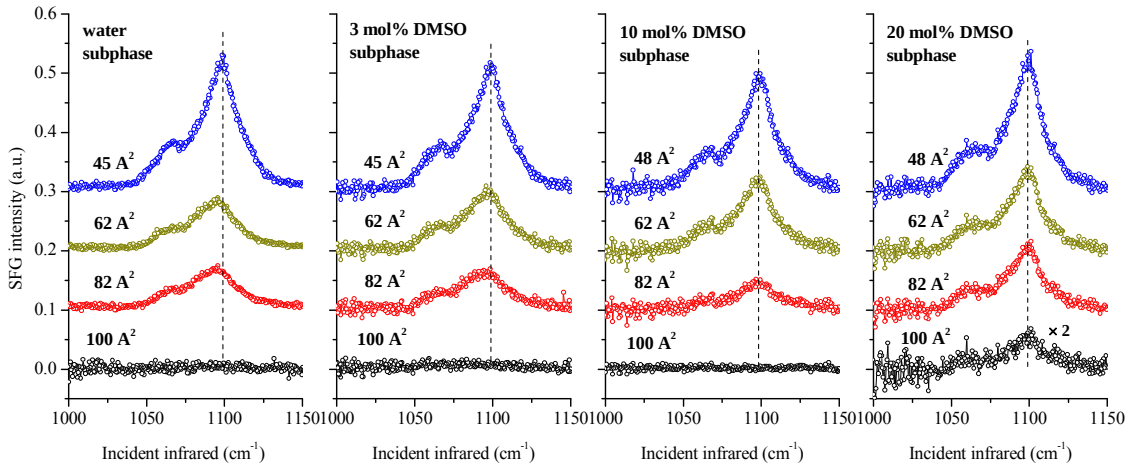

Figure 4.2. P=O region VSFG spectra of DPPC monolayers on different DMSO/water subphases at different surface coverages. From left to right, the subphases are water, 3 mol%, 10 mol% and 20 mol% DMSO respectively. The dash line shows the $-PO_2^-$ SS peak position in the liquid condensed phase. (DPPC is in the LC phase at 45 and 48 $Å^2$/molecule.)

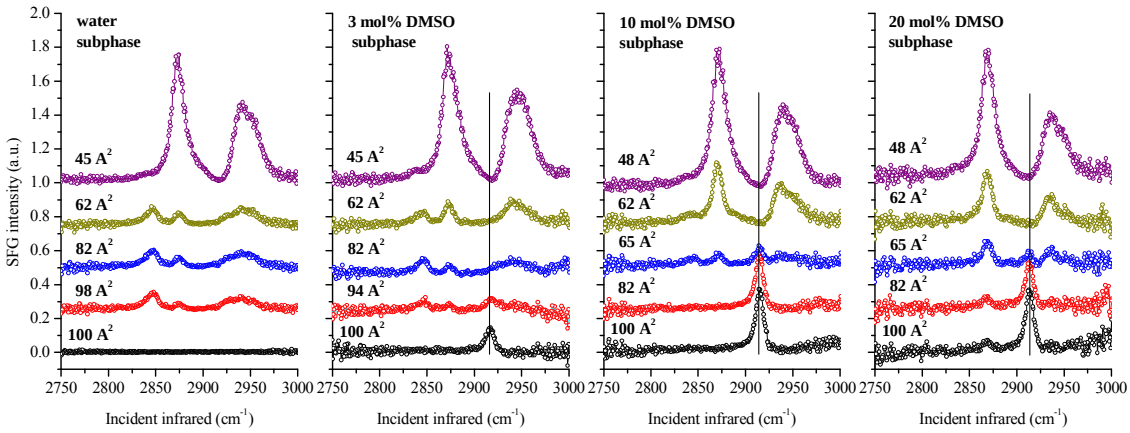

Figure 4.3. C-H stretch region VSFG spectra of DPPC on different DMSO/water subphases. From left to right, the subphases are water, 3 mol%, 10 mol% and 20 mol% DMSO respectively. The solid line shows the DMSO CH_3 SS peak position. (DPPC is in the LC phase at 45 and 48 $Å^2$/molecule.)

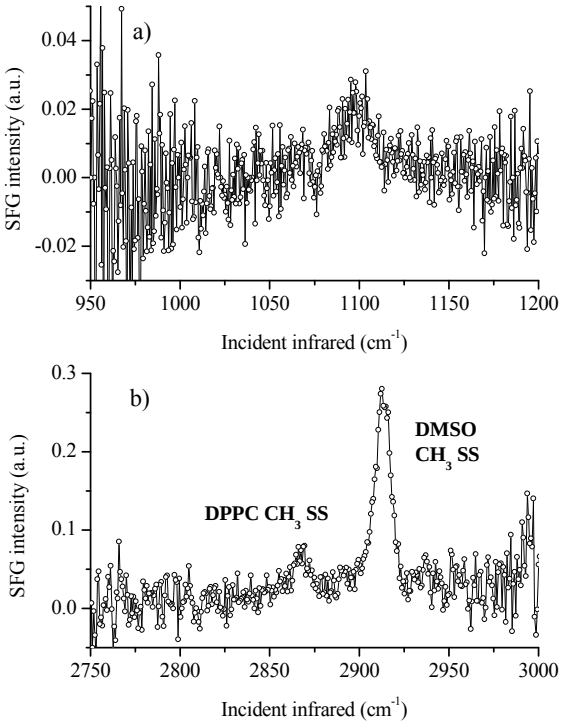

Figure 4.4. Highlight of the VSFG spectra of DPPC obtained on 20 mol% DMSO subphase at 120Å^2/molecule in a) the P=O region and b) the C-H stretch region.

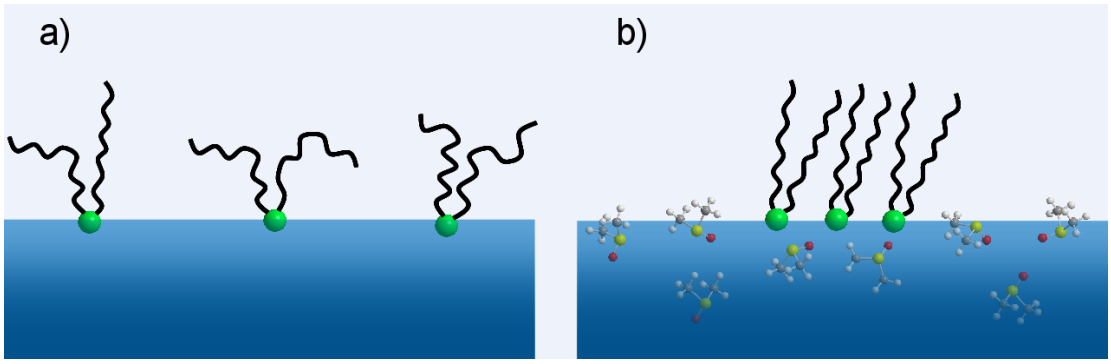

Figure 4.5. Conformation of DPPC molecules at low surface coverage (> 100 $Å^2$/molecule) on a) water subphase and b) 20 mol% DMSO subphase. The condensing effect on the DPPC monolayer induced by high concentration DMSO is illustrated.

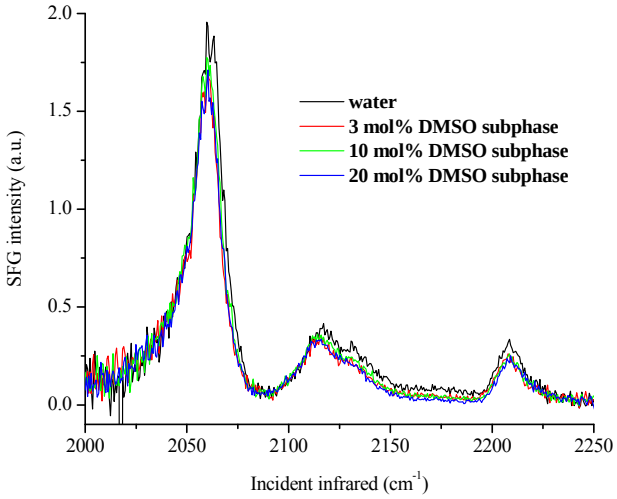

Figure 4.6. C-D stretch region VSFG spectra of condensed DPPC-*d62* monolayers on different DMSO/water subphases.

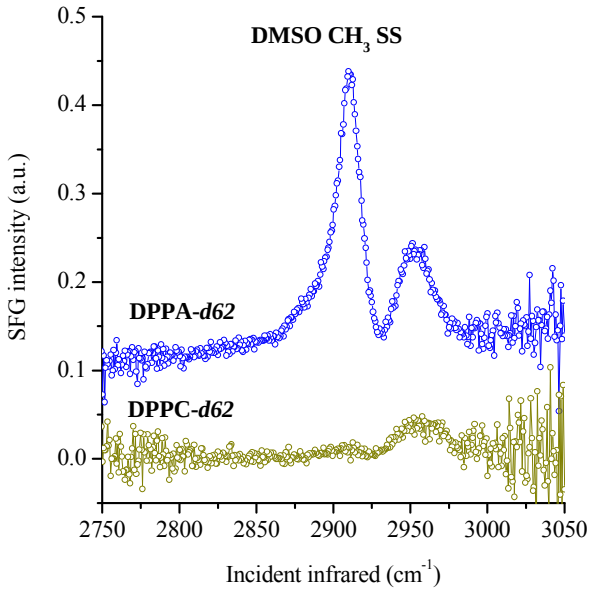

Figure 4.7. C-H stretch region VSFG spectra of LC phase DPPA-*d62* and DPPC-*d62* monolayers on 10 mol% DMSO subphase. The DMSO CH_3 SS peak is absent at the DPPC-*d62* covered interface.

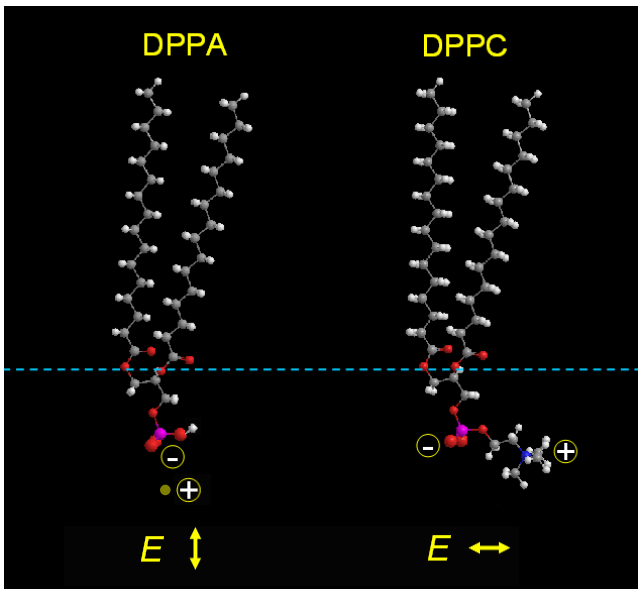

Figure 4.8. Illustration of DPPC and DPPA headgroup conformation and charge at the interface. The directions of the headgroup-induced electric fields are also shown.

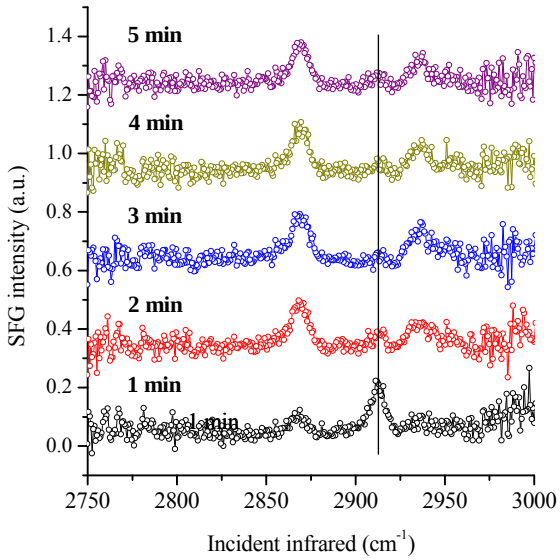

Figure 4.9. Series of C-H region VSFG spectra of DPPC obtained at the onset of the surface pressure rise on the 20 mol% DMSO subphase. The acquisition time is one minute for each spectrum. The solid line shows the DMSO CH_3 SS peak position.

Chapter 5: Permeability enhancement initiated by dimethylsulfoxide on phospholipid monolayers observed by Brewster angle microscopy

Biological membranes are not only a remarkable barrier to keep the cell intact, but they also allow exchange of necessary substances.[1, 3, 85] Molecules that can selectively increase (or decrease) the permeability of membranes are of particular interest for many practical applications such as transdermal drug delivery.[38, 55] The well-organized membrane consists of lipid bilayers with interconnected gel and liquid phase domains that result in a relatively low membrane permeability.[38] An approach to enhance membrane permeability is to perturb and temporarily disrupt the lipid domain structure with certain chemicals called penetration enhancers.[39] To be a successful penetration enhancer in a clinic trial, the agent should be able to promote skin permeability, but also be non-toxic to humans. First introduced 40 years ago, dimethyl sulfoxide (DMSO) is one of the oldest as well as the most widely used penetration enhancer.[86, 87] However, insight on how DMSO modifies lipid membrane structure and function, namely the molecular level interaction mechanism of DMSO on lipid membranes, is still under investigation.[56, 88]

Although lipid molecules show considerable structural diversity, such as sterols, fatty acids, phospholipids and glycolipids, the most important to the bilayer structure backbone

are the phospholipids.[3] The amphiphilic structure of phospholipids gives rise to their unique ability to form elegant bilayers with the long alkyl chain tailgroups congregated together as a hydrophobic center and the charged headgroups facing out to the hydrophilic environment. Phospholipid bilayers can be formed from single constituents, such as dipalmitoylphosphatidylcholine (DPPC), dipalmitoylphosphatidylethanolamine (DPPE), dipalmitoylphosphatidylglycerol (DPPG) or dipalmitoylphosphatidylserine (DPPS), or multiple components of these. Despite the fact that all phospholipids contain a negatively charged phosphate in the headgroup, properties of phospholipids vary significantly due to polar groups attached to the phosphate. For example, the headgroups of DPPC and DPPE are zwitterionic while the headgroups of DPPG and DPPS are net negatively charged (see Figure 3.1). This difference in phospholipid headgroup results in different intermolecular interactions, leading to different packing ability.[4, 5] Due to the complexity of the membrane structure, simpler models such as lipid vesicles, lipid bilayers, and Langmuir monolayers are often studied.[6] Among which, Langmuir monolayers formed at the air/water interface provide the most control, for example a continuously well defined molecular density, surface pressure, and phase.[7, 8]

The interaction of DMSO with phospholipid membranes has been previously studied by various experimental and theoretical approaches, such as differential scanning calorimetry (DSC),[43-45] X-ray diffraction (XRD),[43, 44, 46, 47] small-angle neutron diffraction,[48, 49] nuclear magnetic resonance (NMR),[50] infrared (IR) spectroscopy[45] and molecular dynamics (MD) simulations.[51-55] The influence of DMSO on membranes was

shown to be concentration-dependent.[46] In a water/DMSO mixed solvent the main phase transition temperature of DPPC vesicles increases with DMSO concentration, revealing a stabilization effect by DMSO on the vesicle gel phase.[43] X-ray and neutron diffraction studies revealed that the repeat distance between the bilayers in multilamellar DPPC vesicles decreased with DMSO concentration. This decrease in intermembrane distance inside the vesicles was mainly attributed to the removal of free water molecules in the intermembrane spaces.[46, 49] In addition, Sum et al. showed through MD simulations that DMSO penetrates readily into the polar headgroup region of a bilayer, but only a few DMSO molecules actually cross the bilayer.[54] Recently, Anwar and coworkers reported that DMSO induces water pore formation within a DPPC bilayer by MD simulation, which presented an interesting mechanism for transdermal permeability enhancement.[55, 56] In our recent work the interaction between a DPPC monolayer and DMSO was investigated using vibrational sum frequency generation (VSFG). Results suggested that DPPC monolayers adopt a more condensed packing state at high DMSO concentration, giving room for channel formation inside a membrane.[88]

Brewster angle microscopy (BAM) is a surface sensitive optical technique suitable for "in-situ" studies of phospholipid monolayers.[89, 90] Through coupling with a Langmuir trough, this method is capable of visualizing characteristic domain structures of the monolayer in various phases. The aim of this work is to employ BAM to study the impact of DMSO on the monolayer morphology of various phospholipids, including DPPC,

DPPE, DPPG and DPPS, through which a global view of the interaction between DMSO and membrane lipids is obtained.

5.1 Results and Discussion

DPPC monolayer

The BAM images of phospholipids on water and 0.1 *x* DMSO subphases are shown together to visualize the impact of DMSO on the morphology of the phospholipid domains. Upon addition of DMSO, the refractive index of the interface increases to 1.37 on 0.1 *x* DMSO from 1.33 on water,[68] which corresponds to a Brewster angle change to 53.8° from 53.1°. The contrast in BAM images is based on the difference of refractive index of monolayer domains and the subphase. For the same phospholipid monolayer with full surface coverage, the contrast observed on a water subphase is more than 2 times that of the contrast observed on a 0.1 *x* DMSO subphase, which suggests the refractive index of the monolayer domains is greater than that of water. Moreover, no contrast (homogenously dark image) is observed for phospholipids spread on a 0.2 *x* DMSO subphase (image not shown). This indicates that the refractive index of monolayer domains is equal to that of the subphase, which is 1.40. Therefore, to compare the images taken on water and 0.1 *x* DMSO subphases, the contrast (dark to bright) scale is set to 100 counts on water and 50 counts on 0.1 *x* DMSO subphases. In addition, because the surface may not be homogeneous and the film domains move laterally on the aqueous surface, the images shown are not able to be exactly reproduced. Only typical

images which represent the surface characteristics are therefore shown in the following results.

The surface pressure-area isotherms of a DPPC monolayer on water and 0.1 *x* DMSO subphases are shown in Figure 5.1. DPPC exhibits interesting phase transition properties on water at the room temperature. Several distinct phases, the gas-liquid expanded coexistence region (G-LE, > 100 Å^2), the liquid expanded (LE, 75-100 Å^2) phase, the liquid expanded-liquid condensed coexistence region (LE-LC, ~ 55-75 Å^2), and the liquid condensed (LC, < 55 Å^2) phase, and the collapse phase (not shown, < 40 Å^2) are observed (black square trace).[31] As the DPPC monolayer is compressed to the LE phase, the surface pressure (difference between the surface tension of the subphase and the monolayer covered surface) begins to rise. The LE-LC phase transition plateau occurs at about 5 to 6 mN/m, which is considered to be a first order phase transition.[91] However, the transition plateau is not perfectly horizontal, which seems to be inconsistent with a first order transition. Previous studies on DPPC monolayers show that this nonzero transition slope can be caused by two reasons:[91, 92] 1) impurities in the monolayer, or 2) the compression speed is not slow enough for the phase transition to occur in equilibrium. The compression rate used in the present study was 5 mm/min for each barrier, which corresponds to a rate of 8.5 (Å^2/molecule)/min or higher. This is higher than the sufficiently slow compression rate of 0.1 (Å^2/molecule)/min reported previously. After entering the LC phase the surface pressure increases abruptly with compression, indicating a more rigid packing state of DPPC molecules.

The corresponding BAM images of DPPC in each phase on water and 0.1 *x* DMSO subphases are also shown in Figure 5.1. Each set of images (A, B, C and D, left image is on water subphase while the right image is on 0.1 *x* DMSO subphase) represents the typical morphology of a DPPC monolayer at the indicated mean molecular area (MMA). At MMA of 140 Å^2/molecule (Figure 5.1A) the image is completely dark, which indicates a homogenous G-LE coexistence region. A similarly dark image is observed for the LE phase at the surface pressure of 4 mN/m (image not shown), revealing that the LE phase is also homogenous. This observation is similar to the BAM images reported by Minones et al.[5] However, they observed an average reflectivity increase from the G-LE region to the LE phase, despite the same homogenous feature of these two regions. The brightness of the images is monitored to be the same for these two regions in the present study. Previous vibrational sum frequency generation (VSFG) studies completed in our group[31] show that VSFG spectra intensities can be detected when entering the LE phase (surface pressure > 0.1 mN/m). Because VSFG is sensitive to ordering of molecules, it can therefore be concluded that DPPC molecules are beginning to order at the onset of the LE phase, although the G-LE coexistence phase is dominated by disorder. The homogenous nature of the LE phase image suggests that the LE phase is still monomer rich although molecules are becoming more ordered. Therefore, a significant change in surface reflectivity is not expected.

At the surface pressure of 4.5 mN/m (MMA = 75 Å^2/molecule), the kink point between LE phase and LE-LC transition region is reached. Small, circular domains of DPPC

appear instantaneously (Figure 5.1B) as the phase transition commences. These LC phase domains are bright in contrast (counts > 50) with domain sizes of around 10 μm in diameter (nonuniform focus somewhat distorts the size of the domain in the outer edges of the image). The large increase in contrast from the dark LE phase (counts < 15) to the bright LC phase reveals the different packing density in these phases. LC domains are cluster rich and less compressible, hence resulting in a greater refractive index than the LE phase. In the phase transition region, the circular LC domains grow in size to 30 ~ 40 μm, and form irregular lobe shapes (Figure 5.1C). This kind of shape is typically observed in fluorescence microscopy and is considered to be caused by the chirality of the DPPC molecules. Once the LE-LC transition region is exceeded, the domains merge together with an abrupt increase in surface pressure, and the lobe shape slowly disappears. At the end of compression (Figure 5.1D), the DPPC monolayer becomes homogenous again, but with much greater brightness (counts > 100).

When DPPC is spread on a 0.1 *x* DMSO subphase, the spreading of DPPC at the surface is slower than on water. The surface pressure-area isotherm shows significant differences from that of the water subphase images as seen in Figure 5.1. The LE-LC transition plateau nearly disappears and the DPPC monolayer undergoes a direct G-LC phase transition as being compressed. However, the DPPC monolayer exhibits similar LC phase morphology on both water and 0.1 *x* DMSO subphases as observed in Figure 5.1D, which indicates the exclusion of DMSO molecules out of the condensed monolayer. This observation is also in accordance with previous VSFG[88] and NMR studies.[50]

The BAM images shown in Figure 5.1A, B, C and D visualize the change in the isotherms. Excessively large domain structures and phase boundaries are formed on 0.1 *x* DMSO subphase at MMA = 140 Å^2/molecule (Figure 5.1A) as compared to the all dark gaseous state on water. The brightness of the domains reveals that the domains are predominately in the LC phase. In between the large coalesced domain structures, small circular DPPC domains are also observable. The existence of LC domains indicates the presence of the G-LC coexistence state at this large MMA. Our recent VSFG study of a DPPC monolayer on DMSO containing subphases also pointed to the existence of ordered domains at the MMA of 120 Å^2/molecule.[88] The formation of LC domains at such large MMA is attributed to the condensing effect of DMSO on DPPC monolayer. That is, due to the amphiphilic nature of the DMSO molecule, DMSO molecules show a preference for the aqueous surface. The DMSO molecules occupy large surface regions and exert pressure on the DPPC molecules forcing them to congregate. As the concentration of DMSO exceeds 0.1 *x*, the surface pressure of the subphase alone is 10 mN/m,[68] which is greater than the DPPC LE-LC transition surface pressure for DPPC on water. Therefore, the DPPC monolayer is condensed by surface DMSO molecules and the LC domains are formed on the 0.1 *x* DMSO subphase no matter what the MMA is. These LC domains coexist with the gaseous phase DPPC at large MMA.

As the DPPC monolayer is compressed on the 0.1 *x* DMSO subphase, the LC domains coalesce and gradually merge together (Figure 5.1B, C). Similar homogeneous condensed phase DPPC monolayers are observed on both water and 0.1 *x* DMSO subphases (Figure

5.1D). In addition, some collapse structures such as stripes and dots are also visible when the surface pressure rises above 50 mN/m.

DPPE monolayer

Figure 5.2 shows the surface pressure-area isotherms of a DPPE monolayer on water and 0.1 *x* DMSO subphases. The difference between DPPE and DPPC molecules is that the ammonium group in DPPE is fully methylated to the *N,N,N*-methyl amine group. Unlike the methyl groups on the DPPC headgroup, the hydrogens on the DPPE ammonium group can form hydrogen bonds with neighboring DPPE headgroups. This is thought to account for the more stable DPPE monolayer than the DPPC monolayer, which is evidenced by the higher main transition (gel phase to liquid crystalline phase) temperature of DPPE bilayers (63 °C) than DPPC bilayers (41 °C).[93] Therefore the DPPE molecules more easily interact with each other to form domains. In the surface pressure-area isotherm on water, the DPPE monolayer goes directly through the G-LC coexistence phase to the LC phase and no LE phase is observed. The isotherm on the 0.1 *x* DMSO subphase shows the same character, which suggests that the DMSO molecules have little effect on the condensed DPPE monolayer.

The BAM images of DPPE monolayer at different MMAs are shown in Figure 5.2A, B, C and D. On the water subphase, a pure gaseous phase (dark contrast) is observed when the MMA is greater than 170 Å^2/molecule as shown in Figure 5.2A. At around 170 Å^2/molecule, irregular LC domain structures are formed (Figure 5.2B) although the

surface pressure is still nearly zero. This MMA should be attributed to the G-LC coexistence region. However, on the 0.1 *x* DMSO subphase the large LC domain structures of the DPPE monolayer are clearly observable (Figure 5.2A) at the MMA where only pure gaseous phase is seen on water. This observation suggests that DMSO molecules on the aqueous surface cause the condensation of DPPE molecules to form condensed phase domain structures, which is similar to the effect on the DPPC monolayer.

When the DPPE monolayer on 0.1 *x* DMSO is compressed to the LC phase, a homogeneously condensed monolayer is gradually formed. Finally the bright collapse state is observed in Figure 5.2C, and the 3 dimensional stripe structures are seen in Figure 5.2D.

DPPG monolayer

The surface pressure-area isotherms of net negatively charged DPPG monolayers on water and 0.1 *x* DMSO subphases are shown in Figure 5.3. The shape of the isotherms is similar to that of the DPPE monolayers. As the DPPG monolayer is compressed, only a G-LC coexistence region and the LC phase are observed. The MMA of the onset of the DPPG LC phase is between 50 to 60 $Å^2$/molecule, which is about the same as the DPPC and DPPE monolayers.[5]

As seen from the BAM images of the DPPG monolayer on a water subphase, irregular branch shaped LC domains exist on the water surface (Figure 5.3A and B). These LC domains interconnect with each other as the monolayer is compressed (Figure 5.3C) and a homogeneous LC phase monolayer is formed when the surface pressure is greater than 40 mN/m (Figure 5.3D). On the 0.1 *x* DMSO subphase, the morphology of the LC domains in the G-LC coexistence region is markedly different despite the similar isotherms. Large domain structures of interconnected islands hundreds of μm in diameter are observed in Figure 5.3A. These LC phase islands appear porous as the dark gaseous phase coexists with the bright domain structures. The larger size of the LC domains observed on the 0.1 *x* DMSO subphase as compared to water suggests that the DPPG domains are forced to grow and merge together on the 0.1 *x* DMSO subphase. This is in accordance with the condensing effect of DMSO on the zwitterionic DPPC and DPPE monolayers although DPPG is a negatively charged lipid.

DPPS monolayer

DPPS is another important negatively charged phospholipid. It has three charged centers on the headgroup at physiological pH: the negatively charged phosphate and carboxylic groups, and the positively charged ammonium group.[94] According to previous study, the isoelectric point of DPPS is at a pH of 1.5.[95] At this pH, the carboxylic group of DPPS is completely protonated so that the DPPS molecule becomes zwitterionic. The main transition temperature of a DPPS bilayer is found to be 51 °C, which is higher than DPPG (40 °C).[96] The intermolecular attraction between the DPPS carboxylic group and the

ammonium group are thought to be the cause for the assembly of DPPS molecules at zero surface pressure,[5] resulting in the G-LC coexistence region in the isotherms.

The surface pressure-area isotherms of a DPPS monolayer on water and 0.1 *x* DMSO subphases are similar to the DPPG monolayer as shown in Figure 5.4. In both DPPS isotherms on different subphases, only the G-LC coexistence and LC phases are observed. Changing from water to 0.1 *x* DMSO in the subphase shows insignificant impact on the isotherms.

However, the changes are observed for the DPPS monolayer on different subphases as revealed in the corresponding BAM images in Figure 5.4. Although the morphology of the LC domains is somewhat similar on both subphases, the area covered by the domains is greater on the 0.1 *x* DMSO subphase. In addition, some very bright dots are clearly seen in the interior of the DPPS domains on the 0.1 *x* DMSO subphase, and attributed to collapsed DPPS three dimensional structures. Therefore it can also be concluded that the DMSO molecules cause condensation of the DPPS monolayer.

The four phospholipids studied here account for the major components of biological membranes. The observed condensing effect by DMSO on these phospholipids has implication for understanding the molecular level details of the enhanced permeability of biological membranes. Previous MD simulations of a DPPC bilayer in a DMSO containing subphase suggests that transient water pores could be formed inside the DPPC

bilayer, which then enhances the permeability of the membrane.[55] This effect is a result of the condensing effect of DMSO molecules on the phospholipid monolayers. When the DMSO molecules interact with the phospholipid membranes, DMSO molecules squeeze aside the phospholipids, which cause them to form tightly packed domain structures as well as causing the membrane to expand if the membrane surface area is unconfined. In addition, the miscibility of DMSO with water and its powerful solvation of many substances make the formed pores a transportation corridor across the membrane. As shown in this research, the DMSO-phospholipid interaction is strong and affects phospholipids with headgroups of different chemical properties.

5.2 Conclusions

In-situ Brewster angle microscopy (BAM) together with surface pressure-area isotherm measurement are used to investigate the condensing effect of DMSO molecules on different phospholipid monolayers. It is found that on the 0.1 *x* DMSO subphase, phospholipids form large condensed domain structures readily. When the phospholipid monolayers are compressed to high surface pressures over 40 mN/m, DMSO molecules are squeezed out of the monolayers. The observed condensing effect of DMSO molecules on phospholipids physically changes the morphology of the film. Moreover, DMSO affects phospholipids with different chemical substituents. This physical interaction between DMSO molecules and phospholipids accounts for the enhanced permeability of biological membranes induced by DMSO molecules.

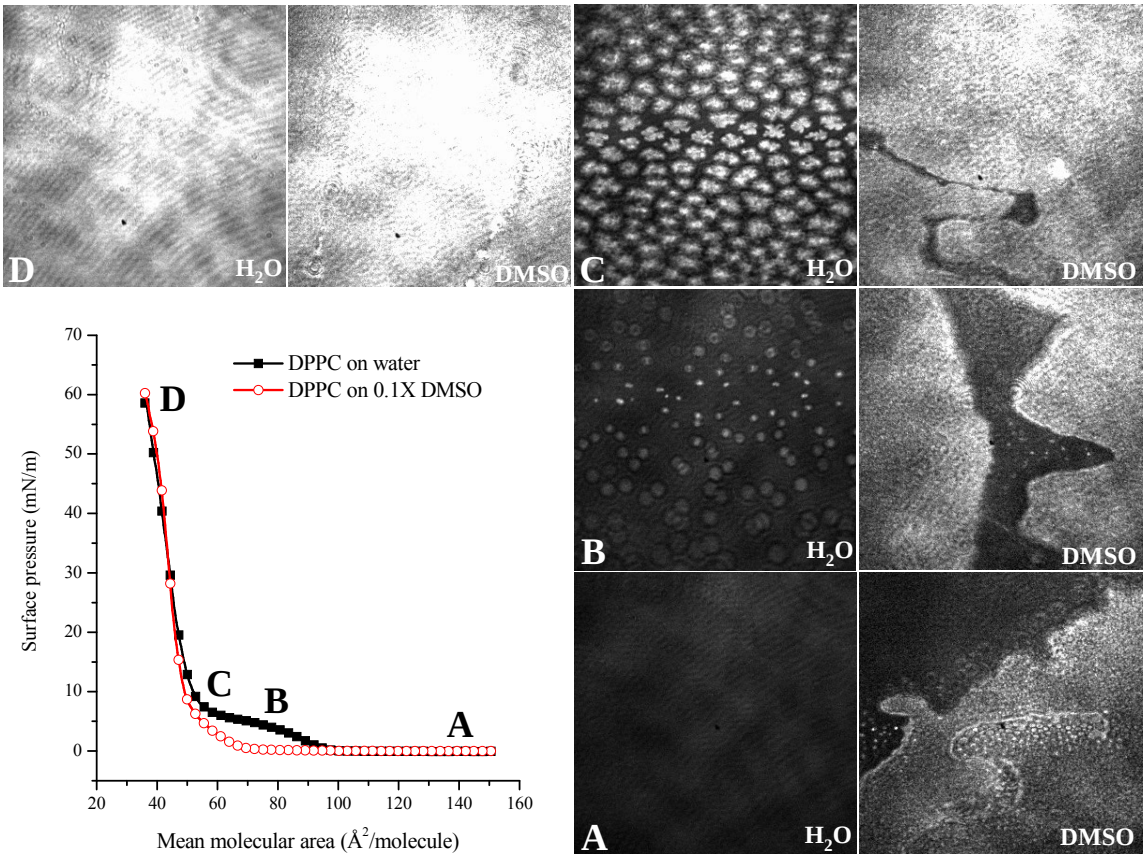

Figure 5.1. Surface pressure-area isotherms of DPPC monolayer on water and 0.1 *x* (mole fraction) DMSO subphases at 22 °C. The BAM images of corresponding points on isotherms are shown in sets of two: A, B, C and D. For each set of BAM images, the left image is on water subphase while the right image is on the 0.1 *x* DMSO subphase. The image scale is 350 μm ×350 μm.

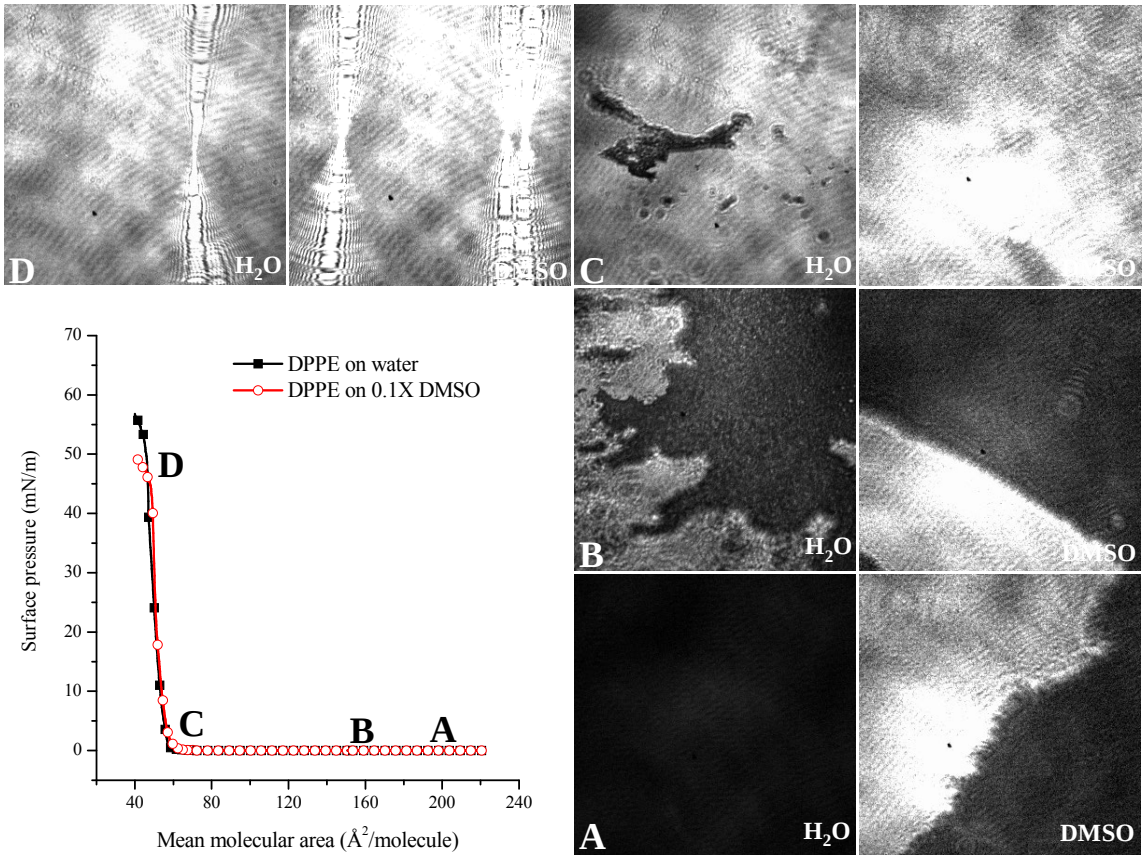

Figure 5.2. Surface pressure-area isotherms of DPPE monolayer on water and 0.1 *x* DMSO subphases at 22 °C. The BAM images of corresponding points on isotherms are shown in sets of two: A, B, C and D. For each set of BAM images, the left image is on water subphase while the right image is on the 0.1 *x* DMSO subphase. The image scale is 350 μm ×350 μm.

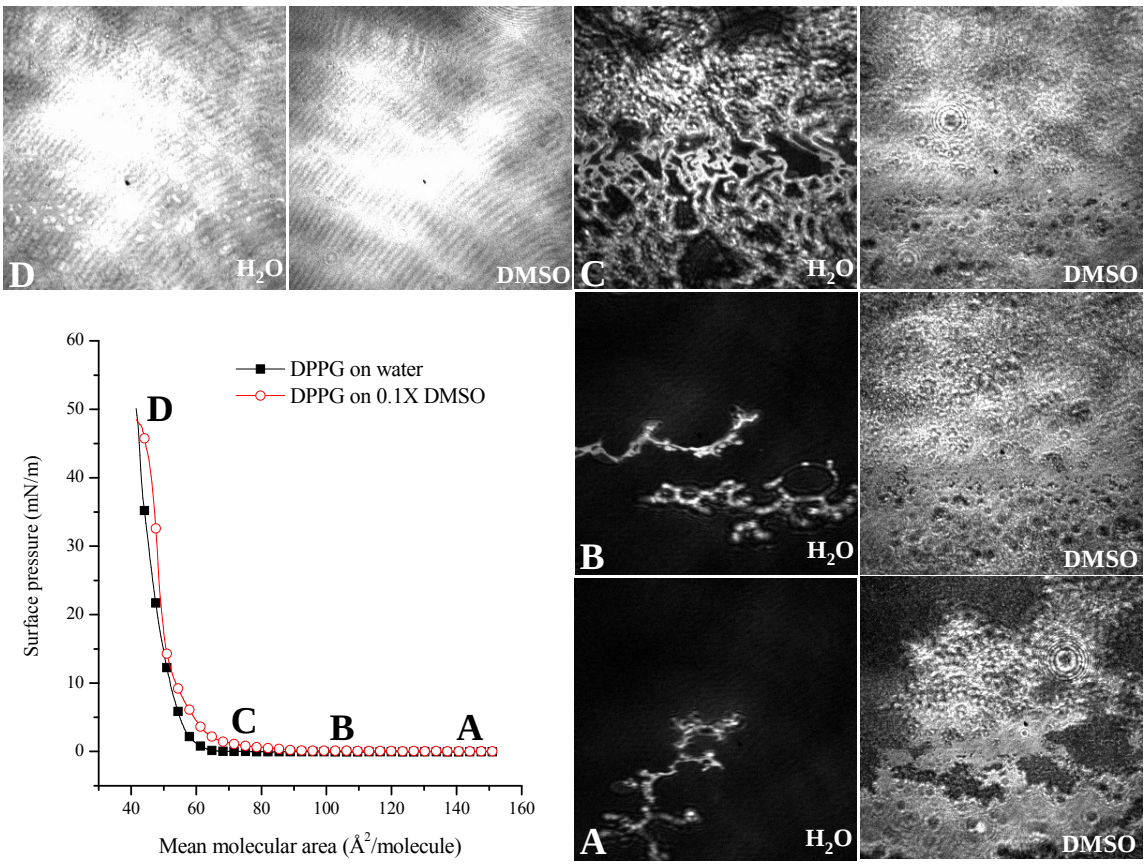

Figure 5.3. Surface pressure-area isotherms of DPPG monolayer on water and 0.1 *x* DMSO subphases at 22 °C. The BAM images of corresponding points on isotherms are shown in sets of two: A, B, C and D. For each set of BAM images, the left image is on water subphase while the right image is on the 0.1 *x* DMSO subphase. The image scale is 350 μm ×350 μm.

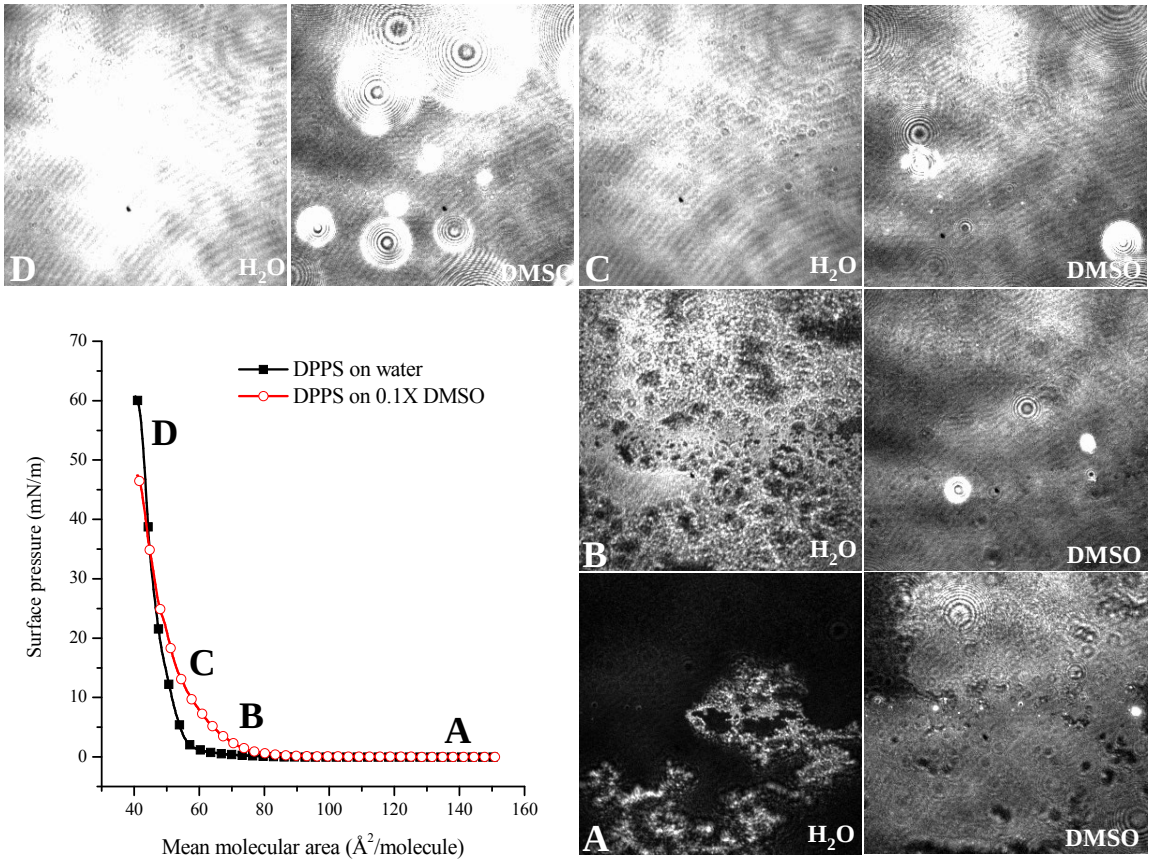

Figure 5.4. Surface pressure-area isotherms of DPPS monolayer on water and 0.1 *x* DMSO subphases at 22 °C. The BAM images of corresponding points on isotherms are shown in sets of two: A, B, C and D. For each set of BAM images, the left image is on water subphase while the right image is on the 0.1 *x* DMSO subphase. The image scale is 350 μm ×350 μm.

Chapter 6: Dangling OD Confined in a Langmuir Monolayer

(The work in this chapter is primarily done by Dr. Gang Ma.)

Waters in confining geometries exist in many physical, chemical, and biological processes and play critical roles in these processes.[97, 98] Protein folding, biological membrane formation, lung surfactant function, catalysis, and heterogeneous aerosol processing are just a few examples involving confined water. A detailed understanding of confined water will not only improve our current knowledge about water itself, but also lead to significant advances in our understanding of the structure and process that confined water is associated with. For instance, recent investigations have demonstrated that adding a water-mediated interaction to an established Hamiltonian can significantly improve protein structure prediction.[99, 100] Studies on interfacial water structure of sea salt solutions have revealed that halides can be present in the interfacial water layer, a seminal finding that has a direct impact on heterogeneous reaction modeling in atmospheric aerosol chemistry.[101, 102] In this report, we present our recent studies on a unique type of water bond, the dangling bond of surface water, confined in a two-dimensional environment, a Langmuir monolayer. D_2O was utilized as a proxy for H_2O.

Dangling bonds of water are observed at air/water,[103] air/ice,[104, 105] and water/hydrophobic interfaces,[106, 107] and at cluster surfaces.[108] They reside at the utmost surface layer, and are sensitive to environmental perturbations of surface reaction and adsorption. Their existence is also characteristic of water structure observed on extended hydrophobic surfaces,[106, 107] thus relevant to hydrophobicity-induced drying.[109]

A Langmuir monolayer is a monomolecular insoluble film spread onto a liquid surface.[110, 111] It is commonly formed with amphiphilic molecules such as lipids on an aqueous surface. The amphiphilic molecule has two distinct moieties, a hydrophobic nonpolar tail and a hydrophilic polar head. The Langmuir monolayer is where hydrophobicity and hydrophilicity meet. In this study, we use vibrational sum frequency generation (VSFG) spectroscopy to investigate how dangling bonds of water (i.e. the dangling OD of D_2O) respond to the presence of a Langmuir monolayer.

6.1 Results and Discussion

The VSFG spectrum of the pure (neat) D_2O surface in the dangling OD stretching region is shown in Figure 6.1A. The dangling OD stretching peak is located at 2735 cm^{-1}. The left-hand portion of the VSFG spectrum is from the hydrogen-bonded OD stretch. Water forms a three-dimensional hydrogen-bonding network in the bulk. While, at the interface, a fraction of the surface water molecules have only one of their two hydrogens hydrogen-bonded to an adjacent water molecule.[103] The non-hydrogen-bonded OH is the dangling OH (free OH), and its OH stretching mode arises at 3700 cm^{-1} in the VSFG spectrum of

H_2O. For D_2O, the isotope effect shifts the frequency to 2735 cm^{-1}. In this study we explore when a Langmuir monolayer covers the D_2O surface. What happens to the dangling OD? The first subject of investigation is the chain-perdeuterated dipalmitoylphosphatidylcholine (*d62*-DPPC) Langmuir monolayer. The chain-perdeuterated DPPC was used to avoid spectral overlap in the 2600 cm^{-1} to 2800 cm^{-1} region.

Figures 6.1B and 6.1C show a series of VSFG spectra in the dangling OD region obtained under different DPPC surface coverages. Here surface pressure is used to indicate surface coverage. Surface pressure is the difference between the surface tension of water and the surface tension of the monolayer. Thus, higher surface pressure corresponds to higher DPPC surface coverage. It is clear from Figures 6.1B and 6.1C that the presence of DPPC causes dramatic spectral changes of the dangling OD band. When DPPC adsorbs at the air/D_2O interface, its hydrophilic head hydrates by forming hydrogen bonds with interfacial waters. This hydration process is expected to consume dangling ODs. As shown in Figure 6.1B, at 0.5 mN/m, the dangling OD indeed decreases its intensity, while its frequency remains constant (refer to the blue curve). Following this trend, one might expect the dangling OD band to eventually vanish if the DPPC surface coverage is increased. However, the 1 mN/m spectrum (green curve) in Figure 6.1B demonstrates that the interfacial dangling OD has a far more complicated behavior than one might expect.

By further increasing DPPC surface coverage to 1 mN/m (Figure 6.1B), the dangling OD peak does not further decrease its intensity, rather, it red-shifts to ~2720 cm^{-1}. In addition, a shoulder grows between 2650 cm^{-1} and 2710 cm^{-1}. With further increasing surface pressure (3, 8 and 42 mN/m; Figure 6.1C), this shoulder continues to grow into a broad peak centered at ~2700 cm^{-1} at a surface pressure of 42 mN/m. At 42 mN/m, the D_2O surface is covered by the DPPC molecules at the maximum surface number density. Yet, we still observe the dangling OD peak. These structural features have not been previously observed.

To understand the spectral variations shown in Figure 6.1, three fundamental questions are addressed. What is the cause of the frequency red-shift? How is the spectral structure (i.e. asymmetric band broadening) explained? How can the dangling OD stretch exist when the D_2O surface is fully covered by DPPC?

The frequency red-shift no doubt indicates a perturbation imposed by DPPC molecules on the dangling OD. The environmental perturbation can be indirect or direct. An indirect perturbation would arise from perturbation through the hydrogen bonded OD that then intramolecularly couples to the dangling OD. The intramolecular coupling can red-shift the dangling OD stretch. This may occur if DPPC can strengthen the hydrogen-bonding network through head group hydration. Direct perturbation would be due to the direct interaction between the DPPC molecule and the dangling OD. This effect is intermolecular.

Previous vibrational studies on water provide a resource for elucidating whether an indirect or direct perturbation is the dominating factor to cause the observed frequency red-shift. A free H_2O monomer has two stretching bands in its vibrational spectrum, the asymmetric stretch (HOH-*as*) and the symmetric stretch (HOH-*ss*). When one OH becomes hydrogen bonded while the other remains free, the HOH-*as* and HOH-*ss* no longer exist due to a decoupling. Two new bands appear. The hydrogen-bonded OH stretch will appear in the low frequency region, below 3500 cm^{-1} (below 2600 cm^{-1} for D_2O), while the dangling OH stretch appears at ~3700 cm^{-1}.[108] Though decoupled, the dangling OH stretch can still be affected by the hydrogen-bonded OH since the decoupling is not absolutely complete.[112, 113] Therefore, there is a possibility that the frequency red-shift observed in Figure 6.1 is due to the hydrogen-bonding network variation induced by the DPPC hydration, instead of a direct intermolecular interaction between DPPC and the dangling OD bond. However, in the studies of benzene-$(H_2O)_n$ clusters (n=2-7) performed by Pribble et al using resonant ion-dip infrared spectroscopy,[108] when the cluster size varied from 2 to 7, the hydrogen-bonded OH stretching modes changed significantly, but the free OH stretch was found virtually unchanged, with 3722 cm^{-1} for $(H_2O)_2$, with 3716 cm^{-1} for $(H_2O)_3$, and with 3713 cm^{-1} for $(H_2O)_7$. This study suggests that the coupling between the two OHs is not strong. A recent quantum-chemical calculation on water clusters with size varying from $(H_2O)_6$ to $(H_2O)_{30}$ demonstrated that the dangling OH stretch is negligibly affected by the hydrogen-bonding network, once again supporting that the coupling between the two ODs in the dangling water is weak.[114] However, these are cluster studies, and one might

argue that the bonding environment is very different relative to the surface of bulk water. Yet, a VSFG study on the surface of water and ice showed that the free OH stretch is located at the same location, 3700 cm^{-1}, even though the water and ice hydrogen-bonded OH stretching mode frequencies and intensities differ significantly.[105] The strengthening of the hydrogen bonded surface water molecules in ice would have red-shifted the free OH peak as compared with that of liquid water if the coupling of the two OHs were strong. Yet, this is not the case. A VSFG study on aqueous acid surfaces showed that even adding acid (HCl, HBr, HI) significantly perturbs the hydrogen-bonded network of surface water; yet, the free OH stretch position remains unchanged at 3700 cm^{-1}.[115] Furthermore, a VSFG study on H_2O and HOD at CCl_4/water interfaces showed that H_2O and HOD gave similar free OH stretching frequencies, 3669 cm^{-1} for H_2O, and 3667 cm^{-1} for HOD.[116] Clearly, coupling between the two ODs is not the dominant cause for the more than 15 cm^{-1} and up to 35 cm^{-1} red-shift observed for the dangling OD bonds in Figure 6.1. Therefore, an indirect perturbation is ruled out.

With respect to the direct perturbation, *d62*-DPPC has several moieties that can be involved including the methylenes in the tail groups and the C-O, C=O, PO_4^-, and $N(CH_3)_3^+$ in the head group. If the dangling OD directly interacts with the oxygen from the C=O, the C-O, or the PO_4^-, a hydrogen bond will form and the OD stretch will red-shift to below 2600 cm^{-1} into the hydrogen-bonded region. The VSFG spectra in Figure 6.1 only show a 15-35 cm^{-1} shift. Thus, an OD – O interaction is easily ruled out. The choline portion of the head group ($N(CH_3)_3^+$) will not form a hydrogen bond with water.

It is also unlikely that the positive charge will interact with the oxygen of the dangling OD because this oxygen prefers bonding with another deuterium from another D_2O through a hydrogen bond. Therefore, quite clearly, the most likely moieties of DPPC that can be involved in a direct perturbation are the CD_2 groups in the hydrocarbon tails. A previous computer simulation on a dilignoceroylphosphatidylcholine monolayer in the condensed phase and an FTIR study on dimyristoylphosphatidylcholine in gel and liquid-crystalline phases support that water penetrates into the hydrophobic tail region.[117, 118] Thus, a direct interaction between the dangling OD and the tail group is spatially feasible. CD_2 is relatively nonpolar, and water is polar. Previous studies by Rowland et al have shown that the interaction between water and a nonpolar molecule is strong enough to cause the dangling OH (or OD) stretch to have a relatively large frequency red-shift in its vibrational spectrum.[104] These researchers performed infrared studies on an ice surface and found that adsorption of H_2, Ar, N_2, and CH_4 red-shifts the dangling OD stretch by as much as ~30 cm^{-1} (in the case of D_2O-CH_4). Scatena et al investigated the dangling OH stretch at the H_2O/CCl_4 and H_2O/hexane interfaces with VSFG spectroscopy.[116] It was found that the dangling OH stretch at 3700 cm^{-1} observed at the air/H_2O interface red-shifted to 3669 cm^{-1} when water is in contact with the nonpolar CCl_4 or hexane solvents at liquid/liquid interfaces. These previous results are consistent with the assertion that the observed frequency red-shift is due to a direct perturbation imposed by the hydrocarbon tail on the dangling OD.

The interaction between water and CD_2 groups is van der Waals by nature. When a polar molecule interacts with a nonpolar molecule, the dispersion force (induced-dipole – induced-dipole) and the induction force (dipole-induced – dipole interaction) contribute to the total van der Waals interaction energy, though the dispersion force usually plays the dominant role.[119] For example, for the CH_4-H_2O complex, the dispersion force contributes 87% of the total van der Waals energy and the induction force contributes the rest.[119] The attraction between a hydrocarbon tail and water is considered to be stronger than the attraction between hydrocarbon tails.[120]

Van der Waals interactions, induction and dispersion forces, are temperature-independent.[119] Therefore, the perturbed dangling OD frequency should be insensitive to temperature. Indeed, lowering the temperature of a *d62*-DPPC monolayer on D_2O does not significantly perturb the dangling OD frequency as shown in Figure 6.2 though the high frequency tail of the hydrogen-bonded region affects the shape of the dangling OD slightly. As a comparison, when the temperature of neat D_2O is lowered to 284 K, the dangling OD peak is almost identical to the room temperature dangling OD spectrum, also shown in Figure 6.2. The low-temperature VSFG comparison study in Figure 6.2 further confirms that the red-shifted OD peaks are correctly assigned to the perturbed dangling OD bonds.

Since the observed frequency red-shift is interpreted to be due to the perturbation imposed by the hydrocarbon tail group, this phenomenon as observed in Figure 6.1,

should be applicable to other types of lipids with different head groups. Figure 6.3 shows the results obtained from DPPC and DPPE Langmuir monolayers in OH region. When the DPPC monolayer is in the condensed phase, the dangling OH stretch red-shifts from 3705 cm^{-1} to 3620 cm^{-1}. Similarly, a dangling OH red-shift to around 3620 cm^{-1} is observed for condensed DPPE monolayer. The frequency of hydrogen bonded OH is typically below 3600 cm^{-1}, which also confirms the assignment of the perturbed dangling OH bonds at the water surfaces covered by DPPC and DPPE monolayers. DPPE has a phosphotidylethanolamine headgroup which is different from the phsophotidylchline headgroup of DPPC.

Both DPPC and DPPE have the same alkyl tail group, but have completely different head groups. The fact that they both can cause the frequency red-shift of the dangling OD/OH, as shown in Figures 6.1, 6.2 and 6.3, confirms that the red-shift of the dangling OD/OH stretch is due to a direct perturbation by the lipid chain.

The spectral structure revealed in Figures 6.1 demonstrates the complexity of the perturbation environment that the dangling ODs experience at the interface. An asymmetric band broadening generally suggests that there are overlapping vibrational modes under the spectral contour. Thus, the presence of a shoulder in Figures 6.1 implies that there is more than one type of dangling OD at the interface. For DPPC, two component peaks, 2700 cm^{-1} and 2720 cm^{-1}, can be deconvolved in the 1 mN/m, 3 mN/m, and 8 mN/m spectra in Figure 6.1. The 42 mN/m spectrum can be fitted with just one

component at 2700 cm^{-1}. The two components correspond to the dangling ODs affected by perturbations of different strengths, 2700 cm^{-1} to a stronger perturbation and 2720 cm^{-1} to a weaker perturbation. It is difficult to explicitly assign the two components at the molecular level only based on the VSFG data. Yet, a tentative assignment is hypothesized. Dangling ODs at close proximity to DPPC are being perturbed the most and thus correspond to the component at 2700 cm^{-1}. This type of OD exists regardless of surface coverage. Dangling ODs that are further away from DPPC can also be perturbed by the tail if the tail can disfigure to interact with the ODs. This occurs at low surface coverage (e.g., 1mN/m, 3 mN/m, and 8 mN/m). This type of ODs gives rise to the 2720 cm^{-1} component. It is also noteworthy that the red-shift and decrease of free OD/OH only occur after the surface pressure of lipid monolayers starts to build up. At zero surface pressure, the free OD/OH peak is intact no matter what the actual surface coverage is. Especially in the case of DPPE, the LC phase domains can already be observed at zero surface pressure.

It is scientifically intriguing that when the D_2O surface is fully covered by DPPC or DPPE, the dangling OD continues to persist. This phenomenon is considered to arise from hydrophobicity-induced drying. When water is in contact with an extended hydrophobic surface (radius larger than 1 nm, as predicted by Lum, Chandler, and Weeks),[121] water tends to move away from the hydrophobic surface to keep the surface dry. This is called a hydrophobicity-induced drying transition. To keep the surface dry (or dewetted) in the vicinity of the hydrophobic surface, water will not be able to maintain its

four-coordination hydrogen-bonding configuration, but must sacrifice one of its hydrogen bonds by forming a dangling OH bond pointing towards the hydrophobic surface. This transition is viewed as an analog to the vapor/water transition. The interfacial layer therefore is similar to the vapor/water interface, possessing dangling OH bonds.[122] The hydrophobicity-induced drying transition has long been envisioned by Stillinger.[122] Supporting evidence is from studies using a variety of methods, such as theoretical analysis,[121] x-ray reflectivity,[123] force measurement,[124, 125] and neutron reflectivity.[126] The dangling water bond is a unique structural feature arising from the drying transition. Previous VSFG studies on water/hydrophobic surfaces provided direct spectroscopic evidence about the existence of the dangling OH bond of water.[106, 107] In a Langmuir monolayer, the long hydrocarbon tail surface of DPPC or DPPE is large enough (if viewed along its axis) to be considered as an extended hydrophobic surface. According to the hydrophobicity-induced drying transition hypothesis, the dangling OD should exist in the vicinity of this hydrophobic region. This is what is observed. Therefore, the existence of a dangling OD even under full monolayer coverage is a natural phenomenon arising from the hydrophobic tail that then induces drying.

It is important to note that in our previous publication,[127] we showed free OD shifts in the presence of PA. However, since that time, we have found that there is an overlap of the perturbed free OD and the COOD-D_2O resonances[32] in the investigated spectral region, which shows that we cannot conclude exclusively that the shifting in the case of PA is due to chain perturbation.

6.2 Conclusions

In conclusion, perturbed dangling OD bonds from interfacial deuterated water exist at the surface of Langmuir monolayers. The perturbation on the dangling OD is attributed to van der Waals interactions between the hydrocarbon chain and the dangling OD bonds. Owing its relevance to hydrophobicity-induced drying, the perturbed dangling bond of water is expected to exist in other types of hydrophobic assemblies, such as micelles, vesicles, and biological membranes.

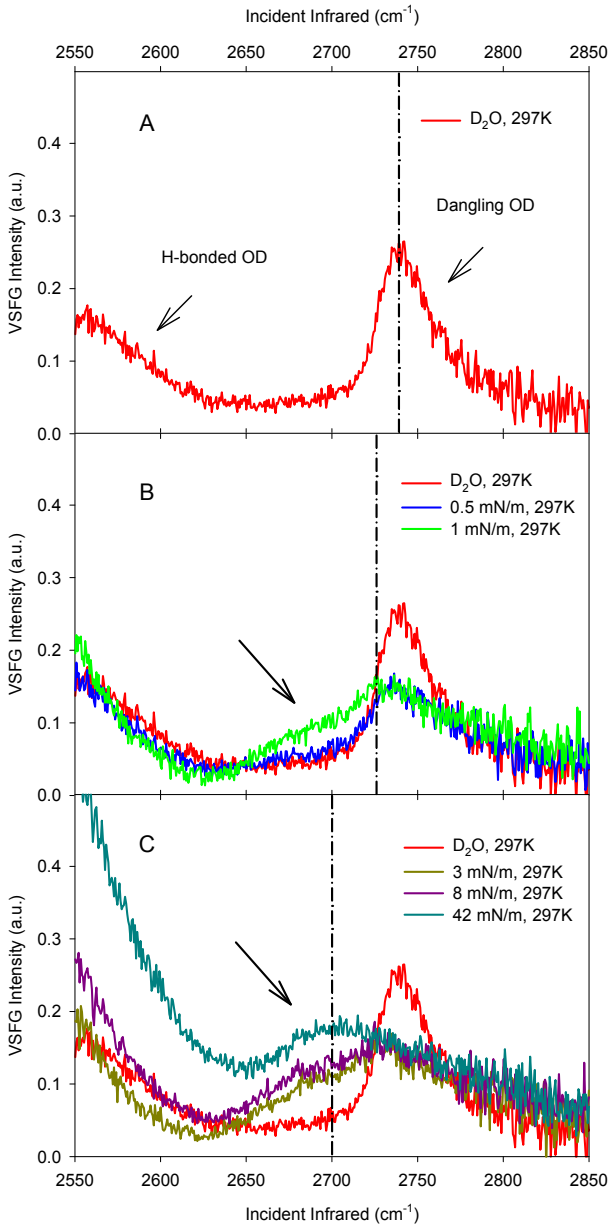

Figure 6.1. *ssp* VSFG spectra of the D_2O surfaces in the dangling OD stretching region at 297 K. A: air/D_2O surface; B and C: air/D_2O/*d62*-DPPC monolayer surfaces under different surface coverages (the air/D_2O surface spectrum, the red curve, is re-shown for comparison).

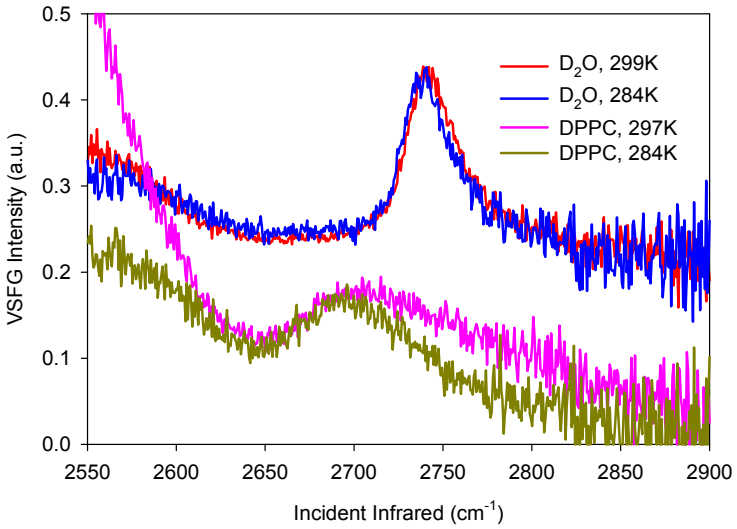

Figure 6.2. *ssp* VSFG spectra of the air/D_2O and the air/D_2O/*d62*-DPPC monolayer surfaces in the dangling OD stretching region in a temperature-dependent study (the 284 K spectra of D_2O and DPPC are scaled by a factor of 1.8 for comparison; the two D_2O spectra are vertically offset by 0.2 units).

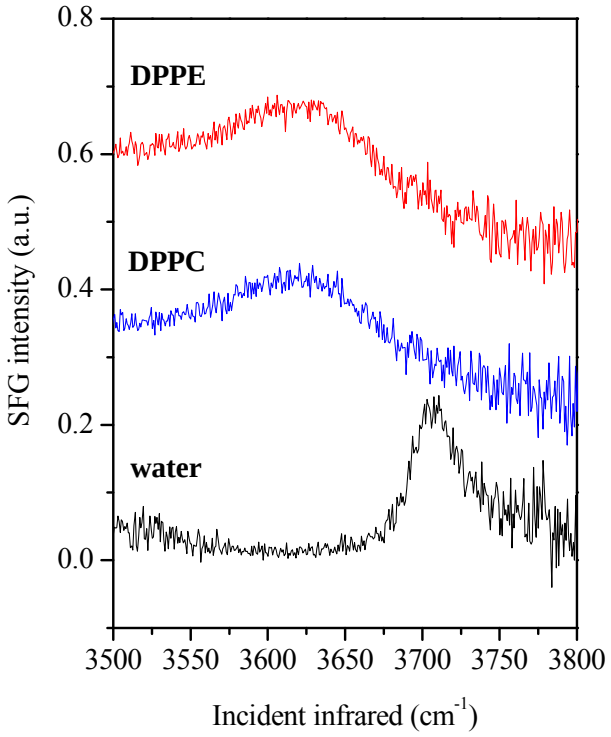

Figure 6.3. *ssp* VSFG spectra of the H_2O surfaces in the dangling OH stretching region for neat water, and covered with DPPC and DPPE monolayers.

Chapter 7: Interfacial water structure associated with phospholipid membranes studied by phase-sensitive vibrational sum frequency generation spectroscopy

Biological membranes are self-assembled bilayers of biomolecules such as lipids, proteins, and carbohydrates.[85] Among such complicated structures, phospholipids are the major constituents of the membrane structural backbone[3] and the phospholipid composition greatly affects membrane functions and properties. The origin of the unique ability of a phospholipid to form self assemblies arises from their amphiphilic nature of its structure and its interaction with the polar water environment. Phospholipids have similar two-part structures, the hydrophobic tail groups and the hydrophilic head group. The tail groups are the alkyl chains of varying lengths which congregate together in the central portion of the bilayer allowing these hydrophobic entities to escape from the surrounding polar environment. The head group of a phospholipid is a negatively charged phosphate linked to a diverse set of functional groups which are immersed in the aqueous medium and thought to be well hydrated. Therefore, it is recognized that water molecules in the region of biomembranes play an important role in the biomembrane structure and function.[6, 128-130]

Different experimental techniques have been employed to study phospholipids and associated water. To simplify the complicated natural biomembrane composition, model membrane bilayers or monolayers containing one type of phospholipid or a mixture of different types are often used. Previous NMR spectroscopic studies revealed that the ordering and dynamics of water near phospholipid head groups are changed upon lipid hydration.[131, 132] X-ray and neutron scattering techniques have elucidated the positions and distances between phospholipid bilayers and provide information on membrane-membrane interactions and the hydration forces.[133, 134] Infrared (IR) vibrational spectroscopy is a method sensitive to characteristic chemical bond strength and interactions and is used extensively to study the hydration sites of lipids and the hydrogen bonding network of water affected by the lipid head groups.[135-138] It has been found that the water molecules that reside near the head groups are hydrogen donors and form strong hydrogen bonds with the lipid phosphate and carbonyl groups. Concurrently, the electrostatic potential due to the charges on the head group leads to ordering of water dipoles and results in stronger hydrogen bonds between neighboring water molecules. In addition to experimental studies, molecular dynamics (MD) simulations provide more insight on the structure and physical properties of the phospholipid/water interface.[6, 129, 139-143] For example, water molecules are suggested to form stronger hydrogen bonds with the lipid phosphate groups than the carbonyl groups and the most probable sites to accept a hydrogen bond are the double bonded oxygens connected to the phosphorus atom.[143] Moreover, at the phospholipid/water interface, water is thought to be perturbed up to 1

nm away by the dipole potential of the head group.[140] Despite ongoing research, direct probing of water molecules at the biomembrane interface has been relatively rare.

Vibrational sum frequency generation (VSFG), an interface-specific spectroscopy, is well suited as a probe to directly study water orientation at the phospholipid/water interface, as is shown here. VSFG spectroscopy is a second-order nonlinear optical spectroscopy that requires lack of inversion symmetry. This unique selection rule enables VSFG spectroscopy to probe the topmost few layers at an interface where the inversion symmetry is naturally broken.[20] To drive a VSFG process, two pulsed laser beams, one visible together with an infrared are used. The VSFG signal is enhanced when the infrared frequency matches the vibrational frequency of an interfacial species, hence giving characteristic molecular information. Moreover, the VSFG response is sensitive to orientation and ordering of surface species, making it an ideal technique for direct probing of the biomembrane/water interface. Application of VSFG has already been well demonstrated on the neat air/water interface[24, 25, 27, 29, 103, 144-148] and phospholipid/water interfaces.[31, 60, 149-151] For VSFG spectra of the neat water surface, the dangling OH bond of surface water molecules with the other OH bond hydrogen bonded to other interfacial water molecules is observed at 3700 cm^{-1}. In addition, hydrogen bonded OH modes (from 3000 cm^{-1} to 3600 cm^{-1}) are clearly seen from the neat water surface spectra, although the detailed spectral assignments relating to specific water structures have not yet been fully agreed upon.[24, 25, 145, 147, 148] When the water surface is covered with a phospholipid monolayer, dangling OH bonds decrease significantly but still persist at the surface with a

red-shifted frequency.[127] However, the VSFG signal in the hydrogen bonded region increases by many times in the presence of various kinds of phospholipids, providing evidence of an ordering of water molecules by the phospholipid head groups.[150]

Although much information about the lipid/water interface has been revealed by VSFG spectroscopy, the important question, namely the average orientation of water molecules at the lipid/water interface is hardly answered. Whether the net interfacial water dipole is pointing towards the lipid tails or the bulk water interior determines the sign of the complex second-order nonlinear susceptibility, $\chi^{(2)}$, of surface modes. A conventional VSFG intensity spectrum is proportional to the absolute square of the nonlinear susceptibility, $|\chi^{(2)}|^2$, hence does not distinguish the net water dipole direction. Recently, a phase-sensitive VSFG (PS-VSFG) method based on interference of the sample response with an additional signal of phase reference has been developed by Shen et al, which enables absolute determination of the sign of the second-order nonlinear susceptibilities of the water surface.[25, 152, 153] The PS-VSFG technique provides the imaginary part of the complex nonlinear susceptibility, Im $\chi^{(2)}$. PS-VSFG data clearly reveal that while the dangling OH bonds of a neat water surface are pointing out into the air side of the interface, the OH bonds that contribute to the hydrogen bonded OH stretching region of the VSFG spectrum are made up of both OH bonds pointing away from and toward the bulk aqueous phase.

Neat water PS-VSFG spectra, similar to Shen et al., were reported by Tahara and coworkers using a broadband SFG system.[27] In addition to direct experiment determination of phase, Bonn et al reported a phase retrieval algorithm applied to a conventional VSFG spectrum containing interfered modes from the phospholipid/water interface.[154] From the phase VSFG spectra deduced from the phase retrieval algorithm, they unexpectedly identified, albeit incorrectly identified as experimentally shown here, that water molecules orient with their hydrogens pointing *down* toward the bulk at a negatively charged phospholipid monolayer interface.[155] To explain this behavior which is contrary with the electrostatic interactions between phospholipid head groups and water, they suggested that the water molecules probed are above the head group hence with their hydrogens still pointing to the negatively charged head group. However, this result is counterintuitive and is also not in agreement with the more recent MD simulation of VSFG from the phospholipid/water interface, which suggests that water dipoles (dipole vector pointing toward the positive charge) are pointing *up* toward the (negatively charged) phospholipids.[156]

To reveal the water orientation at the phospholipid/water interface, we report here a direct PS-VSFG study of water structure associated with a series of phospholipid monolayers at the air/water interface. The five phospholipids that are studied here have differing head group structures and charge (see Figure 3.1), which expectedly affect the nearby water structure. At physiological relevant neutral pH, dipalmitoyl phosphate acid (DPPA), dipalmitoyl phosphatidylglycerol (DPPG), and dipalmitoyl phosphatidylserine (DPPS)

have net negatively charged head groups, while dipalmitoyl phosphatidylcholine (DPPC) and dipalmitoyl phosphatidylethanolamine (DPPE) have zwitterionic head groups. We also examined water orientation in the case of simpler molecules, palmitic acid (PA, negatively charged after deprotonation) and dimethyldioctadecylammonium bromide (DDAB, positively charged) as a check for our phase determination.

7.1 Results and Discussion

It is noteworthy to interpret the VSFG results from a neat water surface before discussing the phospholipid/water interfaces. Despite unambiguous assignment of 3700 cm^{-1} to the dangling OH stretch, also referred to as the free OH, the interpretation of VSFG spectra of the hydrogen bonded OH stretch region (3000 cm^{-1} to 3600 cm^{-1}, Figure 7.1a bottom panel) has been controversial for a long time.[24, 25, 145-148] The intensity spectrum of neat water exhibits two characteristic bands centered at ~3200 cm^{-1} and ~3400 cm^{-1}, which are commonly referred to as "ice-like" and "liquid-like" water structures.[157] Without knowing the sign of the nonlinear susceptibility (χ), interpretations based on fitting of conventional VSFG spectra of the air/water interface are not unique; hence this leads to different structural interpretations.

The Im $\chi^{(2)}$ spectra provide not only the resonant information of modes but also the sign (orientation) of each mode. Our Im $\chi^{(2)}$ spectrum of neat water in the hydrogen bonded stretching region is similar with the result reported by Shen and coworkers[25] (Figure 7.1a, middle panel). It is suggested by Tian et al that the VSFG signal from the neat water

surface is largely due to the top two layers of water molecules and the sublayers are mainly disordered and give little contribution.[158] From previous work[25] in the hydrogen bonded region, the negative region from 3450 cm^{-1} to 3600 cm^{-1} has been assigned to donor-bonded OH stretches of 3-coordinate DDA and DAA water molecules in the topmost layer. (Here D and A denote donor and acceptor hydrogen bonds respectively, with which water molecules hydrogen bond to nearest neighbors.) The negative region from 3200 cm^{-1} to 3450 cm^{-1} has been assigned to asymmetrically donor-bonded 4-coordinate DDAA molecules, while the positive region from 3000 cm^{-1} to 3200 cm^{-1} was mainly attributed to symmetrically donor-bonded DDAA molecules.[25] The above assigned spectral regions overlap with each other, which leads to a crossover point around 3200 cm^{-1}. The negative sign in an Im $\chi^{(2)}$ spectrum corresponds to the OH stretches with a net orientation of the hydrogens pointing down towards the bulk and the positive sign corresponds to a net orientation with hydrogens pointing up.

The fatty acid, surfactant, and phospholipids that were studied here form self-assembled monolayers on water and were over-spread to form a condensed phase monolayer prior to the PS-VSFG measurements. Palmitic acid and DDAB are amphiphilic molecules with relatively simple head groups, i.e. a carboxylic group and ammonium group, respectively. Their monolayers on the water surface therefore serve as references for a negatively charged surface (PA) and a positively charged surface (DDAB). PA on pH 13 water has its carboxylic group in a deprotonated state based on a reported pKa of ~9 from previous studies of an arachidic acid monolayer.[32, 159] The conventional VSFG spectra of a water

surface with deprotonated PA and DDAB monolayers exhibit similar 3200 cm^{-1} and 3400 cm^{-1} bands as that from the neat water surface as shown in the bottom panel of Figure 7.1, but with significantly higher intensities. Such high intensities clearly suggest ordering of water molecules by the strong surface electric field, which increases the probing depth of the VSFG.[146] However, the Im $\chi^{(2)}$ spectra shown in the middle panel of Figure 7.1 in the case of PA and DDAB are completely different. Unlike the coexistence of both negative and positive regions for neat water, broad continuous regions in either purely positive or purely negative phase are observed for PA and DDAB respectively. The negatively charged PA monolayer orients water molecules with hydrogens pointing up toward the air phase and the positively charged DDAB monolayer reveals the opposite water orientation with hydrogens pointing down.

The Im $\chi^{(2)}$ and conventional (power) VSFG spectra of the water surface with net negatively charged phospholipid monolayers DPPA, DPPG, and DPPS are shown in Figure 7.2. These conventional VSFG spectra are also consistent with published VSFG spectra for similarly charged phospholipids,[150] although the 3200 cm^{-1} intensities in our spectra are slightly lower. It has been shown in the early 1990s by Eisenthal and co-workers that the third-order susceptibility ($\chi^{(3)}$) mechanism can make a significant contribution to the detected nonlinear polarization.[160-162] According to a study on a charged monolayer/water surface,[161] the electric-field-induced second harmonic generation (EFISHG) from water molecules induced by the negative charge of an *n*-docosyl sulfonate monolayer shows a decrease in the SHG signal as compared to that

from the neat air/water interface. This is in contrast with the much greater VSFG signal relative to the neat air/water interface for negatively charged phospholipids (Figure 7.2). In addition, the PS-VSFG studies on water at highly charged surfaces completed by Shen and co-workers were interpreted based on $\chi^{(2)}$ contribution.[24, 163] Therefore, the VSFG intensity increase observed in our spectra for the negatively charged phospholipid monolayers are attributed to predominantly a $\chi^{(2)}$ mechanism.

Similar to PA at pH 13, all negatively charged phospholipids order the water molecules with hydrogens pointing up. This indicates that the electrostatic potential of the phospholipid head groups dictates the net interfacial water orientation despite the difference in functional groups and head group orientation. The above phospholipids together with their sodium counterion form an electric double layer (EDL) in the interfacial region. Previous MD simulations on DPPG[164] and dioleoylphosphatidylserine (DOPS)[165] bilayers suggested that sodium ions reside in the vicinity of the negative centers of phospholipid head groups. The order of magnitude higher VSFG intensity in the Im $\chi^{(2)}$ spectra of negatively charged phospholipids compared to that from the neat water surface suggests that water molecules below the negatively charged head groups are aligned preferentially with their hydrogens up toward the surface.

Phospholipids with zwitterionic (net neutral) head groups such as phosphatidylcholine (PC) and phosphatidylethanolamine (PE) are most studied because of their common presence in biomembranes. The water structure associated with these types of net neutral

head groups is particularly intriguing. The Im $\chi^{(2)}$ and conventional VSFG water spectra of DPPC and DPPE monolayers are shown in Figure 7.3. The positive sign for both Im $\chi^{(2)}$ spectra over the full hydrogen bonded OH stretching region indicates that interfacial water molecules orient on average with hydrogens up towards the surface similar to negatively charged monolayers, although the lower relative intensity suggests a weaker orientating effect compared to the net negative DPPA and DPPG phospholipids. Previous studies have also shown that interfacial water structure can be very different at neutral surfaces. For example, specific anions can be absorbed into the air/polymer/water interface and can cause ordering of interfacial water molecules.[166] Interfacial water molecules are also found to be accommodated in neutral 4''-*n*-octyl-4-*p*-cyanobiphenyl (8CB) Langmuir monolayers and give rise to a new band at ~ 3520 cm^{-1}.[167]

Our results are in accordance with the recent MD simulations, which suggest that the charge on a PC head group viewed by the interfacial water molecules is negative despite its zwitterionic nature.[130, 140-142] However, our Im $\chi^{(2)}$ spectra of the phospholipid/water interfaces are *opposite* with the calculated Im $\chi^{(2)}$ results from the phase retrieval algorithm furthered by Bonn et al, although it should be pointed out that our Im $\chi^{(2)}$ spectra of PA and DDAB are similar to the references they use, i.e. lauric acid (LA, negatively charged) and octadecyl trimethyl ammonium bromide (OTAB, positively charged).[155] Bonn et al attributed the negative OH stretch response in their retrieved Im $\chi^{(2)}$ spectra of the phospholipid/water interface to the water molecules sitting above the phospholipid head groups, hence the net orientation of these water OH bonds would point

down to the negative charge of the head groups. Indeed there are water molecules above the head group because significant numbers of dangling OH bonds remain at the phospholipid/water interface even under full monolayer coverage.[127] But the orientation of water in localized regions above as well as directly around the head group, the hydrating water molecules, are not discernable from the larger number of water molecules that are oriented by the electrostatic potential induced by a phospholipid monolayer.

Theoretical simulations help to provide additional insight on the DPPC/water interfacial structure. Berkowitz suggested that water molecules are able to penetrate up to the carbonyl groups of the alkyl chains in the lipid tails.[6] The carbonyl, phosphate, and choline groups are at different positions if projected on the normal to the phospholipid layer with the carbonyl group on the tail ~ 5Å above the PC head.[130, 140, 168] The phosphorus atom to nitrogen atom (P-N) vector is nearly parallel to the surface plane, ~ 10 degrees away from the surface plane as reported by many others, with the phosphate slightly higher than the choline group, although the distribution probability is broad, over several tens of degrees.[83, 169, 170] The electrostatic potential due to the DPPC molecules can be arbitrarily set to continuously increase from zero to positive values as one goes from the tail group to the bulk water.[6] The contributions to this positive electrostatic potential are largely from the negatively charged phosphate, and then from the carbonyl groups.[171] As a result, on average, the interfacial water molecules orient with their dipole (hydrogens) pointing towards the surface (towards the DPPC tails) to compensate for the

electrostatic potential. The orientation of interfacial water molecules can also be explained by the cumulative charge distribution of the DPPC layer that is experienced by the water molecules. Starting from the carbonyl groups on the tails to the bulk water, the simulated cumulative charge becomes more negative until it peaks at the position of the phosphate, and then gradually increases back to zero after the choline group.[142] This suggests that the water molecules between the phosphate and the choline groups experience the strongest orientational ordering. Additionally, the net orientation of water molecules below the carbonyl groups would always be with their hydrogens pointing up towards the DPPC tails, which is in agreement with our measured Im $\chi^{(2)}$ spectra.

The Im $\chi^{(2)}$ water spectra of negatively charged phospholipids clearly show higher amplitudes as compared with net neutral zwitterionic phospholipids. This might suggest that DPPC and DPPE mainly perturb water molecules between the tail carbonyls and the choline of the head group, while the negatively charged head groups could impact the water orientation over a longer range. Recent MD simulated VSFG spectra from the DMPC/water interface suggest as well that the main contribution to the VSFG spectra is the water dipoles located over several Ås in depth, corresponding to the PC head group region.[156]

To further elucidate the influence of zwitterionic head groups on the interfacial water structure, an Im $\chi^{(2)}$ water spectrum of DPPC on a $CaCl_2$ subphase was collected and is also shown in Figure 7.3. The amplitude of the Im $\chi^{(2)}$ water spectra decreases greatly on

the 0.4 M $CaCl_2$ subphase as compared with that of the neat water subphase, although the sign of $\chi^{(2)}$ remains positive over the hydrogen bonded spectral region. (Note that the y axis scales can be directly compared between figures.) Cations are attracted to the carbonyl and phosphate groups of the phospholipids.[172] Owing to the greater negative charge carried by the phosphate group, it is reasonably conceived that Ca^{2+} ions would favor binding to the phosphate compared to the carbonyl group.

Conventional VSFG spectra of the DPPC phosphate group were obtained on neat water and on a 0.4 M $CaCl_2$ subphase as shown in Figure 7.4. Two peaks at ~ 1070 cm^{-1} and ~1100 cm^{-1} are observed in these spectra. The former peak is assigned to the P-O ester stretch and the latter is assigned to the symmetric stretch of PO_2^-.[173] The frequency of the PO_2^- symmetric stretch is sensitive to the hydration state of the phosphate group and blue shifts upon dehydration.[31, 69] A theoretical study of the PO_2^- moiety of methylphosphocholine showed that upon hydration there is a loss of electron density of the P=O bonds due to strong hyperconjugation with the water O-H antibonding orbital, resulting in weakened P=O bonds and a red shift.[72] In the presence of 0.4 M $CaCl_2$, the PO_2^- symmetric stretch blue shifts to ~ 1109 cm^{-1}, suggesting that calcium binding results in phosphate dehydration. The observed spectral blue shift of the PO_2^- peak is also consistent with the theoretical study on dimethyl phosphate in the presence of water and calcium, which showed that as the Ca^{2+} approaches the PO_2^- oxygens, and a blue shift of both the symmetric and asymmetric stretches of the PO_2^- was observed.[174]

Based upon the spectra in Figures 7.3 and 7.4, it can be concluded that the decrease in the amplitude of the Im $\chi^{(2)}$ water spectrum of DPPC on the 0.4 M $CaCl_2$ subphase is due to the binding of Ca^{2+} to the phosphate group. In addition, it should be pointed out that the PO_2^- symmetric stretch frequency remains nearly unchanged at a 0.5 M NaCl subphase (data not shown) relative to that on neat water. This suggests that the electrostatic interaction between sodium ions and the phosphate is relatively weak and does not affect the hydration shell of the phosphate, while the interaction of the calcium ions results in direct binding where calcium replaces hydrating water molecules. As a consequence, the presence of Ca^{2+} shields part of the phosphate charge on the DPPC head group, resulting in a lessened impact on the ordering of the interfacial water molecules as illustrated in Figures 7.5. At the Ca^{2+} concentration studied here, interfacial water molecules still experience a net negative charge from the DPPC molecules so that the Im $\chi^{(2)}$ water spectrum is still positive.

The strength of the water hydrogen bonding network under the influence of a phospholipid monolayer is also of great interest. It is generally thought that water hydrogen bonding strength correlates with the frequency of the OH stretch, namely higher OH stretch frequency equates to weaker hydrogen bonding strength. However, the intermolecular and intramolecular coupling of water O-H bonds causes a splitting of the OH stretch bands, which complicates spectral interpretation.[147] A very recent study of water near the highly charged CTAB/water interface reveals that the 3200 cm^{-1} and 3400 cm^{-1} OH bands merge into one band as the water is gradually replaced by HOD.[175] This

result suggests that decoupling of the O-H bonds is required for determination of the actual OH stretch frequency and the hydrogen bonding strength, although it is suggested by MD simulation that the structure of water molecules in and near the phospholiplid/water interface are heterogeneous and the organization corresponds to different moieties of the head group.[156]

7.2 Conclusions

In summary, direct PS-VSFG measurement of water structure associated with a series of phospholipid monolayers reveals that interfacial water molecules orient accordingly to the net phospholipid head group charges. Negatively charged head groups (DPPA, DPPG and DPPS) have greater impact on water ordering than neutral zwitterionic head groups (DPPC and DPPE). In the case of zwitterionic phospholipids, the negative charge on the phosphate group dominates the interfacial water orientation. Binding of Ca^{2+} to the phosphate group reduces the effective charge experienced by surrounding water molecules, resulting in less influence on water orientation.

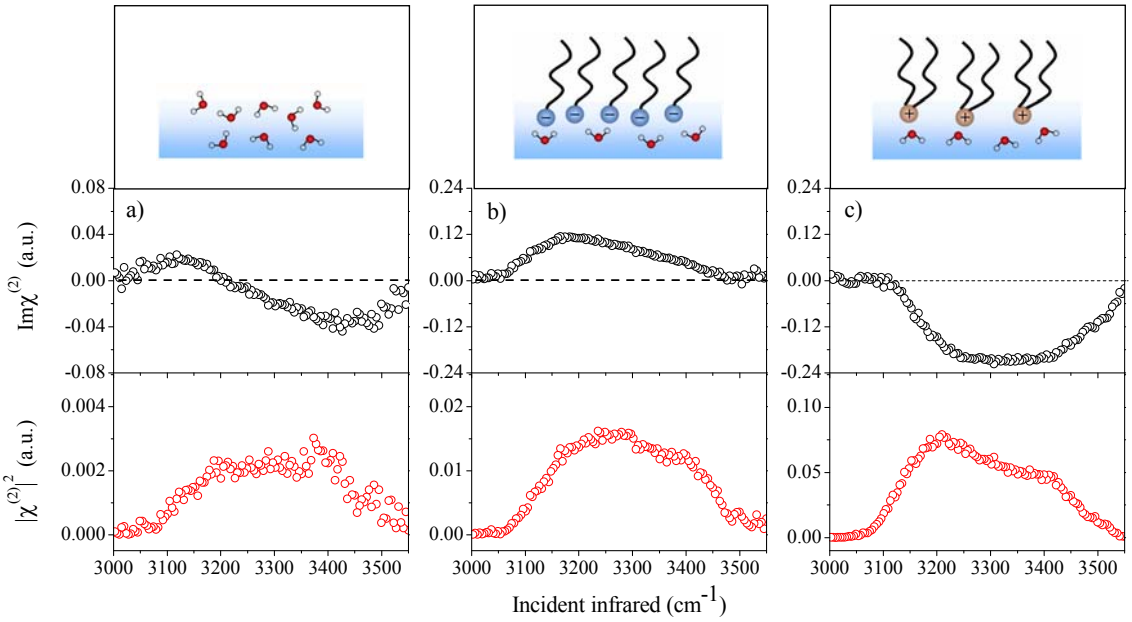

Figure 7.1. Im $\chi^{(2)}$ VSFG spectra (middle panel) and conventional VSFG spectra (bottom panel) of a) water, with b) PA on pH = 13 water, and c) DDAB. Illustrations of each interface are shown in top panel.

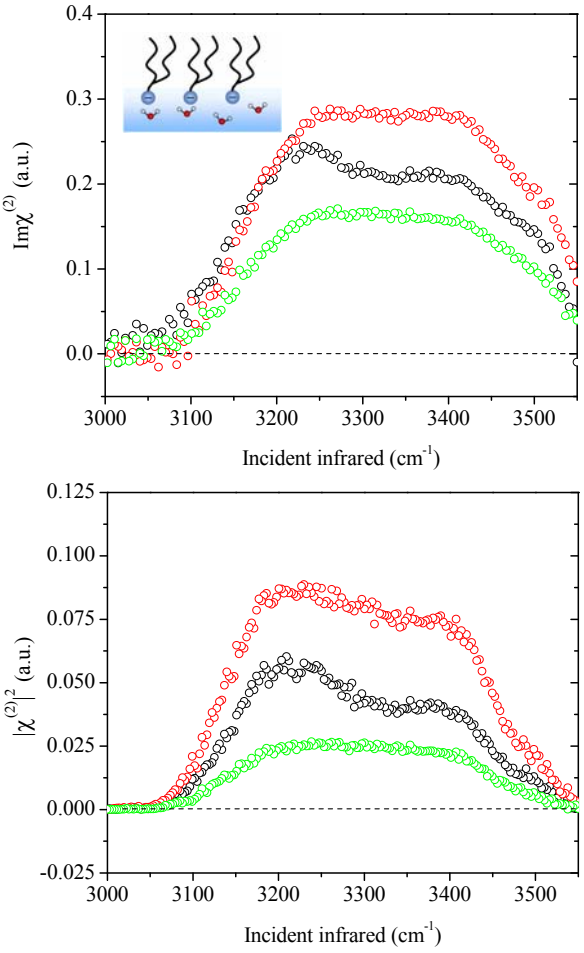

Figure 7.2. Im $\chi^{(2)}$ VSFG spectra (top) and conventional VSFG spectra (bottom) of water with net negatively charged phospholipid monolayers: DPPA (black), DPPG (red), and DPPS (green, lowest intensity spectrum).

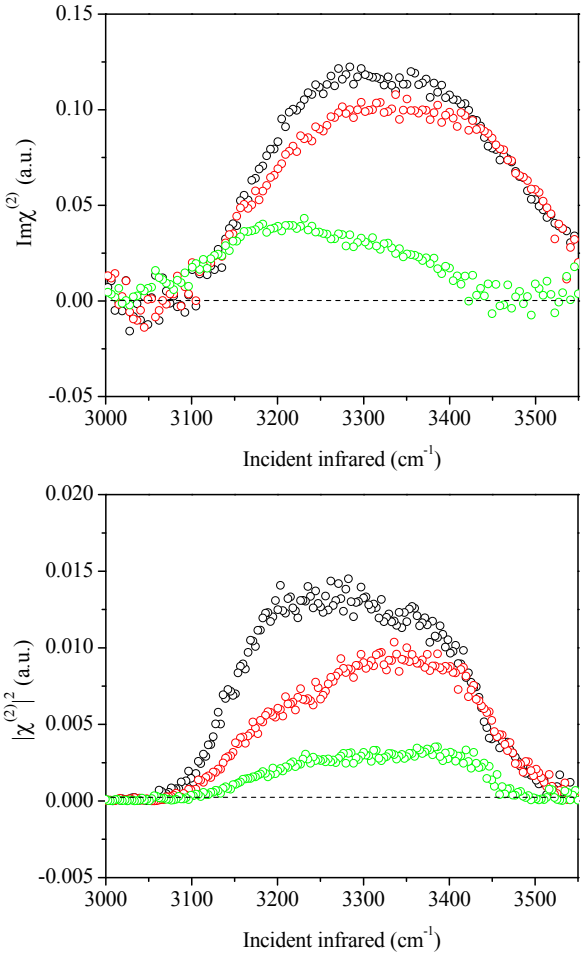

Figure 7.3. Im $\chi^{(2)}$ VSFG spectra (top) and conventional VSFG spectra (bottom) of water with net neutral zwitterionic monolayers: DPPC (black), DPPE (red) and DPPC on 0.4 M $CaCl_2$ (green, lowest intensity spectrum).

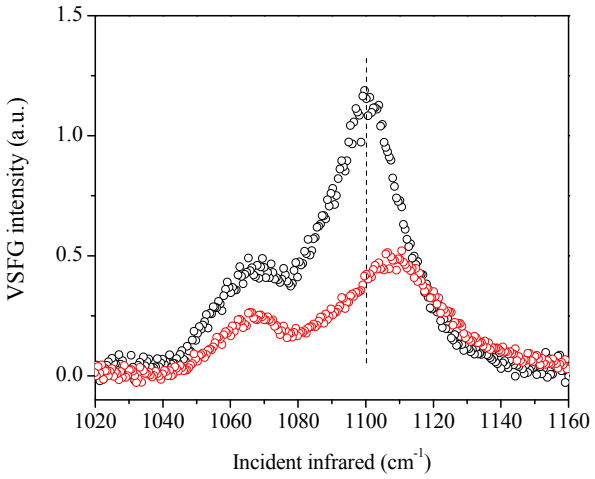

Figure 7.4. Conventional VSFG spectra of DPPC PO_2^- on water (black, highest intensity spectrum) and on 0.4 M $CaCl_2$ (red, lowest intensity spectrum) subphases.

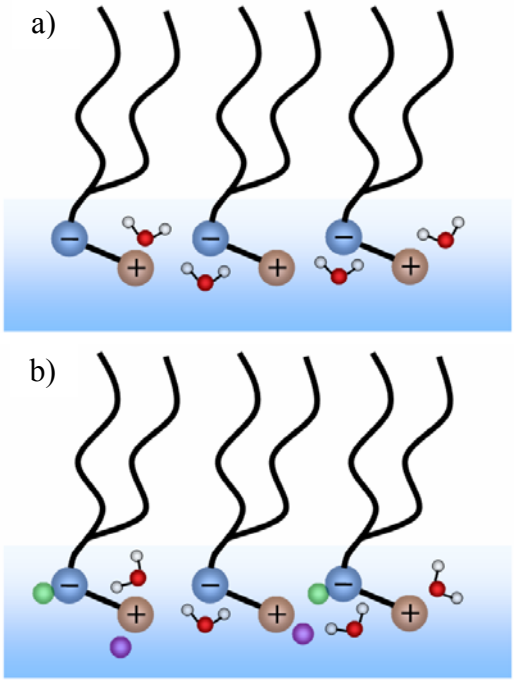

Figure 7.5. Illustration of water orientation at the interface of a) DPPC on neat water and b) DPPC on 0.4 M $CaCl_2$ subphase. The phosphate and choline groups of DPPC are labeled negative and positive charge, respectively. Ca^{2+} ions which bind to the phosphate group and Cl^- ions are represented as green and purple spheres in b). Water orientation becomes less ordered at the interface in the presence of Ca^{2+} ions.

Chapter 8: Interfacial molecular organization at aqueous solutions of atmospherically relevant DMSO and MSA

Organosulfur compounds of both natural and anthropogenic origin have been found to be involved in many reactions taking place at the aerosol surface.[9] In the marine boundary layer (MBL), the sulfur cycle dominates in the gas to particle conversion process and in the growth of aerosols.[176] Tropospheric sulfur containing aerosols play an important role in climate as well as in related heterogeneous atmospheric chemical processes.[15, 17] A significant sulfur source in the MBL is the biogenic dimethyl sulfide (DMS) produced by metabolic processes of algae.[10, 11] Because of its high volatility and reactivity, DMS is easily oxidized in the atmosphere and produces many stable intermediates such as dimethyl sulfoxide (DMSO) and methanesulfonic acid (MSA).[12, 13] Oxidation of DMSO, MSA, and other intermediates can take place at the aerosol surface and in the bulk of the aerosol through reactions with OH radicals, which eventually leads to the formation of H_2SO_4.[14] The sulfur containing aerosols serve as cloud condensation nuclei, influencing the formation of clouds and thereby modifying the earth's albedo.[15-17] Therefore, the uptake of organosulfur species and the molecular organization at the aerosol surface are of great interest in atmospheric chemistry.

Besides the important atmospheric implications, DMSO, MSA, and their aqueous solutions also have a wide range of applications in other chemical processes. In organic chemistry, DMSO is among the most widely used solvents.[177] Biological properties of DMSO are also important. Due to its amphiphilic nature, DMSO interacts strongly with molecules in cell membranes, which promotes membrane permeability[36, 38] and induces cell differentiation[41] and fusion[40]. Because of its strong interaction with water, aqueous DMSO solution displays strong non-ideal behavior. For example, DMSO solutions can reach freezing points below that of liquid nitrogen, and, therefore, DMSO can be used as a cryoprotectant for biological structures such as tissues and proteins.[33] For methanesulfonic acid, similar to DMSO, is completely miscible with water at any concentration. Moreover, MSA is a strong acid (pKa = -1.9) and is widely used as an acid electrolyte in many electrochemical processes.[178]

Extensive efforts have been made to elucidate molecular organization in the bulk solutions of aqueous DMSO and MSA.[179-184] In particular, DMSO-water mixtures have been investigated by a wide variety of experimental techniques such as X-ray and neutron diffraction,[182, 185] infrared (IR) and Raman spectroscopy,[186, 187] nuclear magnetic resonance (NMR),[188, 189] and acoustic spectroscopy[190] as well as computer simulations.[179-181] These studies led to the conclusion that DMSO as a hydrogen bond acceptor forms strong hydrogen bonds with water molecules. The hydrogen bond between DMSO and water is even more pronounced than that between water molecules.[182] The methyl groups of DMSO, although hydrophobic, are loosely hydrated by surrounding water

molecules.[188] Similar hydrogen bonding ability of MSA with water is observed due to the S-O moieties.[183]

Because of the noticeable surface preference of DMSO and MSA, the structure and properties of the surface of their aqueous solutions are also of interest. In contrast with the relatively abundant bulk information, the molecular organization at the surface is still not well understood due to limited surface-specific techniques for aqueous media. Only nonlinear spectroscopic methods such as second harmonic generation (SHG)[191] and vibrational sum frequency generation (VSFG) have been utilized to study the surface of aqueous solutions of DMSO and MSA.[79, 192-194] A concentration VSFG study of aqueous DMSO showed that the square root of the CH_3 intensity was proportional to the determined surface DMSO number density, which suggested that the average orientation of DMSO CH_3 groups remains unchanged with different mixing ratios with water. However, the actual orientation of DMSO at the surface has not been reported. In addition, a VSFG study calculated the MSA orientation based on the CH_3 symmetric stretch intensities in ssp and sps polarizations. Due to the near zero CH_3 intensity in sps polarization, the determined orientation angle of MSA had a large uncertainty range of 0˚ to 60˚.[193] Computational simulations focused solely on DMSO, showing that this molecule is surface active and oriented at the water surface.[195-197] Thus, a general but not complete picture of the surface of aqueous solutions of DMSO and MSA including the surface concentration, molecular interactions and orientation, and interfacial water structure has been presented.

In this chapter, the VSFG technique with complementary infrared (IR) and Raman spectroscopies are employed to present a comprehensive study of the liquid/vapor interface of aqueous solutions of DMSO and MSA to elucidate the molecular organization and orientation, and intermolecular interactions. Taking advantage of the ability to probe in the low frequency vibrational region (fingerprint region), the S-O moieties in DMSO and MSA are investigated here for the first time for these molecules.

8.1 Results and Discussion

DMSO at the surface

DMSO-water mixtures have been investigated by various spectroscopic methods including IR, Raman, and VSFG. The S=O moiety is the key part which accounts for the dipolar interactions of DMSO. Figure 8.1 shows the Raman spectra in S=O stretch region of a series of DMSO-water mixtures. The peak near 950 cm^{-1} is assigned to a rocking mode of DMSO CH_3.[198] For pure DMSO, a broad band peaked at 1043 cm^{-1} is observed for the S=O stretch mode.[187] The asymmetric band shape ranges from 1000 to 1100 cm^{-1} and has a shoulder at ~ 1055 cm^{-1}. This broad shape of S=O stretch shows the existence of different aggregates in pure DMSO. The S=O frequency of DMSO monomer as diluted in carbon tetrachloride was found to be around 1070 cm^{-1}.[198] Because of the negligible interaction between CCl_4 and the DMSO S=O group, this frequency is considered to be unperturbed. In pure DMSO, a strong dipolar interaction was identified between DMSO molecules, leading to formation of DMSO dimers and chain aggregates.[187, 197] Therefore, the peak at 1043 cm^{-1} is assigned to the symmetric stretch of

the cyclic DMSO dimer.[187] As the water content increases in the DMSO-water mixtures, a clear red-shift in the S=O stretch frequency is observed, which is generally attributed to the DMSO-water interaction. The concentration dependence of the S=O frequency red-shift was proposed to be correlated with a cluster model (DMSO)x(H2O)y. When x >> y, as in nearly pure DMSO, the dipolar interaction between DMSO molecules dominates. On the other hand, hydrogen bonding between DMSO and water molecules is more pronounced when y >> x. At 0.66 *x* DMSO the peak intensity at 1030 cm^{-1} is about the same as that at 1043 cm^{-1}, which indicates the coexistence of DMSO in different chemical environments. Previous MD simulation also suggested the tendency of DMSO and water to preserve their own structural order upon mixing.[179] In rather dilute DMSO solutions (< 0.33 *x*) the width of the S=O stretch band becomes narrower, suggesting a more similar or homogeneous environment for DMSO. No significant red-shift is found between the 0.1 *x* and 0.02 *x* DMSO solution spectra, both showing the S=O frequency centered at 1012 cm^{-1}.

Although IR activity of the DMSO S=O stretch is also observed (data not shown), VSFG of the DMSO S=O stretch has not been reported so far. Indeed no VSFG intensity in the S=O stretch region is detected for the 0.1 *x* DMSO in the ssp polarization combination as shown in Figure 8.2. VSFG intensity not only relates to the molecular hyperpolarizability, but also to the molecular orientation at the surface and therefore lack of ssp polarization signal could indicate surface disordered DMSO molecules or orientation of the S=O near the plane of the surface. However, the significant VSFG intensity of DMSO methyl

groups, discussed below, indicates that disorder is not the reason for lack of VSFG signal. Previous MD simulations have predicted the orientation of the S-O vector at the surface of both neat DMSO[197] and aqueous DMSO solutions.[195] The S-O vector orientation of the top layer of molecules was found to be parallel to the surface of neat DMSO, while at the aqueous DMSO (< 0.2 *x*) surface, the average S-O vector orientation was predicted to be ~ 30˚ away from the surface plane. Both theoretical results suggest that the S-O vector in DMSO prefers to orient close to the surface, which as a consequence, leads to a vanishing of the ssp VSFG intensity.

After spreading of negatively charged phospholipid DPPA onto the 0.1 *x* DMSO solution, two broad peaks centered at ~ 1012 cm^{-1} and ~ 1120 cm^{-1} are observed. The higher frequency peak is the DPPA PO_2^- stretch as shown in Figure 8.2. The agreement of the 1012 cm^{-1} DMSO peak position with Raman spectra further proves that the lower frequency 1012 cm^{-1} peak is the S=O stretch of DMSO. This result clearly shows that the S-O vector orientation is affected by the local electric field created by the negative charge of the DPPA headgroup at surface, namely the S-O vector is more perpendicular to the surface with the oxygen pointing to the bulk as shown in Figure 8.3. This result indicates that an applied field can orient the S=O, and that this orientation can be detected. This result still does not clarify the S=O orientation at the surface of an aqueous solution, but at the least, it excludes the possibility of a rather straight down conformation of the S=O bond.

For DMSO, the two CH_3 groups are in a fixed molecular geometry, $\angle$C-S-C = 97.4°, and the angle between the S=O bond and the C-S-C plane is 64°.[195] However, the tilt angle of the CH_3 groups to the surface normal are determined by the angle between the surface normal and the C-S-C plane. Without knowing of the angle between the surface normal and the C-S-C plane, retrieval of DMSO CH_3 orientation angle is not unique.[21] Here we assume the C-S-C plane of DMSO to be perpendicular to the liquid surface, which leaves the S-O vector to be ~ 26° buried close to the surface as suggested by the MD simulation and our VSFG S=O result. The VSFG spectra in the C-H stretch region of 0.2 *x* DMSO is shown in Figure 8.4. In ssp polarization the peak centered at 2913 cm^{-1} is the CH_3 symmetric stretch.[79] This single peak has contribution from both CH_3 groups. Here we also assume that the orientation remains relatively constant at all concentrations studied as suggested by the previous concentration study.[194]

Usually the VSFG intensity ratios of different polarization combinations, i.e. ssp, ppp or sps are used to determine the average orientation of the specified group. This method is convenient when appreciable VSFG intensities can be measured in these polarization combinations. For the DMSO CH_3 groups, although there is decent intensity in ssp polarization, intensity in ppp polarization (data not shown) is more than one order of magnitude less than in ssp polarization. Using the VSFG intensity ratio to determine the DMSO CH_3 orientation could therefore be subject to a relatively large error. In this case, the CH_3 orientation can be more accurately determined through polarization null angle analysis as demonstrated in previous studies.[21, 23] In our experiment, the polarization of

IR is fixed at p while the polarization of visible is set to - 45˚ (equal mixing of s and p), so that both ssp and ppp VSFG signals can be detected. If the detection polarization angle for VSFG is set to s, only half of the intensity will be observed as shown in Figure 8.4. A certain detection polarization angle (so called null angle) can be measured at which the total output VSFG intensity vanishes. For 0.2 *x* DMSO CH_3 groups, the null angle is determined to be -10.8˚ ± 2.0˚ as shown in the inset of Figure 8.4, which corresponds to the $\chi_{eff,ppp}^{(2)}/\chi_{eff,ssp}^{(2)}$ of -0.191 ± 0.036 according to equation (2-19).

In addition, the value of the hyperpolarizability ratio (R) of DMSO CH_3 groups is required. Because the CH_3 groups are linked to sulfur atoms in DMSO, this R value is different from the terminal CH_3 groups in an alkyl chains. One way to experimentally determine the value of R is from the Raman depolarization ratio (ρ), which is 0.03 for DMSO CH_3.[198] As a result, R(CH_3) is calculated using equation (2-15) to be 2.26.

The two CH_3 groups could have different tilt angles, which can be related through the assumed molecular geometry: $\theta_1 = 97.4^\circ - \theta_2$. Using the values above, the two tilt angles are determined through equations (2-10) and (2-11) to be 27.0˚ ± 4.0˚ and 70.4˚ ± 4.0˚, respectively. This indicates that on average, while assuming that the two CH_3 group point toward the air phase, DMSO molecules are only slightly tilted from the surface normal at the surface. However, the above tilt angles of DMSO CH_3 groups are the average values retrieved using a *δ*-distribution assumption. The orientation parameter D retrieved in our experiment is 1.65 (the value at the magic angle is 1.66), which indicates that the DMSO

CH_3 groups could orient at other average tilt angles, but with relatively broad distributions.[22] Although from the relatively strong CH_3 VSFG signal, the partial ordering of DMSO molecules at the surface is anticipated.

MSA at the surface

Unlike DMSO which can only accept hydrogen bonds, MSA is both a hydrogen bond donor and acceptor. The Raman spectra of aqueous MSA in S-O stretch region are shown in Figure 8.5. The spectra reveal the sensitivity of the MSA S-O bond frequency to hydration and deprotonation. The difference between the spectra of 0.02 *x* and pure MSA is marked. A sharp peak at 1050 cm^{-1} is observed at low MSA concentration, which is assigned to the SO_3^- symmetric stretch in the dissociated form.[199] The spectral pattern remains up to 0.1 *x* MSA concentration, which is in agreement with the over 90% ionization degree of MSA at this concentration as reported in the literature.[199] When the molar ratio of MSA:water is 1:1, undissociated MSA is observed to be dominant. Meanwhile the SO_3^- peak intensity decreases significantly as concentration goes up. The peak at 1126 cm^{-1} and the shoulder around 1174 cm^{-1} are assigned to the bending mode of undissociated S-O-H and the SO_2 symmetric stretch respectively, as suggested by previous studies.[183, 199] Molecular MSA can easily form hydrogen bonds with water and itself.[183] In pure MSA, self association to form cyclic dimers should prevail, while a 1:1 MSA-water complex exists in a 0.5 *x* MSA solution. However, the Raman peak positions and intensities of the S-O-H bend and SO_2 symmetric stretch are almost identical for pure and 0.5 *x* MSA regardless of the fact that they are different species. This suggests that the

hydrogen bonds formed between MSA molecules and between MSA and water molecules are similar.

Orientation of MSA molecules at the surface is reasonably different for its molecular and ionized forms. At low concentrations (< 0.1 *x*) MSA molecules dissociate almost completely and the anion has two co-axial C_{3v} groups, the CH_3 and SO_3^-. Therefore the molecular orientation can be determined from the orientation of either the CH_3 or SO_3^- groups.

The VSFG spectra of 0.1 *x* aqueous MSA in both C-H stretch and S-O stretch regions are shown in Figure 8.6. In the C-H stretch region the sharp peak observed at 2944 cm^{-1} is from the symmetric stretch of the CH_3 group. The negative interference feature around 3030 cm^{-1} is the position of the CH_3 asymmetric stretch. The apparent peak positions are not the exact peak positions of the component peaks due to interference of adjacent resonances. In addition, the broad proton continuum intensity is clearly seen to extend down below 2800 cm^{-1}. The VSFG intensities in ppp and sps polarizations, however, are nearly undetectable, which is in accordance with previous reports.[193] Therefore it is not possible to accurately measure the CH_3 orientation based on such low spectral intensities. In contrast, the VSFG intensities of the SO_3^- group in both ssp and ppp polarizations can be collected with relatively good signal-to-noise ratios as shown in Figure 8.6. Similarly the Raman depolarization ratio $\rho(SO_3^-)$ is measured to be 0.039 ± 0.001 from a polarized Raman experiment (see Chapter 3), which then gives the hyperpolarizability ratio $R(SO_3^-)$

of 2.65 ± 0.05. Therefore based on the measured intensity ratio of ssp/ppp and the $R(SO_3^-)$ above, the average tilt angle of SO_3^- group can be determined through equation (2-10) and (2-11) to be 16.0˚ ± 2.0˚, indicating a relatively straight up conformation of MSA, aligned with the surface normal.

To check the validity of the orientation angle of SO_3^- group, one can back out this value with the measured C-H stretch intensities. The tilt angle of CH_3 group is the same as the SO_3^- group in dissociated MSA, and as determined here, it is 16˚. In addition, the Raman depolarization ratio and the hyperpolarizability ratio of the MSA CH_3 group are determined to be 0.009 ± 0.001 and 1.49 ± 0.03 (see Chapter 3). It is noticeably different between the R value of the CH_3 groups in DMSO and MSA which arises from different molecular structure and electron density. The deduced VSFG intensity ratio of ssp/ppp from the values above is ~ 20 at the 16˚ tilt angle, which in agreement with the fact that the ppp and sps intensities are almost undetectable.

8.2 Conclusion

A comprehensive investigation of the molecular structure at the aqueous DMSO/MSA surface has been completed using VSFG spectrposcopy. For DMSO molecules at the aqueous surface, the two CH_3 groups are pointing outwards into the air with tilt angles of ~ 27° and ~ 70°, respectively.. The S=O group is hydrated by the aqueous phase and points only slightly inwards to the interior of the solution. MSA molecules completely dissociate into hydrated ions at low concentrations (< 0.1 *x*). Deprotonated

methanesulfonate anions reside at the surface in a relatively straight up conformation with their SO_3^- axis pointing inward and their CH_3 axis pointing outward, with both moieties oriented ~16° from the surface normal in their residing phase, aqueous and gas, respectively.

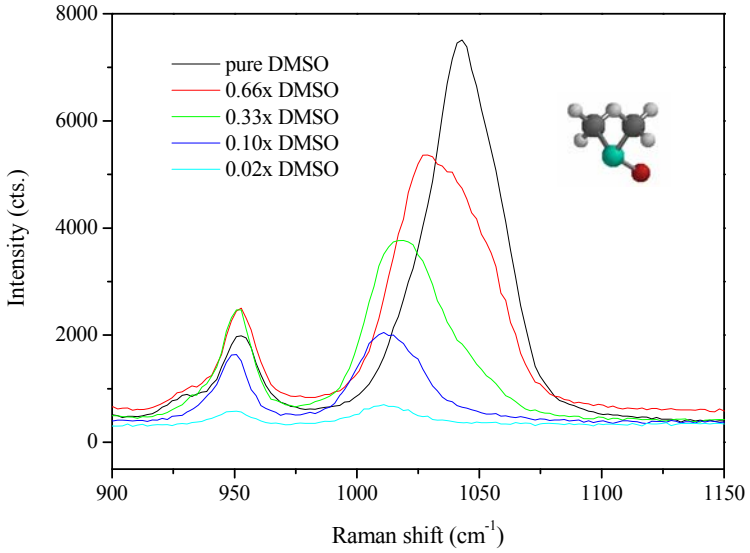

Figure 8.1. S=O stretch region Raman spectra of a series of DMSO-water mixtures. Structure of DMSO is shown in graph.

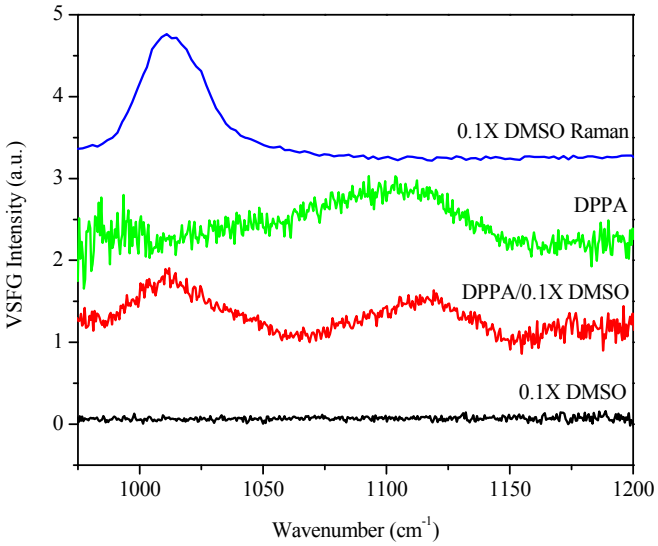

Figure 8.2. VSFG spectra in S=O region of 0.1 *x* aqueous DMSO. The impact of DPPA on DMSO orientation is shown.

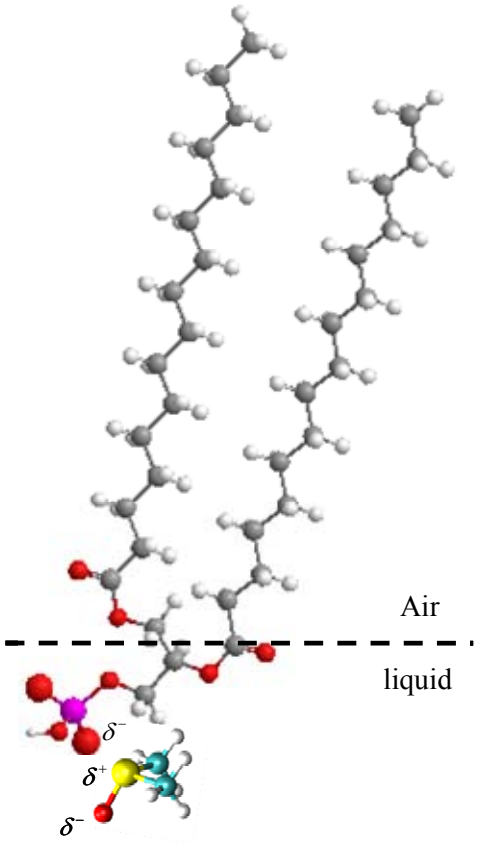

Figure 8.3. Influence of DPPA on DMSO orientation at the interface.

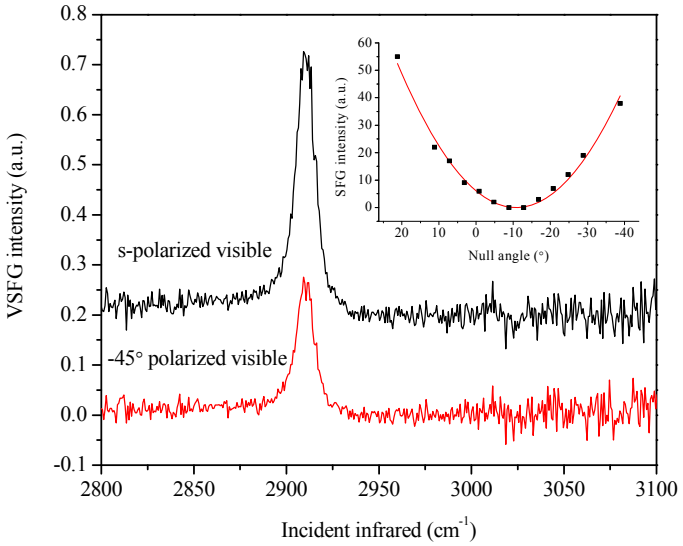

Figure 8.4. Polarization null angle study of 0.2 *x* aqueous DMSO CH_3 group. The null angle is shown in the inset.

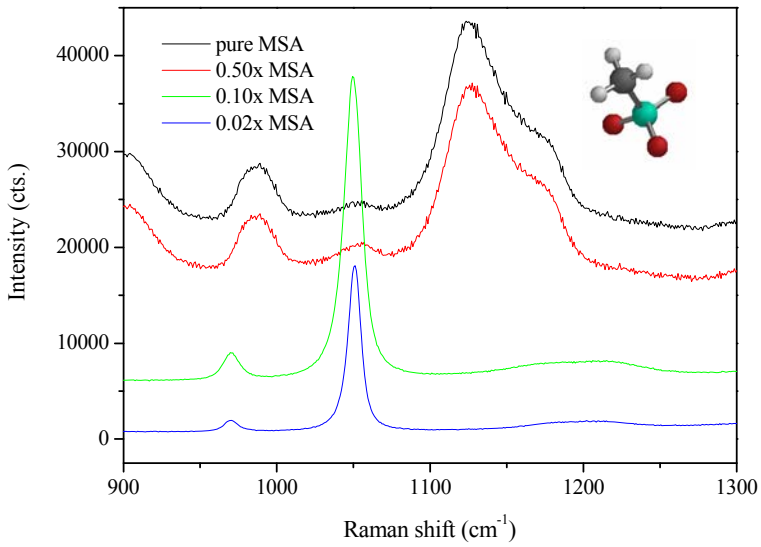

Figure 8.5. S-O stretch region Raman spectra of a series of MSA-water mixtures. Structure of dissociated MSA is shown in graph.

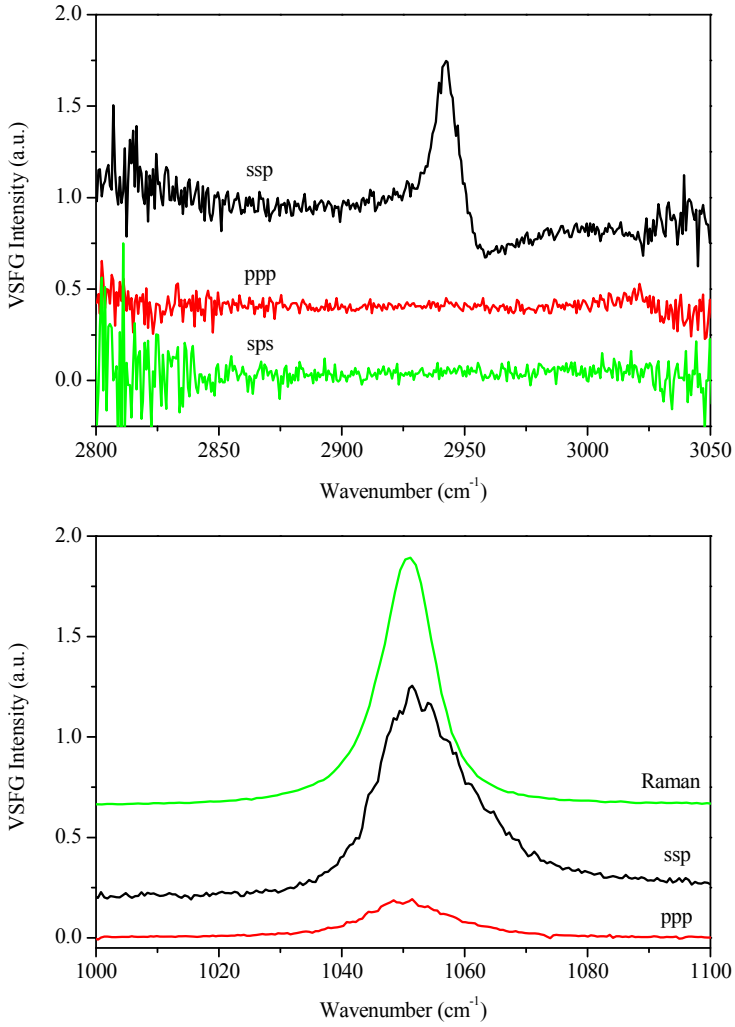

Figure 8.6. VSFG spectra in both C-H stretch (upper graph) and S-O stretch (lower graph) region of 0.1 *x* aqueous MSA.

Chapter 9: Interfacial Water structure at the air/aqueous solution surfaces of atmospherically relevant DMSO and MSA

The DMSO-water mixture represents one of the more complicated binary systems as strong interactions not only happen between the molecules of a single component but also between the two components. Even the hydrogen bonding properties of pure water alone are not completely understood.[200] Early studies of bulk DMSO-water mixtures presented various results and some do not appear consistent with each other. It has been suggested that addition of a small amounts of DMSO to water: (1) can increase the molecular ordering of water,[179, 201] (2) has little effect on the hydrogen bond of water[186] and, (3) results in "structure breaking" of water.[202, 203] From DMSO rich solutions to dilute DMSO solutions, a red-shift trend was observed for ν_b, ν_d, and ν_w (OH bonded, OH dibonded, and OH weakly bonded, respectively) in Raman spectra, revealing a disruption of long range ordering of the water hydrogen bonding network.[202]

Despite different views on the DMSO-perturbed water structure, it is unambiguously accepted that DMSO can form strong hydrogen bonds with water as a hydrogen bond acceptor. The hydrogen bond between DMSO and water is stronger than the hydrogen bond between water molecules.[182, 204] The strong hydrogen bonds formed between

DMSO and water can be evidenced by the red shift of the DMSO S=O stretching frequency with increasing water concentration.[187] The two electron lone pairs on the DMSO oxygen can accept hydrogens from water molecules, which causes the red-shift of the S=O frequency.

The MSA-water binary solution is less studied compared to DMSO-water systems. It has been shown that among the organosulfur species $DMSO_2$, DMSO, and MSA, MSA-water clusters require the least number of molecules to serve as the critical cluster for nucleation of water vapor.[176] This suggests a strong interaction between water and MSA molecules.

The formation and growth of aerosols initiated by DMSO and MSA relate to their interactions with water vapor, which addresses the importance of understanding the perturbed interfacial water structure in addition to that of the bulk aqueous solutions. In contrast with the relative abundant bulk information, the molecular structure at aqueous surfaces is still not well understood due to limited surface-specific techniques. Vibrational sum frequency generation (VSFG) spectroscopy, one of the nonlinear spectroscopic methods that can probe the thin layers of the surface, was the only characterization method utilized to study the surface water structure of aqueous solutions of DMSO and MSA.[79, 192-194] The VSFG spectra of the water hydrogen bonding region (3000 cm^{-1} to 3600 cm^{-1}) showed, as compared to the neat water surface, slight changes induced by DMSO[194] and a significant red-shift induced by MSA.[193] This was interpreted

that DMSO molecules could well incorporate into the water network and cause minimal change on the surface water structure, while MSA molecules could enhance the hydrogen bonding of surface water molecules.

However, as is shown in this work, the interpretation of VSFG water spectra would be less informative and sometimes misleading without the phase information (net polar orientation) of the vibrational modes.[24] The recently developed phase-sensitive vibrational sum frequency generation (PS-VSFG) methods[24, 25, 27] have firmly demonstrated the ability of revealing not only the *energetic* states of vibrational modes but also the net *polar orientation*, which can greatly clarify the controversial issues in VSFG spectra interpretation.

In this chapter, both conventional VSFG and phase-sensitive vibrational sum frequency generation (PS-VSFG) methods are employed to present a comprehensive study of the air/aqueous interface of DMSO and MSA solutions, revealing new information on the interfacial water structure and absolute orientation of the water molecules in the interfacial region. Water structure is elucidated at relatively low solute concentrations to explore the hydrogen bonding character changes and orientation changes of the water in different spectral regions. Typical solute concentrations are 0.02 x (mole fraction, ~ 1 M), 0.04 x (~ 2 M) and 0.1 x (~ 5 M). VSFG spectra below are denoted as conventional VSFG spectra, while phase-sensitive VSFG spectra is denoted as Im $\chi^{(2)}$ spectra.

9.1 Results and Discussion

Bulk water structure of aqueous DMSO/MSA solutions

Before discussing the influence of DMSO and MSA on the interfacial water structure, it is helpful to investigate the structural change of water in bulk. Spectroscopic methods, such as IR and Raman have been extensively used to reveal the water structure, hydrogen bonding properties, and the hydrated structure around solutes. Although much work has been done, structural understanding is still incomplete.

The Raman spectra of water and aqueous DMSO/MSA solutions are shown is Figure 9.1, and are consistent with previously published Raman data.[202] The main spectral feature of neat water is the bimodal shape centered at ~ 3220 cm^{-1} and ~ 3440 cm^{-1}, with a slight but detectable high frequency shoulder around 3630 cm^{-1}. Questions arise on how to interpret the water spectra as some try to fit the spectra with several Gaussians and attribute each to a particular molecular environment,[202, 205] while others view liquid water as a dynamical continuum and the spectra are complicated by intramolecular and intermolecular vibrational couplings.[206, 207] Upon adding DMSO or MSA into the water, the bimodal shape remains despite the decrease in intensity due to less water content. A closer examination of the spectra finds that for DMSO, there is no change in peak position up to 0.1 *x* and the bimodal shape becomes narrower at 0.33 *x* DMSO. In contrast, a blue shift of the 3440 cm^{-1} peak is observed in the presence of 0.1 *x* MSA, and the baseline of the low frequency side is clearly elevated. The spectral narrowing at relatively high DMSO concentration can come from either the DMSO-water interaction

or the reduced coupling between water molecules due to less water concentration. The blue-shift of OH stretch frequency in aqueous MSA, however, seems to imply a weakening of water hydrogen bonding network. In addition, the broad continuum which causes baseline lift indicates the existence of hydrated hydronium ions,[208] confirming the dissociation of MSA at this concentration.

Spectra of isotopically diluted water, in particular, the dilute HOD in H_2O are much simplified as most intramolecular and intermolecular vibrational couplings of OD stretch to other vibrational modes are minimized.[200, 206, 207] As a result the decoupled OD stretch displays a monomodal shape and can be used as a sensitive local probe for the water structure. The most important information from the HOD spectra is the OD peak position, which is considered to be empirically proportional to the hydrogen bond strength.[209] Figure 9.2 shows the Raman spectra of OD stretch in the presence of DMSO/MSA up to 5 M concentration (~ 0.1 *x*). As expected from the slight change of H_2O spectra by DMSO, both the band position and the width of OD stretch show no change in these DMSO concentrations. The small sharp peaks lay on the OD stretch are from DMSO CH_3 moieties. This result is in agreement with previous studies[186] and indicates that DMSO forms strong hydrogen bonds with water similar in strength to that of water-water interactions. Therefore accommodation of a relatively low amount of DMSO into the water hydrogen bonding network should not significantly change the energetic states of the overall water hydrogen bonds. This observation does not necessarily contradict with the ordering of water molecules at low DMSO concentrations. An increase in the radial

distribution function (RDF) intensity shows ordering in the spatial arrangement of oxygen atoms, while the strength of individual hydrogen bonds might remain almost unchanged.

By adding MSA, a similar blue shift of the OD stretch is observed at 5 M (~ 0.1 *x*) as in the H_2O spectra. Because MSA is mostly dissociated into hydrated ions at this concentration, the OD spectra should be considered as the "cation + anion affected" water spectra.[209] The water structure affected by other cations and anions has been systematically studied using HOD spectra.[209, 210] Terms like "structure makers" and "structure breakers" continue to be commonly used to describe the impact of solutes on water hydrogen bond strength based on the red shift and blue shift of the OD frequency, respectively. Structure making and breaking refers to the structure of water around the solute. The OD peak position was found to be correlated with surface charge density of the cations.[209, 210] Typically the affected OD peak occurs at higher frequency by monovalent metal cations and at lower frequency by divalent or trivalent metal cations. Hydronium ion, because of its high surface charge density, was shown to cause a red shift on the OH/OD stretch frequency and thus considered as a "structural maker".[211] Many anions, especially large species such as ClO_4^- are typically termed "structural breakers" and cause a blue shift of the OD stretch frequency.[209] The OD stretch in MSA blue shifts from ~ 2510 cm^{-1} to ~ 2550 cm^{-1}, which coincidences with the OD frequency shift caused by methanesulfonate anion ($CH_3SO_3^-$).[209] Therefore the overall hydrogen bond strength of dilute OD is weakened by 0.1 *x* MSA, which is mainly due to the hydrated

methanesulfonate anion through ion-dipole interaction. The OD stretch shift caused by MSA is not only observed in Raman spectra, but is also observed in FT-IR absorption spectra as shown in Figure 9.3.

Surface water structure of aqueous DMSO/MSA solutions

The different interaction mechanism of DMSO and MSA with water will certainly alter the surface water structure due to their notable surface preference.[79, 193] The VSFG spectra in water stretch region of 1 M (~ 0.02 *x*) and 2 M (~ 0.04 *x*) DMSO/MSA are shown in Figure 9.4. Our conventional VSFG spectra of neat water and aqueous DMSO/MSA solutions agree well with previous studies. Our PS-VSFG data are the first to be published however for these systems. For conventional VSFG neat water spectra, the unbound dangling OH stretch manifests as a sharp peak at 3700 cm^{-1} and the hydrogen bonded OH stretch is observed in bimodal shape between 3000 cm^{-1} and 3600 cm^{-1}. Similar to bulk water, the interpretation of the VSFG spectra of the hydrogen bonded region has not been fully agreed upon. The two characteristic bands centered at ~ 3200 cm^{-1} and ~ 3400 cm^{-1} are commonly labeled as "ice-like" and "liquid-like" water structures owing to their spectral similarity with the bulk ice and liquid water.[103] Other assignments such as "strongly/weakly hydrogen bonded" or "symmetrically/asymmetrically 4-coordinated" water structures are also mentioned.[145, 146]

For the dangling OH region, a decrease in intensity is observed for 1 M DMSO and MSA solutions. This decrease becomes much more obvious for 2 M DMSO and MSA

concentration, indicating the topmost water molecules are replaced or hydrogen bonded by solutes. The perturbation of DMSO and MSA on the dangling OH is very different with the effect of solvated simple ions, i.e. H^+, OH^-, Na^+ and halogen anions which leave the dangling OH little changed.[158] This difference should arise from the hydrophobic CH_3 moieties of DMSO and MSA, which lead to their preferential existence at the outermost surface. Previous MD simulations also suggested the free OH decrease with increasing DMSO concentration.[195]

The VSFG spectra of hydrogen bonded region of aqueous DMSO and MSA are quite different. The change in this region induced by DMSO seems to be small. The 3200 cm^{-1} band is little affected, which was explained by the well incorporation of DMSO into the interfacial water and the preservation of symmetrical hydrogen bonding environment. The slightly increased intensity near ~ 3300 cm^{-1} was attributed to a strengthened tetrahedral water environment due to strong DMSO-water interactions.[194] On the contrary, significant decrease in the hydrogen bonded region, especially the 3400 cm^{-1} band is observed in 2 M aqueous MSA and the overall hydrogen bonded region is somewhat red-shifted. This seems to suggest that MSA enhances the interfacial hydrogen bonding network.[193]

However, because the conventional VSFG intensity is proportional to the absolute square of the nonlinear susceptibility, $|\chi^{(2)}|^2$, the phase (polar orientation) of each band and their interference are unknown and subject to arbitrary fitting procedures. Therefore

interpretation of water structure based on VSFG spectra is less informative and even could be wrong.[25, 152] Recently phase-sensitive VSFG (PS-VSFG) methods have been developed on both scanning SFG system and broad bandwidth SFG systems.[25, 27] In PS-VSFG spectra, the imaginary part of $\chi^{(2)}$ is obtained hence giving implications on the net polar orientation on the isotropic liquid surface. Figure 9.5 shows the Im $\chi^{(2)}$ spectra in the hydrogen bonded region of neat water and 2 M aqueous DMSO and MSA. Remarkable differences are revealed as compared to the VSFG spectra and are discussed below. The assignment of Im $\chi^{(2)}$ spectrum of neat water has been suggested by Shen and co-workers, [25] the negative region from 3450 cm^{-1} to 3600 cm^{-1} has been assigned to donor-bonded OH stretches of 3-coordinate DDA and DAA water molecules in the topmost layer. (Here D and A denote donor and acceptor hydrogen bonds respectively, with which water molecules hydrogen bond to nearest neighbors.) The negative region from 3200 cm^{-1} to 3450 cm^{-1} has been assigned to loosely hydrogen bonded 4-coordinate DDAA molecules, while the positive region from 3000 cm^{-1} to 3200 cm^{-1} was mainly attributed to strongly hydrogen bonded DDAA molecules. The above assigned spectral regions overlap with each other, which leads to a crossover point around 3200 cm^{-1}. The negative sign in an Im $\chi^{(2)}$ spectrum corresponds to the OH stretches with a net orientation of the hydrogens pointing down towards the bulk and the positive sign corresponds to a net orientation with hydrogens pointing up.

For 2 M aqueous DMSO, the surface water structure is greatly changed despite the resemblance of the VSFG spectra. As seen in Figure 9.5, the sign of OH stretch becomes

positive throughout the hydrogen bonded region in 2 M aqueous DMSO, revealing a net up orientation of water dipoles (pointing from oxygen to hydrogen). That is, the presence of sufficient DMSO molecules at the surface re-orients the loosely hydrogen bonded DDAA molecules at surface. This reorientation should be directly related to the hydrogen bond formed between DMSO and water. As shown previously,[79, 195] surface DMSO molecules would prefer to orient with the CH_3 groups pointing up and the S=O group pointing slightly inwards. Water fraction at the topmost layer is therefore greatly reduced. To form hydrogen bonds with the oxygen on S=O moiety at the surface, interfacial water molecules thus reorient and point with their hydrogen up to the DMSO oxygen. The reorientation of water molecules under perturbation of DMSO was noticed in previous VSFG study but is not firmly concluded because the strengthening of hydrogen bond could result in similar change in VSFG spectra.[194]

The Im $\chi^{(2)}$ spectrum of 2 M MSA is also interesting, with the positive band below 3200 cm^{-1} less affected and the negative band around 3400 cm^{-1} nearly vanished. Surface water structure is perturbed by both the hydrated methanesulfonate anion and the hydrated hydronium cations. The resulted Im $\chi^{(2)}$ spectrum, however, looks like neither the anion affected nor the hydronium ion affected Im $\chi^{(2)}$ spectra. For the Im $\chi^{(2)}$ spectra of water in the presence of anions at the outmost surface, i.e. deprotonated fatty acid, the sign of the overall hydrogen bonded region is all positive, as dictated by the surface anions.[212] On the contrary, for acidic HCl and HI solutions, the sign of the overall hydrogen bonded region is all negative in Im $\chi^{(2)}$ spectra,[158] suggesting that hydronium ions have more

surface excess than the halogen anions and thus create a surface field inducing OH pointing down. In the case of MSA, both the methanesulfonate anion and the hydronium ion have surface preference as compared to the bulk. However, the methanesulfonate anions should have more surface excess than the hydronium ions as evidenced by their impact on the dangling OH. Overall, the surface methanesulfonate anions tend to orient interfacial water molecules with their dipoles pointing up, which however, are partially offset by the hydronium ions at the surface. The resulted surface electric double layer (EDL) is thin and the overall VSFG power spectrum intensity is low.

9.2 Conclusion

A comprehensive investigation of the molecular structure at the aqueous DMSO and MSA surfaces has been made. The results imply that both DMSO and MSA molecules have surface preference which decreases the dangling OH fraction at the surface. For surface DMSO molecules, the S=O group at the surface forms strong hydrogen bonds with water, which results in reorientation of interfacial water molecules with their hydrogens pointing up towards the oxygen of the S=O group. MSA molecules completely dissociate into hydrated ions at low concentrations ($< 0.1\ x$). The interfacial water structure is therefore affected by both the methanesulfonate anions and the hydronium ions residing at the surface. The electric double layer (EDL) at the surface formed by the methanesulfonate anions and the hydronium ions is thin which leads to an overall decrease in the VSFG intensity.

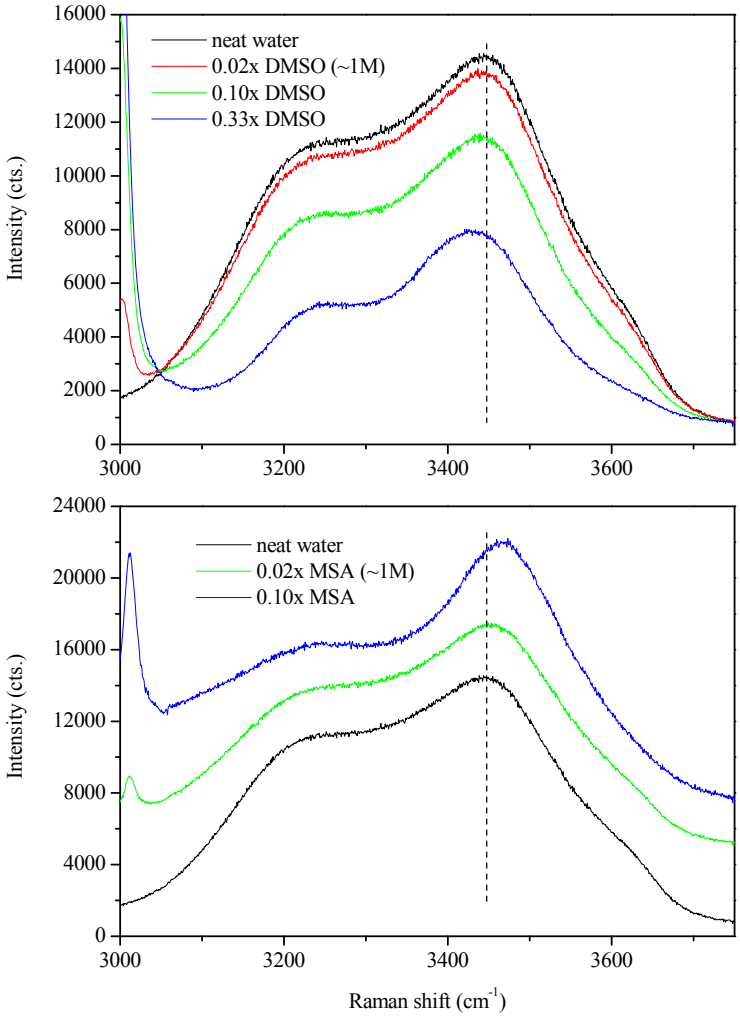

Figure 9.1. Water region Raman spectra of a series of DMSO-water (top) and MSA-water mixtures (bottom)

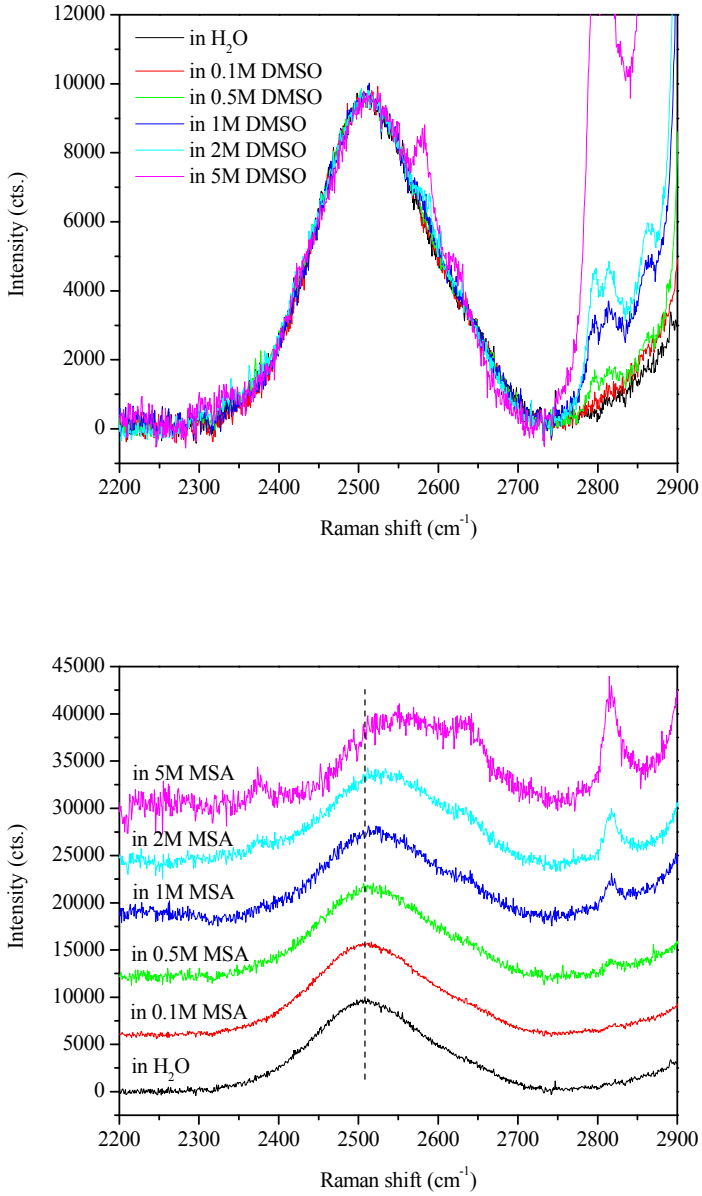

Figure 9.2. O-D stretch region Raman spectra of dilute OD (D_2O : H_2O = 4: 96) in DMSO-H_2O (top) and MSA-H_2O mixtures (bottom).

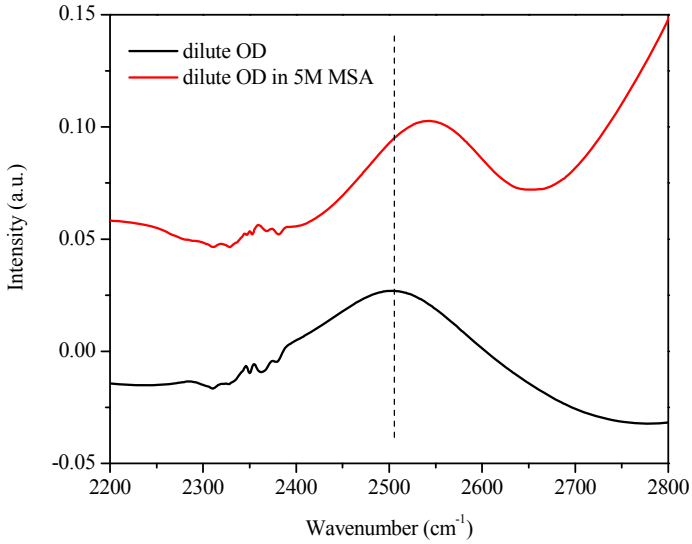

Figure 9.3. Transmission IR absorption spectra of dilute OD (D_2O : H_2O = 4: 96) in MSA-H_2O mixtures.

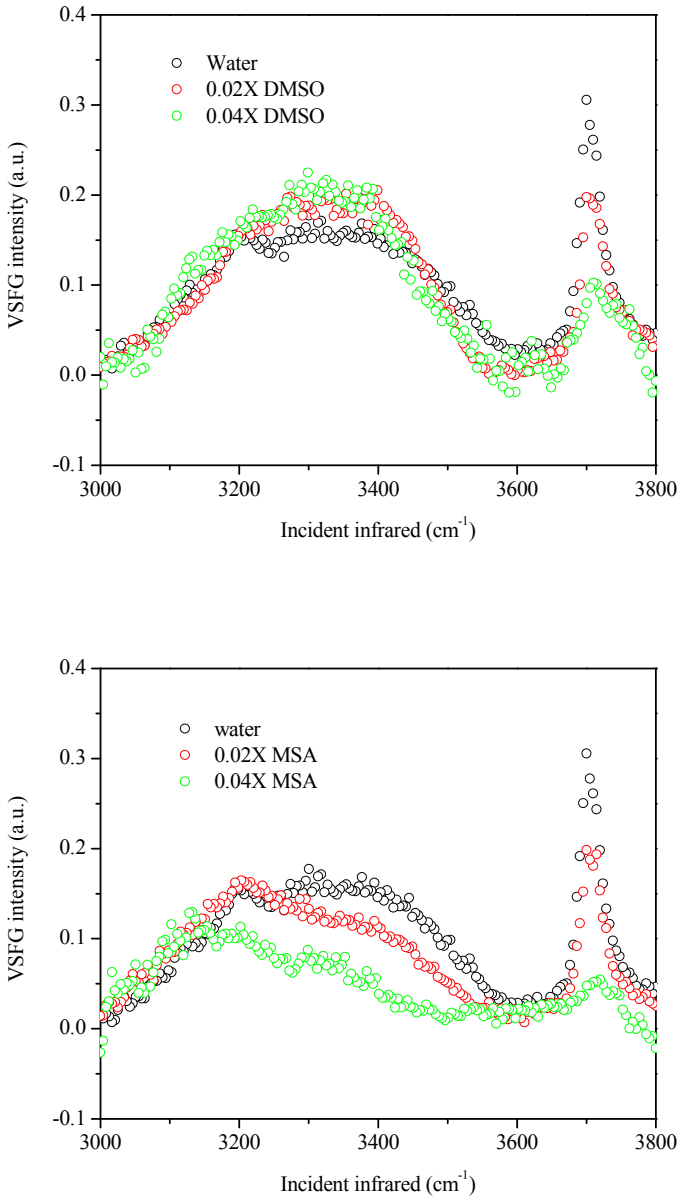

Figure 9.4. VSFG in water stretch region of DMSO-water mixtures (top) and MSA-water mixtures (bottom).

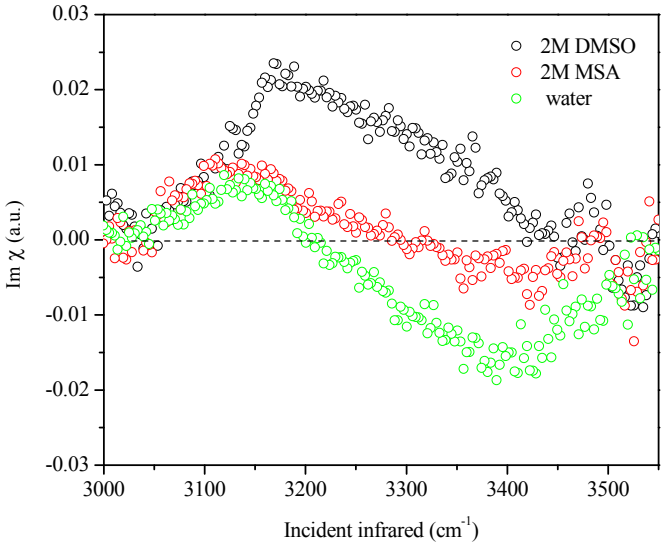

Figure 9.5. Im $\chi^{(2)}$ spectra in water region of 2 M DMSO, 2 M MSA, and neat water.

Chapter 10: Biological and Environmental Implications

The work presented in this dissertation was motivated by the growing interest for the understanding of the molecular organization and interaction at the biological and atmospheric relevant interfaces. For this aim, vibrational sum frequency generation (VSFG), a surface (interface) specific nonlinear spectroscopic technique, is utilized to investigate the air/membrane/water interfaces and air/aqueous DMSO/MSA interfaces.

The VSFG study of model phospholipid (DPPC) monolayer demonstrates the advantages, i.e. the surface specificity, the sub-monolayer sensitivity, and the unique selection rule provided by VSFG. With these advantages, various important properties such as the phospholipid organization, hydration, and phase behavior can be directly probed. The application of VSFG to study model membranes sets forth an example for study of a broad variety of biomolecules, i.e. lipids, nucleic acid, and proteins which form self-assemblies at the biologic interfaces.

The interactions between DMSO and model phospholipid monolayers observed in this work provide direct experimental evidence for the possible molecular mechanism of the membrane permeability enhancement. Especially the shown permeability enhancement

by DMSO is not due to chemical-specific interactions but the physical surface pressure, which broadens its implication to various biological membranes which are not comprised mainly of phospholipids, i.e. skin. This observed mechanism could apply to other substances with similar structure properties as DMSO, giving insight for future choice of membrane penetration enhancers. In addition, to effectively enhance the membrane permeability, it has been revealed that the surface pressure of DMSO must be higher than the liquid expanded (LE) to liquid condensed (LC) phase transition plateau of DPPC monolayer, which provide guidance for the usage of the penetration enhancers. Moreover, other membrane involved interactions, i.e. membrane-protein interactions, membrane-DNA interactions, and membrane-ion interactions are similarly could be investigated.

The interfacial water structures have always been important because of the involvement of water in many processes happened at the biological interfaces. Compared with the conventional VSFG, the phase-sensitive VSFG points out the future direction for surface studies because it provides both the spectral and polar orientation information. The spectral information of interfacial water structure reveals the nature of lipid-water interactions, while the orientation information provides insights for the origin of the hydration forces between membranes. Therefore the role of water in the interactions at the membrane surfaces, such as membrane and vesicle fusion can be better understood.

The surface activity and organization of DMSO and MSA are shown. Their strong hydrogen bonding ability with water facilitates the water vapor nucleation at the interface

and the growth of aerosols. In addition, the surface activity is the prerequisite for further heterogeneous reactions taking place, which leads to formation of H2SO4 eventually. For aqueous MSA solutions, the presence of hydronium ions at the surface shown in this work would affect the physical properties and the chemistry of atmospheric aerosol surfaces, which can lead to absorption of volatile molecules, oxidation reactions and particle growth.

References

1. Edidin, M., *Nat. Rev. Mol. Cell Biol.* **2003,** 4, 414.
2. Zimmerberg, J.; Gawrisch, K., *Nat. Chem. Biol.* **2006,** 2, 564.
3. Singer, S. J.; Nicolson, G. L., *Science* **1972,** 175, 720.
4. Lindblom, G.; Rilfors, L.; Hauksson, J. B.; Brentel, I.; Sjolund, M.; Bergenstahl, B., *Biochemistry* **1991,** 30, 10938.
5. Minones, J.; Patino, J. M. R.; Conde, O.; Carrera, C.; Seoane, R., *Colloid Surf. A-Physicochem. Eng. Asp.* **2002,** 203, 273.
6. Berkowitz, M. L.; Bostick, D. L.; Pandit, S., *Chem. Rev.* **2006,** 106, 1527.
7. Phillips, M. C.; Chapman, D., *Biochimica Et Biophysica Acta* **1968,** 163, 301.
8. Paltauf, F.; Hauser, H.; Phillips, M. C., *Biochimica Et Biophysica Acta* **1971,** 249, 539.
9. Ellison, G. B.; Tuck, A. F.; Vaida, V., *J. Geophys. Res.-Atmos.* **1999,** 104, 11633.
10. Schwartz, S. E., *Nature* **1988,** 336, 441.
11. Wakeham, S. G.; Dacey, J. W. H., *Acs Symposium Series* **1989,** 393, 152.
12. Yin, F. D.; Grosjean, D.; Seinfeld, J. H., *J. Atmos. Chem.* **1990,** 11, 309.
13. Barone, S. B.; Turnipseed, A. A.; Ravishankara, A. R., *Faraday Discuss.* **1995,** 100, 39.
14. Schweitzer, F.; Magi, L.; Mirabel, P.; George, C., *J. Phys. Chem. A* **1998,** 102, 593.
15. Charlson, R. J.; Lovelock, J. E.; Andreae, M. O.; Warren, S. G., *Nature* **1987,** 326, 655.
16. Charlson, R. J.; Schwartz, S. E.; Hales, J. M.; Cess, R. D.; Coakley, J. A.; Hansen, J. E.; Hofmann, D. J., *Science* **1992,** 255, 423.
17. von Glasow, R.; von Kuhlmann, R.; Lawrence, M. G.; Platt, U.; Crutzen, P. J., *Atmos. Chem. Phys.* **2004,** 4, 2481.
18. Hirose, C.; Akamatsu, N.; Domen, K., *J. Chem. Phys.* **1992,** 96, 997.
19. Zhuang, X.; Miranda, P. B.; Kim, D.; Shen, Y. R., *Phys. Rev. B* **1999,** 59, 12632.
20. Lambert, A. G.; Davies, P. B.; Neivandt, D. J., *Appl. Spectrosc. Rev.* **2005,** 40, 103.
21. Wang, H. F.; Gan, W.; Lu, R.; Rao, Y.; Wu, B. H., *Int. Rev. Phys. Chem.* **2005,** 24, 191.
22. Simpson, G. J.; Rowlen, K. L., *J. Am. Chem. Soc.* **1999,** 121, 2635.
23. Groenzin, H.; Li, I.; Shultz, M. J., *J. Chem. Phys.* **2008,** 128.
24. Shen, Y. R.; Ostroverkhov, V., *Chem. Rev.* **2006,** 106, 1140.

25. Ji, N.; Ostroverkhov, V.; Tian, C. S.; Shen, Y. R., *Phys. Rev. Lett.* **2008,** 100, 096102.
26. Stiopkin, I. V.; Jayathilake, H. D.; Bordenyuk, A. N.; Benderskii, A. V., *J. Am. Chem. Soc.* **2008,** 130, 2271.
27. Nihonyanagi, S.; Yamaguchi, S.; Tahara, T., *J. Chem. Phys.* **2009,** 130, 204704.
28. Yamaguchi, S.; Tahara, T., *J. Chem. Phys.* **2008,** 129, 101102.
29. Gan, W.; Wu, D.; Zhang, Z.; Feng, R. R.; Wang, H. F., *J. Chem. Phys.* **2006,** 124, 114705.
30. Hommel, E. L.; Allen, H. C., *Anal. Sci.* **2001,** 17, 137.
31. Ma, G.; Allen, H. C., *Langmuir* **2006,** 22, 5341.
32. Tang, C. Y.; Allen, H. C., *J. Phys. Chem. A* **2009,** 113, 7383.
33. Rall, W. F.; Fahy, G. M., *Nature* **1985,** 313, 573.
34. Anchordoguy, T. J.; Rudolph, A. S.; Carpenter, J. F.; Crowe, J. H., *Cryobiology* **1987,** 24, 324.
35. Anchordoguy, T. J.; Cecchini, C. A.; Crowe, J. H.; Crowe, L. M., *Cryobiology* **1991,** 28, 467.
36. Anchordoguy, T. J.; Carpenter, J. F.; Crowe, J. H.; Crowe, L. M., *Biochimica Et Biophysica Acta* **1992,** 1104, 117.
37. Yu, Z. W.; Quinn, P. J., *Mol. Membr. Biol.* **1998,** 15, 59.
38. Barry, B. W., *Nat. Biotechnol.* **2004,** 22, 165.
39. Williams, A. C.; Barry, B. W., *Adv. Drug Deliv. Rev.* **2004,** 56, 603.
40. Ahkong, Q. F.; Fisher, D.; Tampion, W.; Lucy, J. A., *Nature* **1975,** 253, 194.
41. Lyman, G. H.; Preisler, H. D.; Papahadjopoulos, D., *Nature* **1976,** 262, 360.
42. Yu, Z. W.; Quinn, P. J., *Biosci. Rep.* **1994,** 14, 259.
43. Yu, Z. W.; Quinn, P. J., *Biophys. J.* **1995,** 69, 1456.
44. Tristram-Nagle, S.; Moore, T.; Petrache, H. I.; Nagle, J. F., *Biochim. Biophys. Acta-Biomembr.* **1998,** 1369, 19.
45. Long, C. J.; Hmel, P. J.; Kennedy, A.; Quiles, J. G.; Seelbaugh, J.; Reid, T. J., *J. Liposome Res.* **2003,** 13, 249.
46. Kiselev, M. A.; Lesieur, P.; Kisselev, A. M.; Grabielle-Madelmond, C.; Ollivon, M., *J. Alloy. Compd.* **1999,** 286, 195.
47. Krasteva, N.; Vollhardt, D.; Brezesinski, G.; Mohwald, H., *Langmuir* **2001,** 17, 1209.
48. Gorshkova, J. E.; Gordeliy, V. I., *Crystallogr. Rep.* **2007,** 52, 535.
49. Kiselev, M. A., *Crystallogr. Rep.* **2007,** 52, 529.
50. Kennedy, A.; Long, C. J.; Hmel, P. J.; Hicks, R.; Reid, T. J., *Spectr.-Int. J.* **2004,** 18, 265.
51. Paci, E.; Marchi, M., *Mol. Simul.* **1994,** 14, 1.
52. Smondyrev, A. M.; Berkowitz, M. L., *Biophys. J.* **1999,** 76, 2472.
53. Sum, A. K.; de Pablo, J. J., *Biophys. J.* **2003,** 85, 3636.
54. Leekumjorn, S.; Sum, A. K., *Biochim. Biophys. Acta-Biomembr.* **2006,** 1758, 1751.
55. Notman, R.; Noro, M.; O'Malley, B.; Anwar, J., *J. Am. Chem. Soc.* **2006,** 128, 13982.

56. Gurtovenko, A. A.; Anwar, J., *J. Phys. Chem. B* **2007,** 111, 10453.
57. Gordeliy, V. I.; Kiselev, M. A.; Lesieur, P.; Pole, A. V.; Teixeira, J., *Biophys. J.* **1998,** 75, 2343.
58. Richmond, G. L.; Walker, R. A.; Smiley, B. L., *Spectroscopy* **1999,** 14, 18.
59. Roke, S.; Schins, J.; Muller, M.; Bonn, M., *Phys. Rev. Lett.* **2003,** 90, 128101.
60. Sovago, M.; Wurpel, G. W. H.; Smits, M.; Muller, M.; Bonn, M., *J. Am. Chem. Soc.* **2007,** 129, 11079.
61. Liu, J.; Conboy, J. C., *J. Am. Chem. Soc.* **2004,** 126, 8894.
62. Anderson, N. A.; Richter, L. J.; Stephenson, J. C.; Briggman, K. A., *Langmuir* **2006,** 22, 8333.
63. Anderson, N. A.; Richter, L. J.; Stephenson, J. C.; Briggman, K. A., *J. Am. Chem. Soc.* **2007,** 129, 2094.
64. McConlogue, C. W.; Malamud, D.; Vanderlick, T. K., *Biochim. Biophys. Acta-Biomembr.* **1998,** 1372, 124.
65. Can, S. Z.; Chang, C. F.; Walker, R. A., *Biochim. Biophys. Acta-Biomembr.* **2008,** 1778, 2368.
66. Tabak, S. A.; Notter, R. H., *Rev. Sci. Instrum.* **1977,** 48, 1196.
67. Notter, R. H.; Tabak, S. A.; Mavis, R. D., *Journal of Lipid Research* **1980,** 21, 10.
68. Markarian, S. A.; Terzyan, A. M., *J. Chem. Eng. Data* **2007,** 52, 1704.
69. Pohle, W.; Selle, C.; Fritzsche, H.; Bohl, M., *J. Mol. Struct.* **1997,** 408, 273.
70. Grabiellemadelmont, C.; Perron, R., *Journal of Colloid and Interface Science* **1983,** 95, 483.
71. Shashkov, S. N.; Kiselev, M. A.; Tioutiounnikov, S. N.; Kiselev, A. M.; Lesieur, P., *Physica B* **1999,** 271, 184.
72. Mrazkova, E.; Hobza, P.; Bohl, M.; Gauger, D. R.; Pohle, W., *J. Phys. Chem. B* **2005,** 109, 15126.
73. Gauger, D. R.; Selle, C.; Fritzsche, H.; Pohle, W., *J. Mol. Struct.* **2001,** 565-566, 25.
74. Harper, K. L.; Allen, H. C., *Langmuir* **2007,** 23, 8925.
75. Walker, R. A.; Conboy, J. C.; Richmond, G. L., *Langmuir* **1997,** 13, 3070.
76. Walker, R. A.; Gruetzmacher, J. A.; Richmond, G. L., *J. Am. Chem. Soc.* **1998,** 120, 6991.
77. Gurau, M. C.; Lim, S.-M.; Castellana, E. T.; Albertorio, F.; Kataoka, S.; Cremer, P. S., *J. Am. Chem. Soc.* **2004,** 126, 10522.
78. Liu, J.; Conboy, J. C., *J. Phys. Chem. C* **2007,** 111, 8988.
79. Allen, H. C.; Gragson, D. E.; Richmond, G. L., *J. Phys. Chem. B* **1999,** 103, 660.
80. Ye, S.; Noda, H.; Nishida, T.; Morita, S.; Osawa, M., *Langmuir* **2004,** 20, 357.
81. Ohe, C.; Ida, Y.; Matsumoto, S.; Sasaki, T.; Goto, Y.; Noi, A.; Tsurumaru, T.; Itoh, K., *J. Phys. Chem. B* **2004,** 108, 18081.
82. Brezesinski, G.; Dietrich, A.; Struth, B.; Boehm, C.; Bouwman, W. G.; Kjaer, K.; Moehwald, H., *Chem. Phys. Lipids* **1995,** 76, 145.
83. Dominguez, H.; Smondyrev, A. M.; Berkowitz, M. L., *J. Phys. Chem. B* **1999,** 103, 9582.

84. Cascales, J. J. L.; Otero, T. F.; Smith, B. D.; Gonzalez, C.; Marquez, M., *J. Phys. Chem. B* **2006,** 110, 2358.
85. Zubay, G., *Biochemistry, second edition, Macmillan, New York* **1988**, 154.
86. Jacob, S. W., *CURRENT THERAPEUTIC RESEARCH-CLINICAL AND EXPERIMENTAL* **1964,** 6, 134.
87. Kligman, A. M., *Journal of the American Medical Association* **1965,** 193, 796.
88. Chen, X. K.; Allen, H. C., *J. Phys. Chem. A* **2009,** 113, 12655.
89. Henon, S.; Meunier, J., *Rev. Sci. Instrum.* **1991,** 62, 936.
90. Honig, D.; Mobius, D., *J. Phys. Chem.* **1991,** 95, 4590.
91. Hifeda, Y. F.; Rayfield, G. W., *Langmuir* **1992,** 8, 197.
92. Pallas, N. R.; Pethica, B. A., *Langmuir* **1985,** 1, 509.
93. Mason, J. T.; Oleary, T. J., *Biophys. J.* **1990,** 58, 277.
94. Seimiya, T.; Ohki, S., *Nature-New Biology* **1972,** 239, 26.
95. Hauser, H.; Darke, A.; Phillips, M. C., *Eur. J. Biochem.* **1976,** 62, 335.
96. Jing, W. G.; Prenner, E. J.; Vogel, H. J.; Waring, A. J.; Lehrer, R. I.; Lohner, K., *J. Pept. Sci.* **2005,** 11, 735.
97. Levinger, N. E., *Science* **2002,** 298, 1722.
98. Buch, V.; Devlin, J. P., *Water in Confining Geometries*. Springer: Berlin, 2003.
99. Papoian, G. A.; Ulander, J.; Eastwood, M. P.; Luthey-Schulten, Z.; Wolynes, P. G., *Proc. Natl. Acad. Sci. U. S. A.* **2004,** 101, 3352.
100. Levy, Y.; Onuchic, J. N., *Proc. Natl. Acad. Sci. U. S. A.* **2004,** 101, 3325.
101. Knipping, E. M.; Lakin, M. J.; Foster, K. L.; Jungwirth, P.; Tobias, D. J.; Gerber, R. B.; Dabdub, D.; Finlayson-Pitts, B. J., *Science* **2000,** 288, 301.
102. Garrett, B. C., *Science* **2004,** 303, 1146.
103. Du, Q.; Superfine, R.; Freysz, E.; Shen, Y. R., *Phys. Rev. Lett.* **1993,** 70, 2313.
104. Rowland, B.; Fisher, M.; Devlin, J. P., *J. Chem. Phys.* **1991,** 95, 1378.
105. Wei, X.; Miranda, P. B.; Shen, Y. R., *Phys. Rev. Lett.* **2001,** 86, 1554.
106. Du, Q.; Freysz, E.; Shen, Y. R., *Science* **1994,** 264, 826.
107. Scatena, L. F.; Brown, M. G.; Richmond, G. L., *Science* **2001,** 292, 908.
108. Pribble, R. N.; Zwier, T. S., *Science* **1994,** 265, 75.
109. Chandler, D., *Nature* **2005,** 437, 640.
110. Gaines, G. L., *Insoluble Monolayers at Liquid-Gas Interfaces*. Interscience Publishers: New York, 1966.
111. Kaganer, V. M.; Mohwald, H.; Dutta, P., *Reviews of Modern Physics* **1999,** 71, 779.
112. Morita, A.; Hynes, J. T., *Chem. Phys.* **2000,** 258, 371.
113. Liu, W.-T.; Zhang, L.; Shen, Y. R., *J. Chem. Phys.* **2006,** 125, 144711.
114. Lenz, A.; Ojamaee, L., *J. Phys. Chem. A* **2006,** 110, 13388.
115. Mucha, M.; Frigato, T.; Levering, L. M.; Allen, H. C.; Tobias, D. J.; Dang, L. X.; Jungwirth, P., *J. Phys. Chem. B* **2005,** 109, 7617.
116. Scatena, L. F.; Richmond, G. L., *J. Phys. Chem. B* **2001,** 105, 11240.
117. Sun, F., *Biophys. J.* **2002,** 82, 2511.
118. Blume, A.; Huebner, W.; Messner, G., *Biochemistry* **1988,** 27, 8239.

119. Israelachvili, J. N., *Intermolecular and Surface Forces*. 2nd ed.; Academic Press: San Diego, 1991.
120. Tanford, C., *Science* **1978,** 200, 1012.
121. Lum, K.; Chandler, D.; Weeks, J. D., *J. Phys. Chem. B* **1999,** 103, 4570.
122. Lee, C. Y.; McCammon, J. A.; Rossky, P. J., *J. Chem. Phys.* **1984,** 80, 4448.
123. Jensen, T. R.; Ostergaard Jensen, M.; Reitzel, N.; Balashev, K.; Peters, G. H.; Kjaer, K.; Bjornholm, T., *Phys. Rev. Lett.* **2003,** 90, 086101.
124. Zhang, X.; Zhu, Y.; Granick, S., *Science* **2002,** 295, 663.
125. Singh, S.; Houston, J.; van Swol, F.; Brinker, C. J., *Nature* **2006,** 442, 526.
126. Doshi, D. A.; Watkins, E. B.; Israelachvili, J. N.; Majewski, J., *Proc. Natl. Acad. Sci. U. S. A.* **2005,** 102, 9458.
127. Ma, G.; Chen, X. K.; Allen, H. C., *J. Am. Chem. Soc.* **2007,** 129, 14053.
128. Rand, R. P.; Parsegian, V. A., *Biochimica Et Biophysica Acta* **1989,** 988, 351.
129. Gawrisch, K.; Ruston, D.; Zimmerberg, J.; Parsegian, V. A.; Rand, R. P.; Fuller, N., *Biophys. J.* **1992,** 61, 1213.
130. Milhaud, J., *Biochim. Biophys. Acta-Biomembr.* **2004,** 1663, 19.
131. Volke, F.; Eisenblatter, S.; Galle, J.; Klose, G., *Chem. Phys. Lipids* **1994,** 70, 121.
132. Konig, S.; Sackmann, E.; Richter, D.; Zorn, R.; Carlile, C.; Bayerl, T. M., *J. Chem. Phys.* **1994,** 100, 3307.
133. Fitter, J.; Lechner, R. E.; Dencher, N. A., *J. Phys. Chem. B* **1999,** 103, 8036.
134. Nagle, J. F.; Tristram-Nagle, S., *Biochim. Biophys. Acta-Rev. Biomembr.* **2000,** 1469, 159.
135. Hubner, W.; Blume, A., *Chem. Phys. Lipids* **1998,** 96, 99.
136. Pohle, W.; Selle, C.; Fritzsche, H.; Binder, H., *Biospectroscopy* **1998,** 4, 267.
137. Binder, H., *Appl. Spectrosc. Rev.* **2003,** 38, 15.
138. Binder, H., *Eur. Biophys. J. Biophys. Lett.* **2007,** 36, 265.
139. Alper, H. E.; Bassolinoklimas, D.; Stouch, T. R., *J. Chem. Phys.* **1993,** 99, 5547.
140. Marrink, S. J.; Berkowitz, M.; Berendsen, H. J. C., *Langmuir* **1993,** 9, 3122.
141. Zhou, F.; Schulten, K., *J. Phys. Chem.* **1995,** 99, 2194.
142. Jedlovszky, P.; Mezei, M., *J. Phys. Chem. B* **2001,** 105, 3614.
143. Lopez, C. F.; Nielsen, S. O.; Klein, M. L.; Moore, P. B., *J. Phys. Chem. B* **2004,** 108, 6603.
144. Gragson, D. E.; Richmond, G. L., *J. Phys. Chem. B* **1998,** 102, 3847.
145. Richmond, G. L., *Chem. Rev.* **2002,** 102, 2693.
146. Gopalakrishnan, S.; Liu, D. F.; Allen, H. C.; Kuo, M.; Shultz, M. J., *Chem. Rev.* **2006,** 106, 1155.
147. Sovago, M.; Campen, R. K.; Wurpel, G. W. H.; Muller, M.; Bakker, H. J.; Bonn, M., *Phys. Rev. Lett.* **2008,** 100, 173901.
148. Fan, Y. B.; Chen, X.; Yang, L. J.; Cremer, P. S.; Gao, Y. Q., *J. Phys. Chem. B* **2009,** 113, 11672.
149. Kim, J.; Kim, G.; Cremer, P. S., *Langmuir* **2001,** 17, 7255.
150. Watry, M. R.; Tarbuck, T. L.; Richmond, G. L., *J. Phys. Chem. B* **2003,** 107, 512.
151. Chen, X. Y.; Clarke, M. L.; Wang, J.; Chen, Z., *Int. J. Mod. Phys. B* **2005,** 19, 691.

152. Ostroverkhov, V.; Waychunas, G. A.; Shen, Y. R., *Phys. Rev. Lett.* **2005,** 94, 046102.
153. Tian, C. S.; Shen, Y. R., *J. Am. Chem. Soc.* **2009,** 131, 2790.
154. Sovago, M.; Vartiainen, E.; Bonn, M., *J. Phys. Chem. C* **2009,** 113, 6100.
155. Sovago, M.; Vartiainen, E.; Bonn, M., *J. Chem. Phys.* **2009,** 131, 161107.
156. Nagata, Y.; Mukamel, S., *J. Am. Chem. Soc.* **2010,** 132, 6434.
157. Tian, C. S.; Shen, Y. R., *Chem. Phys. Lett.* **2009,** 470, 1.
158. Tian, C. S.; Ji, N.; Waychunas, G. A.; Shen, Y. R., *J. Am. Chem. Soc.* **2008,** 130, 13033.
159. Le Calvez, E.; Blaudez, D.; Buffeteau, T.; Desbat, B., *Langmuir* **2001,** 17, 670.
160. Ong, S. W.; Zhao, X. L.; Eisenthal, K. B., *Chem. Phys. Lett.* **1992,** 191, 327.
161. Zhao, X. L.; Ong, S. W.; Eisenthal, K. B., *Chem. Phys. Lett.* **1993,** 202, 513.
162. Geiger, F. M., *Annu. Rev. Phys. Chem.* **2009,** 60, 61.
163. Tian, C. S.; Shen, Y. R., *Proc. Natl. Acad. Sci. U. S. A.* **2009,** 106, 15148.
164. Pimthon, J.; Willumeit, R.; Lendlein, A.; Hofmann, D., *J. Mol. Struct.* **2009,** 921, 38.
165. Bhide, S. Y.; Berkowitz, M. L., *J. Chem. Phys.* **2005,** 123, 224702.
166. Chen, X.; Yang, T.; Kataoka, S.; Cremer, P. S., *J. Am. Chem. Soc.* **2007,** 129, 12272.
167. Zhang, Z.; Zheng, D. S.; Guo, Y.; Wang, H. F., *Phys. Chem. Chem. Phys.* **2009,** 11, 991.
168. Pandit, S. A.; Bostick, D.; Berkowitz, M. L., *Biophys. J.* **2003,** 84, 3743.
169. Gabdoulline, R. R.; Vanderkooi, G.; Zheng, C., *J. Phys. Chem.* **1996,** 100, 15942.
170. Mashl, R. J.; Scott, H. L.; Subramaniam, S.; Jakobsson, E., *Biophys. J.* **2001,** 81, 3005.
171. Pandit, S. A.; Bostick, D.; Berkowitz, M. L., *J. Chem. Phys.* **2003,** 119, 2199.
172. Binder, H.; Zschornig, O., *Chem. Phys. Lipids* **2002,** 115, 39.
173. Casal, H. L.; Mantsch, H. H.; Paltauf, F.; Hauser, H., *Biochimica Et Biophysica Acta* **1987,** 919, 275.
174. Petrov, A. S.; Funseth-Smotzer, J.; Pack, G. R., *Int. J. Quantum Chem.* **2005,** 102, 645.
175. Nihonyanagi, S.; Yamaguchi, S.; Tahara, T., *J. Am. Chem. Soc.* **2010,** 132, 6867.
176. Debruyn, W. J.; Shorter, J. A.; Davidovits, P.; Worsnop, D. R.; Zahniser, M. S.; Kolb, C. E., *J. Geophys. Res.-Atmos.* **1994,** 99, 16927.
177. Martin, D.; Weise, A.; Niclas, H. J., *Angew. Chem.-Int. Edit.* **1967,** 6, 318.
178. Gernon, M. D.; Wu, M.; Buszta, T.; Janney, P., *Green Chem.* **1999,** 1, 127.
179. Vaisman, II; Berkowitz, M. L., *J. Am. Chem. Soc.* **1992,** 114, 7889.
180. Soper, A. K.; Luzar, A., *J. Chem. Phys.* **1992,** 97, 1320.
181. Luzar, A.; Chandler, D., *J. Chem. Phys.* **1993,** 98, 8160.
182. Soper, A. K.; Luzar, A., *J. Phys. Chem.* **1996,** 100, 1357.
183. Givan, A.; Loewenschuss, A.; Nielsen, C. J., *J. Mol. Struct.* **2005,** 748, 77.
184. Li, S. J.; Qian, W.; Tao, F. M., *Chem. Phys. Lett.* **2007,** 438, 190.
185. Bertagnolli, H.; Schultz, E., *Ber. Bunsen-Ges. Phys. Chem. Chem. Phys.* **1989,** 93, 88.

186. Brink, G.; Falk, M., *J. Mol. Struct.* **1970,** 5, 27.
187. Bertoluzza, A.; Bonora, S.; Battaglia, M. A.; Monti, P., *J. Raman Spectrosc.* **1979,** 8, 231.
188. Mizuno, K.; Imafuji, S.; Ochi, T.; Ohta, T.; Maeda, S., *J. Phys. Chem. B* **2000,** 104, 11001.
189. Catalan, J.; Diaz, C.; Garcia-Blanco, F., *J. Org. Chem.* **2001,** 66, 5846.
190. Kaatze, U.; Brai, M.; Scholle, F. D.; Pottel, R., *J. Mol. Liq.* **1990,** 44, 197.
191. Karpovich, D. S.; Ray, D., *J. Phys. Chem. B* **1998,** 102, 649.
192. Allen, H. C.; Raymond, E. A.; Richmond, G. L., *Curr. Opin. Colloid Interface Sci.* **2000,** 5, 74.
193. Allen, H. C.; Raymond, E. A.; Richmond, G. L., *J. Phys. Chem. A* **2001,** 105, 1649.
194. Tarbuck, T. L.; Richmond, G. L., *J. Phys. Chem. B* **2005,** 109, 20868.
195. Benjamin, I., *J. Chem. Phys.* **1999,** 110, 8070.
196. Senapati, S., *J. Chem. Phys.* **2002,** 117, 1812.
197. Darvas, M.; Pojjak, K.; Horvai, G.; Jedlovszky, P., *J. Chem. Phys.* **2010,** 132, 134701.
198. Forel, M. T.; Tranquil.M, *Spectrochimica Acta Part a-Molecular Spectroscopy* **1970,** A 26, 1023.
199. Covington, A. K.; Thompson, R., *J. Solut. Chem.* **1974,** 3, 603.
200. Auer, B. M.; Skinner, J. L., *J. Chem. Phys.* **2008,** 128.
201. Safford, G. J.; Schaffer, P. C.; Leung, P. S.; Doebbler, G. F.; Brady, G. W.; Lyden, E. F. X., *J. Chem. Phys.* **1969,** 50, 2140.
202. Scherer, J. R.; Go, M. K.; Kint, S., *J. Phys. Chem.* **1973,** 77, 2108.
203. Devisser, C.; Heuvelsland, W. J. M.; Dunn, L. A.; Somsen, G., *Journal of the Chemical Society-Faraday Transactions I* **1978,** 74, 1159.
204. Puranik, S. M.; Kumbharkhane, A. C.; Mehrotra, S. C., *J. Chem. Soc.-Faraday Trans.* **1992,** 88, 433.
205. Brubach, J. B.; Mermet, A.; Filabozzi, A.; Gerschel, A.; Roy, P., *J. Chem. Phys.* **2005,** 122, 184509.
206. Wall, T. T.; Hornig, D. F., *J. Chem. Phys.* **1965,** 43, 2079.
207. Falk, M.; Ford, T. A., *Canadian Journal of Chemistry* **1966,** 44, 1699.
208. Janosche.R; Weideman.Eg; Zundel, G.; Pfeiffer, H., *J. Am. Chem. Soc.* **1972,** 94, 2387.
209. Stangret, J.; Gampe, T., *J. Phys. Chem. A* **2002,** 106, 5393.
210. Mikenda, W., *Mon. Chem.* **1986,** 117, 977.
211. Tarbuck, T. L.; Ota, S. T.; Richmond, G. L., *J. Am. Chem. Soc.* **2006,** 128, 14519.
212. Chen, X. K.; Hua, W.; Huang, Z. S.; Allen, H. C., *J. Am. Chem. Soc.* **2010,** in press.